

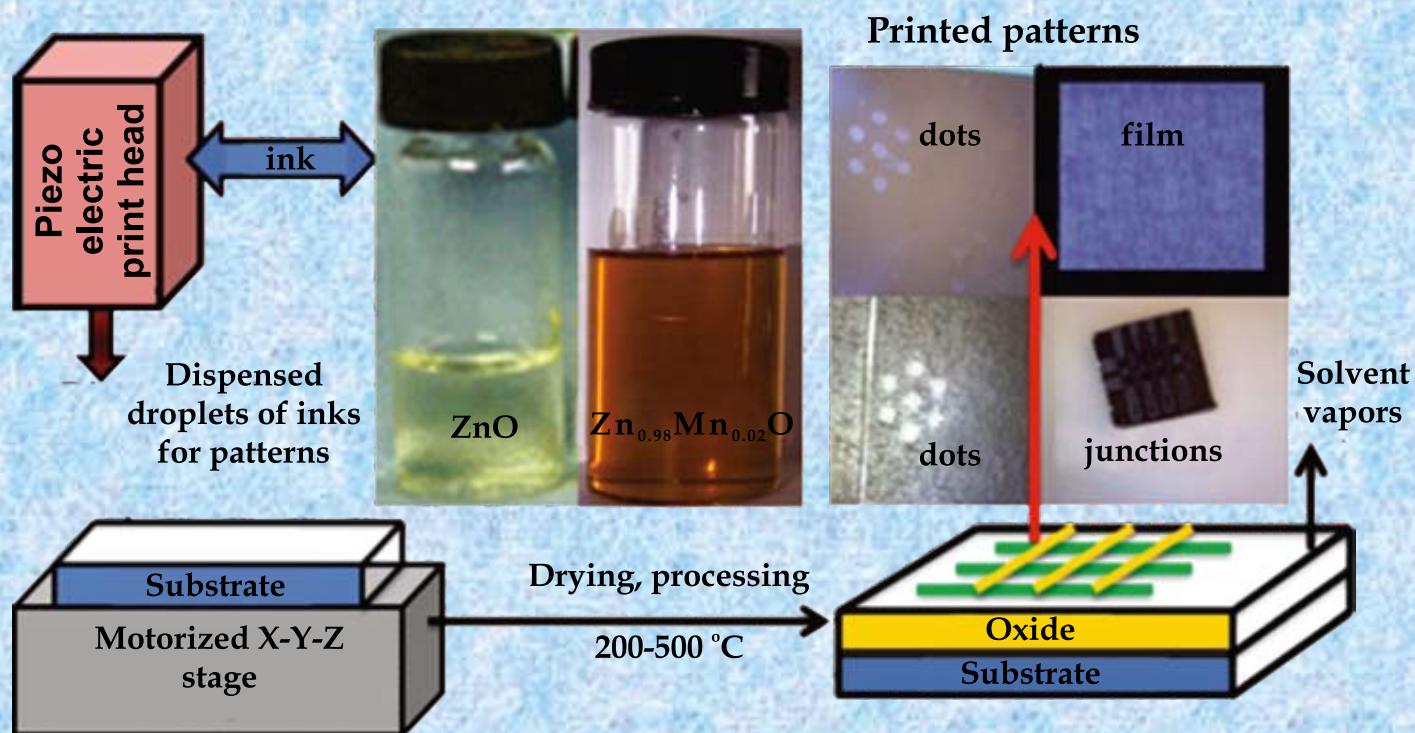
SMC Bulletin

A Publication of the Society for Materials Chemistry

Volume 2

No. 1

June 2011



SOCIETY FOR MATERIALS CHEMISTRY

Society for Materials Chemistry was mooted in 2007 with following aims and objectives:

- (a) to help the advancement, dissemination and application of the knowledge in the field of materials chemistry,
- (b) to promote active interaction among all material scientists, bodies, institutions and industries interested in achieving the advancement, dissemination and application of the knowledge of materials chemistry,
- (c) to disseminate information in the field of materials chemistry by publication of bulletins, reports, newsletters, journals.
- (d) to provide a common platform to young researchers and active scientists by arranging seminars, lectures, workshops, conferences on current research topics in the area of materials chemistry,
- (e) to provide financial and other assistance to needy deserving researchers for participation to present their work in symposia, conference, etc.
- (f) to provide an incentive by way of cash awards to researchers for best thesis, best paper published in journal/national/international conferences for the advancement of materials chemistry,
- (g) to undertake and execute all other acts as mentioned in the constitution of SMC.

Executive Committee

President

Dr. T. Mukherjee
Bhabha Atomic Research Centre
Trombay, Mumbai, 400 085
mukherji@barc.gov.in

Vice-Presidents

Dr. D. Das
Bhabha Atomic Research Centre
Trombay, Mumbai, 400 085
dasd@barc.gov.in

Dr. K. Nagarajan
Indira Gandhi Centre for Atomic
Research
Kalpakkam, 603102 (TN)
knag@igcar.gov.in

Secretary

Dr. A.K. Tyagi
Bhabha Atomic Research Centre
Trombay, Mumbai, 400 085
aktyagi@barc.gov.in

Treasurer

Dr. R.K. Vatsa
Bhabha Atomic Research Centre
Trombay, Mumbai, 400 085
rkvatsa@barc.gov.in

Members

Dr. P.R. Vasudeva Rao
Indira Gandhi Centre for Atomic
Research
Kalpakkam, 603102 (TN)
vasu@igcar.gov.in

Dr. S.K. Kulshrestha
Atomic Energy Education Society
Western Sector, AEES-6
Anushaktinagar, Mumbai, 400 094
kulshres@gmail.com

Dr. V.K. Jain
Bhabha Atomic Research Centre
Trombay, Mumbai, 400 085
jainvk@barc.gov.in

Dr. C.G.S. Pillai
Bhabha Atomic Research Centre
Trombay, Mumbai, 400 085
cgspil@barc.gov.in

Dr. S.R. Bharadwaj
Bhabha Atomic Research Centre
Trombay, Mumbai, 400 085
shyamala@barc.gov.in

Dr. Manidipa Basu
Bhabha Atomic Research Centre
Trombay, Mumbai, 400 085
deepa@barc.gov.in

Dr. Sandeep Nigam
Bhabha Atomic Research Centre
Trombay, Mumbai, 400 085
snigam@barc.gov.in

Co-opted Members

Dr. Aparna Banerjee
Bhabha Atomic Research Centre
Trombay, Mumbai, 400 085
aparnab@barc.gov.in

Dr. A.K. Tripathi
Bhabha Atomic Research Centre
Trombay, Mumbai, 400 085
catal@barc.gov.in

Prof. S.D. Samant
Institute of Chemical Technology
Matunga, Mumbai-400 019
samantsd@udct.org

Prof. G.P. Das
Indian Association for the Cultivation
of Science (IACS)
Jadavpur, Kolkata-700 032,
msgpd@iacs.res.in

Prof. Ashok K. Ganguli
Indian Institute of Technology
Hauz Khas, New Delhi 110 016
ashok@chemistry.iitd.ernet.in

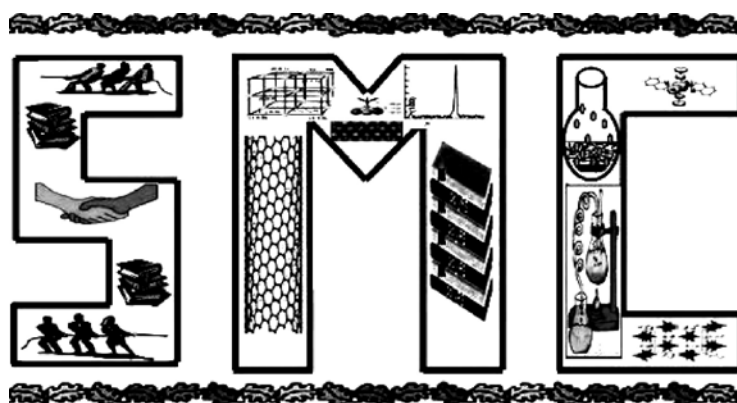
SMC Bulletin

A Publication of the Society for Materials Chemistry

Volume 2

No. 1

June 2011



SOCIETY FOR MATERIALS CHEMISTRY

SMC Bulletin

Vol. 2, No.1

June 2011

Editorial Board

Dr. Arvind Kumar Tripathi
Chemistry Division
Bhabha Atomic Research Centre
Trombay, Mumbai, 400 085
e-mail: catal@barc.gov.in

Dr. Shyamala Bharadwaj
Chemistry Division
Bhabha Atomic Research Centre
Trombay, Mumbai, 400 085
e-mail: shyamala@barc.gov.in

Dr. Manidipa Basu
Chemistry Division
Bhabha Atomic Research Centre
Trombay, Mumbai, 400 085
e-mail: deepa@barc.gov.in

Dr. Aparna Banerjee
Product Development Division
Bhabha Atomic Research Centre
Trombay, Mumbai, 400 085
e-mail: aparnab@barc.gov.in

Dr. Sandeep Nigam
Chemistry Division
Bhabha Atomic Research Centre
Trombay, Mumbai, 400 085
e-mail: snigam@barc.gov.in

Published by
Society for Materials Chemistry
C/o. Chemistry Division
Bhabha Atomic Research Centre, Trombay, Mumbai, 400 085
E-mail: socmatchem@gmail.com,
Tel: +91-22-25592001

*"Please note that the authors of the paper are alone responsible for the technical contents of papers and references cited therein.
Front cover shows a schematic of Ink-jet printing method to prepare thin films of functional materials."*

Editorial Note

After a successful release of the inaugural issue of SMC bulletin during 3rd International Symposium on Materials Chemistry (ISMC-2010) we are happy to present the second issue, a thematic one, on “Nanomaterials and their applications”. This issue contains total six research articles on this theme including one feature article on chemistry of nanomaterials and their applications. These articles present synthesis of different oxides, mixed oxides, metallic nanoparticles, nano-composites in various shapes and sizes (sphere, nanoplate etc.) via evaporation, polyol method or by employing reactive polymers like poly(vinylidene fluoride) as templates. Applications of these materials include variety of areas like white light generation, photocatalysis, tissue engineering.

The next issue of the bulletin will be a thematic one on “Chemistry of functional materials”. Readers are encouraged to send their feedbacks which will enable us to improve the SMC bulletin.

Editors

From the President's Desk

Dear Fellow members,

The Society for Materials Chemistry (SMC) is a fast growing national body with around 540 life members. In the past, the Society has successfully organized international symposia on Materials Chemistry (ISMC-2006, ISMC-2008 and ISMC-2010) and we are now planning to organise a National Workshop on Materials Chemistry: Functional Materials, NWMC-2011 (FUN-MAT) on 7th and 8th December 2011 in Mumbai.

I am happy to note that the inaugural issue of the SMC bulletin brought out during the 3rd DAE-BRNS International Symposium on Materials Chemistry at BARC was well received by our members. I earnestly request all members to contribute towards SMC bulletin which is publishing articles on various themes e.g., present issue is on nanomaterials and its applications. I hope that the theme based issues of our bulletin will be quite useful for our members, particularly for the young researchers working in the area of materials chemistry. I expect that the bulletin will continue to provide a platform to highlight the advances made in the field of materials chemistry and hope that the members will contribute articles to enrich the goals of the bulletin.

T. Mukherjee

CONTENTS

Feature Articles	Page No
1. Chemistry and applications of nanomaterials <i>A.K. Tyagi</i>	1
2. Evaporation induced self assembly of nanoparticles by spray drying <i>D. Sen, J. Bahadur, S. Mazumder, J.S. Melo and S.F. D' Souza</i>	12
3. Light absorption and emission in gold nanoplates assembled in small groups via poly(vinylidene fluoride) molecules <i>B. Susrutha, A.D. Phule and S. Ram</i>	22
4. Preparation and characterization of Collagen-based Liposome Nanoparticles composite matrix <i>Krishnamoorthy Ganesan, Praveen Kumar Sehgal, Asit Baran Mandal and Sadulla Sayeed</i>	29
5. Application of nanophosphors in solid state white light generation <i>Dimple P. Dutta</i>	34
6. Photocatalytic Properties of mixed oxides of BaCrO₄ and TiO₂ <i>Tanmay K. Ghorai, Chirantan Roy Chaudhyry, Suman Biswas, Mukut Chakraborty, Ranjan Das, Jhimli Sengupta</i>	40
News and Forthcoming Events	48
Honours and Awards	49

Chemistry and Applications of Nanomaterials

A. K. Tyagi

*Chemistry Division,
Bhabha Atomic Research Centre
Mumbai- 400 085, India
E-mail: aktyagi@barc.gov.in*

Abstract

The world of science has witnessed a tremendous upsurge in the field of nanoscience and nanotechnology in the last few years. The term 'Nano' has now become a theme in almost all the established disciplines of science. Some of the broad fields like separation science, catalysis, energy conversion, nano-ceramics, biological formulations, coatings, bio-imaging and semiconductors etc. have witnessed revolutionary changes after the advent of nanoscience and nanotechnology. Nanomaterials are likely to play an important role in Department of Atomic Energy's programmes also ranging from front end to back end of the nuclear fuel cycle, The recovery of valuable from nuclear waste and design of new sorbents for radio-isotopes for health applications, just to name a few. This article is intended to give a broad over view of chemistry and wide range of applications of nanomaterials.

Key-words: Soft-Chemical routes, optical materials, magnetic materials, energy conversion materials, sensors.

Introduction

Nanoparticles are small clusters of atoms about 1 to 100 nanometers long. 'Nano' derives from the Greek word "nanos", which means dwarf or extremely small. Essentially, the reason is that nanocrystals in the 1 to 10 nm range make up a new realm of matter in which physical and chemical properties change as size changes. Contemplating that any nanostructured solid material can have variable properties based on size essentially makes the periodic table of the elements "three dimensional". The properties that change in the nano regime include band gaps (for semiconductors), magnetic moments (for ferro- ferrimagnetisms), specific heats, melting points, surface chemistry, and morphology/particle shape. For consolidated nanoparticles, metal pieces can be harder, and ceramic pieces can be more plastic than normal materials made from microcrystal-polycrystal consolidation. Metal oxide nanoparticles are an important class of materials for their optical, magnetic and electronic properties [1,2]. These properties make nanostructured metal oxides useful for a wide range of applications such as catalysts, sensors, optical materials, electrical materials and magnetic storages [3]. Hence, over the past half-decade, research in functional oxide-based nanostructures has attracted considerable attention due to their unique and innovative applications in optics, optoelectronics, catalysis, ferro and piezoelectricity.

Synthesis methods

The synthesis and characterization of nanoparticles, nano-tubes and other nano-units at a length scale of about 1-100 nm (at least in one direction) is a subject of intense research. In this direction, material chemists play a crucial role in the preparation, structural elucidation and property measurements of the materials, which are important ingredients in the discovery and commercialization of nanotechnologies and devices. The materials synthesis methods can be classified in to two broad categories namely (i) Solid state method and (ii) Soft-chemical methods. The latter classes of methods are basically low energy synthesis methods which are often used under ambient or slightly above ambient conditions. Of late, the soft-chemical methods such as combustion synthesis, metal nanocrystals by reduction, template method, coprecipitation, arrested precipitation, radiation assisted synthesis, polyol method, sono-chemical, miceller methods, impregnation, microwave assisted synthesis, hydro & solvothermal methods, xerogel method and solid state metathesis etc. have gained tremendous momentum. By these methods it is possible to have an excellent control on shape and size of nanomaterials. There is yet another category of synthesis of nanomaterials, which is primarily bio-inspired. Nature makes most of the materials at ambient or slightly above ambient conditions.

As far as thin films of are concerned, in addition to energy and cost intensive Physical Vapor Deposition (PVD) techniques, chemical methods like ink-jet printing, screen printing and spin coating have also become prominent to prepare thin films of functional nanomaterials.

Some of the soft-chemical synthesis methods for nanomaterials are briefly described in the next section:

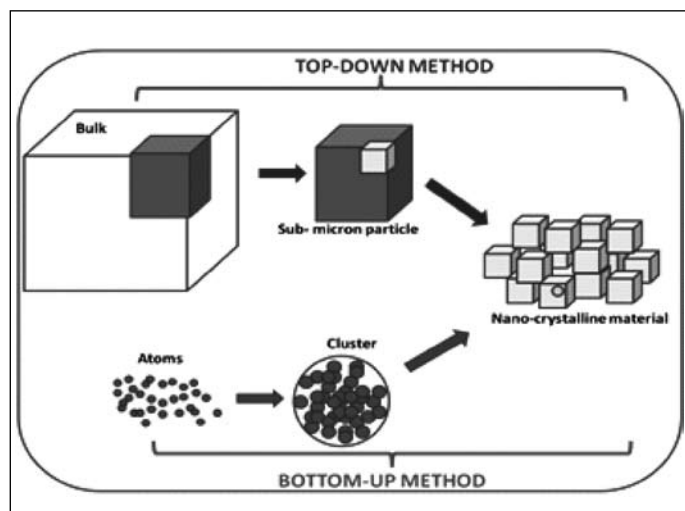


Fig. 1: Two broad synthesis methods of nano materials

Gel-Combustion synthesis

It is a facile synthesis technique [4] which can be easily employed on a lab-scale to prepare nano-crystalline ceramic powders with reproducible characteristics. Combustion is basically a redox reaction between the oxidant and fuel, which is controlled by various factors such as nature and amount of fuel. First the nitrate/oxynitrate salts of the metals, in a required molar ratio, are mixed together in an aqueous media to produce a transparent mixed metal-nitrate solution. A suitable fuel (glycine, citric acid, urea etc.) is then added in an appropriate amount to this solution. The aqueous solution of fuel and oxidants is subsequently thermally dehydrated on a hot plate (at about 80-100 °C) or a muffle furnace to obtain a viscous gel. The gel, as formed in the above step, is further heated at a higher temperature (200-250 °C) which initiates a self-propagating combustion. The exothermic decomposition of the fuel-oxidant precursor is visible in the form of flame, which rapidly propagates throughout the gel. Therefore, this step is also termed as "auto-ignition". The auto-ignition is a very short-lived phenomenon as the flame persists for only about few (5-10) seconds. It is within this short duration that the product formation takes place.

Sol gel synthesis

The sol-gel process [5] is a low temperature approach for synthesizing various oxide materials. A sol is a colloidal suspension of solid particles in a liquid whereas the gel is a solid whose pore contains liquids. It is generally a two step process which involves hydrolysis of precursors followed by their condensation to form oxide frameworks. Product properties are affected by the rate of hydrolysis and condensation. Generally, slower and controlled hydrolysis leads to smaller particle sizes. Pore size, distribution, and interconnectivity are also affected by other processing parameters, such as the type and amount of solvent and/or catalyst, temperature. This low temperature soft chemical method is safe, inexpensive and can give nanomaterials with complex shapes.

Template synthesis

Template method involves the fabrication of the desired material within the pores or channels of a nanoporous template [6]. In general, a template may be defined as a central structure within which a network forms in such a way that removal of the template creates a filled cavity with morphological and/or stereochemical features related to those of the template. Templates can be of several types' e.g. hard templates, soft templates and soft-hard templates. Some of the examples of hard templates are ordered mesoporous siliceous materials, track-etch membranes, porous alumina etc. The typical examples of soft templates are surfactants, colloidal particles, shape-directing molecules, soap bubbles and colloids. Some of the polycarbonates are neither too-hard not too-soft and hence they form yet another class of templates namely soft-hard templates. It is important to note that nearly all the materials can be synthesized within nanoporous templates, provided a suitable chemical pathway can be developed. One can achieve an excellent shape control by template method. There are essentially five representative strategies to carry out template synthesis of nanostructures. They are electrochemical deposition, electrodeless deposition, chemical polymerization, sol gel deposition and chemical vapor deposition techniques.

Sonochemical synthesis

Ultrasound has become an important tool for the synthesis of nanoparticles [7,8]. When liquids are irradiated with ultrasonic irradiation, ultrasonic cavitation will form. Ultrasonic cavitation is concerned with the formation, growth, and implosive collapse of bubbles. Inherently the

cavitation bubbles are vacuum bubbles. The vacuum is created by a fast moving surface on one side and an inert liquid on the other. The resulting pressure differences serve to overcome the cohesion and adhesion forces within the liquid. Ultrasonic cavitation produces a variety of physical and chemical effects, such as high temperature (>5000 K), pressure (>20 MPa), and cooling rate ($>10^{10}$ Ks⁻¹), which could provide a unique environment for chemical reactions under extreme conditions. The sonochemical effects observed in chemical reactions and processes can involve increase in reaction speed, increase in reaction output, more efficient energy usage, sonochemical methods for switching of reaction pathway, activation of metals and solids, improvement of particle synthesis and also coating of nanoparticles. The temperature plays an important role in sonochemical reactions.

Nano-metals by reduction process

A large number of metals and their alloys can be prepared in nanoform by a facile chemical reduction method [9]. The prerequisite of this method is a water soluble metal salt, which can be reduced by using a variety of reducing agents, such as borohydride, alcohols and hydrazine etc., to obtain the corresponding metal or alloys in nanocrystalline state. The common metals which have been prepared by this method are noble metals, Cu, Co, Ni, Au etc. It is also possible to modify the surface of these nanometals during the course of reduction itself. For example, PVP coated Pd, Ag, Au and Cu nanocrystals can be prepared [10] by refluxing the corresponding metal salts and ethyl alcohol (reducing agent) in the presence of PVP. The basic reaction in case of the borohydride reduction is hydrolysis of borohydride to generate hydrogen, which in turn reduces the metal ions. In ideal cases, it is also possible to prepare alloys and intermetallics, such as FePt, FePd etc., by this method.

Radiation-induced synthesis of semiconductor nanomaterials

The radiation-induced synthesis of nanomaterials like metallic and semiconductor is very effective and powerful method. Unlike in the chemical methods, the usage of high temperature, inert atmosphere and several chemical reagents is avoided in this method of synthesis. The synthesis is mainly carried out by the solvated electrons generated upon interaction of high energy radiations with solvents. In the case of water as the solvent, these are called as hydrated electrons. These hydrated electrons are highly

reactive species and react with the positively charged metal ions as well as other precursors ions present in the aqueous solutions. Synthesis of several metal nanoparticles of silver, gold, nickel etc. and semiconductor nanoparticles of cadmium sulfide, cadmium selenide, zinc oxide etc. through the radiation-induced route in neat aqueous solutions as well as in the presence of different capping agents or polymers can be achieved. In this case, the reaction mixture does not have too many chemical reagents which otherwise need to be removed if it is required. Furthermore, the shape and size of the nanomaterials are controlled by the absorbed dose, dose rate, precursor concentrations and the proper choice of a microenvironment. These reactions are performed by both cobalt-60 gamma irradiation and electron beam irradiation in an electron accelerator like linear electron accelerator, LINAC.

A typical example is synthesis [11] of cadmium selenide, CdSe quantum dots in aqueous solutions containing equimolar ammoniated cadmium sulfate and sodium selenosulfate by gamma and electron beam irradiations. The as-grown CdSe quantum dots exist in agglomerated form and exhibit ferromagnetic behavior at room temperature (RTFM). The RTFM was about 30% higher in the case of CdSe synthesized by electron beam irradiation as compared to that in the case of gamma irradiation. CdSe quantum dots synthesized via electron beam irradiation were found to be decomposed upon exposure to air and light when they are present in aqueous solutions. The decomposed solutions again produced CdSe quantum dots upon electron beam irradiations and this cycle was repeated for several times. However, these nanomaterials are quite stable when dispersed in organic solvents and removed from water. The CdSe quantum dots synthesized in CTAB microemulsions exhibit strong photoluminescence with an emission peak at 600 nm at room temperature. It was confirmed that the formation of CdSe nanomaterials proceeds through the reactions of hydrated electrons with both cadmium and selenosulfate ions, with the formation of a transient intermediate species having an absorption maximum at 520 nm.

Thin films of nanomaterials by chemical methods

Inkjet printing technology is a simple and low cost method which has recently become an attractive technique of patterning and printing of thin films of semiconductors, conductive polymers and organic LEDs, electronic circuits and bio-nanoparticles at ambient conditions [12]. Its versatility to deliver small volumes of inks with spatial

accuracy and direct-writing ability in a non-contact deposition mode makes it a novel patterning technique. Nevertheless, reports of inkjet printing of inorganic materials are in scarce. Only a handful of inorganic materials have been ink-jet printed, mainly due to the difficulty in synthesizing printable inorganic inks. Few inkjet printed microstructures of oxides, nanoparticles and polymers, using dispersions have been recently reported [13]. The formulation of printable sulfide based (ZnS and doped ZnS) quantum dots dispersions in water [14] have been reported. Dispersed particles can often cause agglomeration, which cause clogging of the print head. This clogging problem can be overcome by formulating solvent based precursor inks, which form crystalline nanoparticles on the substrate after printing and annealing. Recently fabrication of inkjet printed films and patterns (dots, lines and junctions) of ZnO and $Zn_{0.98}Mn_{0.02}O$ on Si and polyimide substrates was reported [15] using their precursor based solvent inks, that have been fine tuned to match the desired viscosity, surface tension and adhesive property by adding suitable additives. It was found by Atomic Force Microscopy that the surface morphology of these thin films was smoother than that of ZnO based films prepared by other cost intensive method. Typical scheme showing printing, processing and patterning of ZnO based ink is given below (Fig. 2).

Bio-inspired synthesis of metal nanoparticles

Nature synthesizes nanoparticles in a most energy efficient way that makes use of no hazardous chemicals

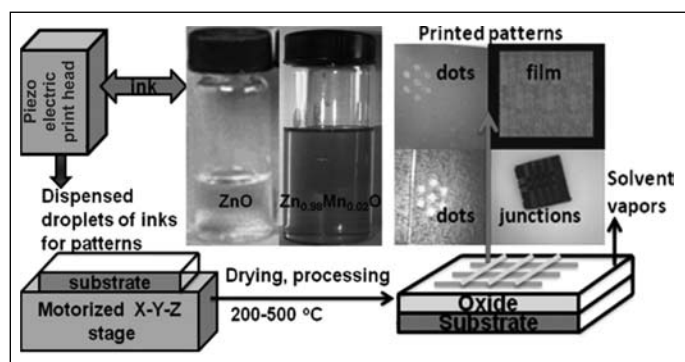


Fig. 2: Scheme representing the Ink-jet printing of functional materials

and/or any high-boiling solvents, typically employed in large-scale industrial production of the same. For example, magnetotactic bacteria synthesize well-aligned magnetic nanoparticles within their cells. Inspired by

this approach, researchers from all over the world started synthesizing nanoparticles using extract from plants and microorganisms. These methods involving a wide variety of biological processes provide great control over kinetics of the nano-particle production that often results in exotic morphologies and unique optical and electronic properties. Metal nanoparticles synthesized via biological route also exhibit excellent microbial properties. Organisms ranging from bacteria to fungi and even plants have been used to synthesize nanoparticles. Extract from plant pathogenic fungus *Fusarium Oxysporum* has been used for the synthesis of Au, Ag, Au-Ag alloy, SiO_2 , TiO_2 , ZrO_2 , Fe_3O_4 , CdS and $BaTiO_3$ nanoparticles [16]. Cell-free extract from *T. asperellum*, a non-pathogenic, commercial bio-control agent was used for the synthesis of variety of nano-materials including silver nanoparticles [17] Lemon grass and Aloe vera extracts [18] have been used to synthesize gold nanoprisms that exhibit anisotropic electron transport behavior. Palladium nanoparticles were synthesized using sulfate reducing bacteria [19]. DNA, proteins and virus were also used to produce nanoparticles, nanowires etc. [20]. In brief, bio-inspired synthesis of nanoparticles has led to the exploitation of a simple but altogether new area of research that was hitherto largely unexplored.

Applications of Nanomaterials

The broad areas in which nanomaterials have potential to an impact are (a). Energy (b). Environment (c) Biomedical and (d) Engineering. Some of the applications are summarized briefly.

Nanomaterials for energy conversion applications

Nanomaterials have immense applications in energy conversion devices such as Fuel Cells (SOFC), oxygen storage capacitors, Li ion batteries, hydrogen generation and storage, and wavelength shifters (optical materials). There is a growing need to develop better soft chemical synthesis routes as the conventional solid state method has several limitations. Among the available chemical routes, the combustion technique is capable of producing the nanocrystalline powders of the oxide ceramics at lower calcination temperature. A wide range of materials for SOFC applications have been synthesized. In SOFC technology, the electrolyte and interconnect materials need to be have near theoretical densities whereas anode and cathode materials need a high degree of porosity. These opposite requirements pose a challenge to the synthetic and processing scientists. Sof-chemical routes have played

in important role in circumventing some of the materials problems of SOFC technology. Several SOFC materials such as Gd and Sm doped ceria, $Zr_{0.8}Ce_{0.2}O_2$, YSZ, CeO_2 - Y_2O_3 solid solution, $La_{1-x}M_xCrO_3$ ($M = Ca, Sr$), Sr-doped $LaCoO_3$ and doped $LaGaO_3$ have been prepared by combustion method [21-23]. The powder properties were tailored to achieve near theoretical density sintered pellets. A major emphasis was on the optimization of the processing parameters so as to get a highly sinterable phase pure materials. The size and nature of agglomeration was found to be a crucial parameter affecting the sinterability. The desired extent of porosity in cathode and anode materials was introduced by using pore-formers like graphite or starch. The shape of pores was found to crucially depend on powder properties of the pore formers.

Another key issue of SOFC technology is the design of better ionic conductors. It is well known that ionic conductivity is a highly structure-driven property. Several new ionic conductors, such $Nd_{2-x}Gd_xZr_2O_7$ and $Ba_2In_{2-x}Ti_xO_{5+x/2}$ were prepared [24] based on the structure-property correlation. Detailed XRD and Raman spectroscopy studies revealed that an optimum degree of disorder enhances the ionic conductivity. Recently, a two steps synthesis was developed involving a combustion reaction followed by a reduction step, which was used to prepare [25-28] of a number potential oxygen storage materials such as $Ce_2Zr_2O_{7+x}$, $Gd_{2-x}Ce_xZr_2O_7$ ($x = 0.0$ to 2.0), $Ce_{0.5}Sc_{0.5}O_{1.75}$ and interesting magnetic materials like $La_{1-x}Ce_xCrO_3$ in nanocrystalline form. All compounds in $La_{1-x}Ce_xCrO_3$ series were found to be predominantly antiferromagnetic in nature with a remarkable linear increasing trend in Neel temperature (T_N) from 257 K to 281.5 K as a function of decreasing Ce^{3+} content. Interestingly, the band-gap also shows a linear decrease from 3.21eV to 3.02 eV as a function of increasing Ce^{3+} concentration in the $La_{1-x}Ce_xCrO_3$ series. It was found that on oxidation $Ce_2Zr_2O_7$ transforms to $Ce_2Zr_2O_8$ via an intermediate lattice at $Ce_2Zr_2O_{7.5}$. The retention of cubic pyrochlore type arrangements is observed even up to the fully oxidized $Ce_2Zr_2O_8$ composition. A complete oxidation of Ce^{3+} to Ce^{4+} is observed in contrast to kinetically/sterically hindered oxidation proposed by other researchers. The deep crystallographic insights [29] associated with the oxygen intercalation and deintercalation process in Ce_2O_3/CeO_2 - ZrO_2 will have immense importance in the development and understanding of new oxygen storage capacitors (OSC). Likewise, the ease of oxygen intercalation and deintercalation process in $Gd_{2-x}Ce_xZr_2O_{7+x}$

without any collapse of the structure empowers these materials with various properties like OSC.

Biomedical applications

Nanostructured materials with well defined particle size, morphology, microstructure and surface characteristics are currently offering great promise as supports in a large number of biotechnological, pharmaceutical and medical applications such as diagnostics (assays), bioseparation, NMR imaging, cosmetics and drug delivery systems [30]. In view of this, a large amount of work has been done in Chemistry Division, BARC to the design and preparation of nanomaterials with appropriate properties for interacting with biologically active macromolecules. Stable immobilization of one of the assay reagents (biomolecules) on a suitable substrate with complete retention of their biological recognition properties is a crucial step in developing efficient biosensors. Amine/imine functional groups of polyaniline modified surfaces have shown improved binding of triiodothyronine (T_3) antibodies on polystyrene surface that can be used as a substrate for the detection of human thyroid hormone in nanograms/ml level using radioimmunoassay (RIA) [31]. Metal nanoparticles such as gold and silver exhibit an intense color in the visible region due to the well-known surface plasmon absorption. It has been shown in literature [32] that triangular silver nanoprisms can be used to detect proteins by monitoring shifts in their surface plasmon resonance after binding of target proteins. Silver nanoparticles are generated on surfaces using nanosphere lithography, and then biotin is immobilized on the surfaces of the particles. The shift in the surface plasmon resonance of the silver triangles by the addition of streptavidin allows detection of streptavidin at concentrations as low as ~ 0.1 -1 pM. The formation of particulate systems with defined particle size and shape is of eminent interest in drug delivery applications, as well. The pH sensitive hydrogels can be designed to respond to specific chemical triggers, such as glucose for controlled release of insulin in diabetic patients. Self assembled stimuli responsive hydrogels can also be prepared from worm-like micelles using surfactants and other pH-sensitive moieties. Among the different polymer-based drug delivery systems, polymeric micelles represent a promising delivery vehicle especially intended for poorly water-soluble pharmaceutical active ingredients in order to improve their oral bioavailability. Polymeric micelles have been studied extensively as delivery vehicles for injectable drug formulations of poorly water-soluble drugs such as

paclitaxel, indomethacin, amphotericin B, adriamycin, and dihydrotestosterone. Overall, they proved to be highly effective drug delivery vehicles. The doxorubicin loaded mixed micelles were evaluated for in vitro cytotoxicity against various cancer cell lines to establish their potential in improving delivery of the drug. Attempts have also been made to use dendrimers in the targeted delivery of drugs and other therapeutic agents. Dendrimers have been used as coating agents to protect or deliver drugs to specific sites in the body or as time-release vehicles.

Research on rare-earth nano-fluorides has been an intense area of investigations in last few years from the point of view of their applications as phosphors for solid state lighting. They have distinct advantages compared to other materials because of their outstanding properties such as very low phonon frequencies, high thermal stability and sometimes tunable crystal phases and related photo physical properties. Rare earth fluoride compounds can be synthesized by wet chemical routes like the hydrothermal method, microwave irradiation, sonication and also by employing ionic liquids. Polyol mediated synthesis is a simple one pot synthesis for obtaining nano-fluorides at low temperature. In this method, the precursors (generally nitrates) are refluxed in a polyol (ethylene glycol, glycerol etc.) in the presence of a fluorinating agent (NaF, NH_4F , KBF_4 etc.) for 2-3 hours. The product thus obtained has uniform size distribution and the resulting nonpowders are readily dispersible in polar solvents like methanol and water. Rare earth nanofluorides (YF_3 , CeF_3 and GdF_3) were explored as potential phosphors for ultra-violet based light emitting diodes for solid state lighting. Preliminary studies on human breast cancer cells have shown good uptake of these nanoparticles by carcinoma cells (MCF-7), which give bright colors corresponding to that of nanoparticles after being illuminated with UV light.

Magnetic nanoparticles (MN) are used in many applications such as data storage/recording medium, catalysis, magnetic resonance imaging as a contrast agent and targeted drug delivery in cancer therapy. Biocompatibility, size and magnetic properties make Fe_3O_4 nanoparticles primary candidates of choice for numerous biomedical applications such as drug delivery, cell separation, immunoassay, magnetic resonance imaging, contrast enhancement, tissue repair and hyperthermia. Following administration, these nanoparticles could get transferred through blood stream to desired areas of treatment. Water dispersible Fe_3O_4 nanoparticles (coated

with Poly Vinyl Pyrolidone (PVP) and Poly oxy ethylene 25- propylene glycol stearate (POES) and complexed with Doxorubicin has been prepared [33] and characterized using X-ray diffraction (XRD), transmission electron microscopy (TEM) and vibrating sample magnetometer (VSM). The antitumor activity of these particles has been studied by targeting the complex to the tumor site, using an externally applied magnetic field, after oral administration of the magnetic nanoparticle-drug complexes. Our results reveal that the chemotherapy effect of Doxorubicin could be considerably enhanced by combination of the application of the drug conjugated-magnetic Fe_3O_4 nanoparticles, which are biocompatible and stable, and targeted drug delivery with a magnet.

Magnetic nanoparticles (MN) smaller than 20 nm size are more useful in cancer therapy because of their high effective surface area for easy attachment of ligands and better tissue diffusion. MN can produce heat under AC magnetic field, which is required for hyperthermia temperature (42-44 °C). Sources of heat-generation of MN are from hysteresis loss, eddy current, Brownian rotational loss and spin relaxation. When MN have high resistance, contribution from eddy current is negligible. Sometimes, particles becomes non-ferromagnetic (i. e. coercivity, H_c is zero) as the particle size becomes less than critical size (single domain), but individual particles have large moment (10^3 - $10^5 \mu_B$). In such situation, particles are considered as superparamagnetic. If the particle size is smaller than single domain, heat generation from hysteresis loop is almost negligible, and thus, main contribution to heat-generation will be from Brownian rotational loss and spin relaxation under AC induction magnetic field. In order to get the fast or high heat generation and also important in cancer therapy, the particle size of magnetic nanoparticles should not be too small. Otherwise, more particles, more duration of heat-treatment and high AC frequency will be necessary to achieve hyperthermia temperature (42-45 °C). Particularly, Fe_3O_4 and its derivative compounds are important in hyperthermia application. The increasing attention to these Fe_3O_4 nanoparticles for various biomedical applications are due to their biocompatibility, injectibility, chemical stability over physiological circumference and substantial accumulation at the diseased site. Thus, monodispersed Fe_3O_4 nanoparticles with size of 8-11 nm are desirable. Every sample with different particle size can have specific absorption rate (SAR) in AC magnetic field and this information will help in amount of heat generation from 1

mg of sample. Recently at Chemistry Division, BARC Fe_3O_4 and Co, Ni doped $\text{Fe}_{3-x}\text{O}_4$ nanoparticles were prepared by co-precipitation method. In order to functionalize surface of particle, particles are capped with PEG (polyethylene glycol) and OA (oleic acid) so as to minimize agglomeration among smaller magnetic particles. About 2-5 mg of Fe_3O_4 (pure) can reach hyperthermia temperature within 5-10 min at 256 kHz and 400-600 A. Heating ability of MN capped with OA or PEG up to 42°C was observed at reasonably low concentration (10 mg) suggesting their suitability for hyperthermia applications. The efficacy of capped MN was further validated [34] in human breast cancer cells with their enhanced killing ability under induction heating conditions suggesting to extend these studies for hyperthermic cancer therapy in suitable in vivo experimental models. Control release of anticancer drug at tumor site is important in order to reduce side-effect to other normal cells while delivery/injecting to blood vessels.

Nanomaterials in catalysis

The structure sensitive catalytic properties of small-size particles are relevant for both metal and non-metal catalyst surfaces. In addition, due to the changes in the electron density as a function of particle size, there is a disparity in chemical properties also, thereby resulting in different binding modes of the adsorbate molecules than that observed in the case of corresponding bulk materials. Effectively, for the supported catalysts, the chemisorption properties are generally guided by the electronic interaction between the nano-dispersed metal crystallites and the support matrix. These aspects are immensely important for the semiconductor-assisted photocatalytic processes. The alteration in the particle size in the case of nanocrystalline TiO_2 photocatalysts leads to changes in the transfer and the recombination rate of surface charge carriers (e^- or h^+) are, thereby resulting in improved quantum yields. A considerable work is going on in Chemistry Division, BARC on application of designed nanomaterials in the field of catalysis for various applications such as water splitting for hydrogen generation, volatile organic compounds (VOC) degradation, oxidation of CO and NH_3 etc. Photocatalytic oxidation of the volatile organic compounds, under the ambient conditions by the photocatalysts such as TiO_2 and TiO_2 -dispersed in the host matrix of MCM-41 doped TiO_2 , and TiO_2 dispersed on cloth have been investigated [35-38]. The structure-activity correlation is elucidated, with factors like particle size effect, effect in the change of the band gap, effect of the oxidation state for the effective change in the

photo-oxidation property of the catalysts. The host matrix of MCM-41 was synthesized and the TiO_2 was impregnated in it by the incipient wet impregnation technique, which lead to formation of different particle size of the guest molecules as a function of loading in the host matrix. The oxidation of methanol was studied as a function of different particle size of the TiO_2 nano particles in MCM-41 matrix, it was found that as a function of size the activity decreased for the TiO_2 nano particles. The reaction mechanism for the oxidation of the methanol under these conditions was illustrated by the insitu FT-IR technique, which showed that there were different species produced in the bulk TiO_2 and pristine host MCM-41. In case of TiO_2 dispersed in the MCM-41 there was a combined effect of these two systems (host-guest). There was an increase in the band gap as a function of the vanadium doping in the TiO_2 system. The oxidation of ethylene under ambient conditions was studied, which lead to the conclusion that not only the change in the band gap is required but also the oxidation state of the vanadium also plays a very important role. Higher the amount of the V^{5+} lower is the photocatalytic activity of these catalysts.

Nanomaterials in separation science

Separation processes often make use of one or combination of processes like precipitation, membrane filtration, ion exchange, and adsorption. However, adsorption using simple and cheap adsorbents is gaining lot of importance due to its economic benefits as well as easy availability of different kinds of adsorbents. Hence the research in developing new adsorbents can be focused on the development of simple and economic procedures for the synthesis of the sorbents or on the development of methods for the reusability of these sorbents. Activated high surface area carbon is the "gold standard" in sorbent technology. There are, many other solids that serve as high surface area (high capacity) sorbents. This has become especially the case in recent years when new synthetic methods have allowed nanoscale metal oxides like magnesium oxide (MgO), calcium oxide (CaO), titanium oxide (TiO_2), aluminum oxide (Al_2O_3), iron oxide (Fe_2O_3), and zinc oxide (ZnO) to be prepared. These oxides in high surface area form, and their physical mixtures and intimate (molecular or nanoscale) mixtures have proven to be excellent sorbents for many applications. Toxic species such as heavy metal ions and fluoride ions etc has received much attention. The World Health Organization (WHO) has specified the tolerance limit for fluoride content in drinking water as 1.5 mg L^{-1} . The presence of heavy metals in the environment is a serious

global, social, and environmental problem and every possible care should be taken to keep them isolated from getting mixed into air, water, and soil. Based on its toxicity the US Environmental Protection Agency (EPA) has set the maximum permissible limit for lead ions in drinking water as 0.05mgL^{-1} and the Bureau of Indian Standards as 0.1mg L^{-1} . These limits suggest more stringent requirement for the removal of lead from aqueous environment, which necessitated the development of innovative and cost-effective treatment methods for the effluents containing the ions before discharging into natural water bodies. The use of nanocrystalline compounds as simple adsorbents appeared as a good alternative. Likewise, defluoridation of water is another important societal need. An oxide $\text{Mg}_{0.8}\text{Al}_{0.2}\text{O}_{1.1}$ was prepared by combustion method an average crystallite size of 8 nm. It was found [39] to be an excellent adsorbent for uptake of fluoride anion of up to 120 mg L^{-1} concentration with a uptake capacity of $10\text{ mg F}^{-}/\text{g}$. Nanosize pure and mixed metal oxides like nanocrystalline cobalt ferrite and MnO_2 showed good uptake capacity for lead ion. Titania-silica ($\text{TiO}_2/\text{SiO}_2$) binary mixed oxide was also found to be a good sorbent for lead ions. A novel hybrid adsorbent HMO-001 was fabricated by impregnating nanosized hydrous manganese dioxide (HMO) onto a porous polystyrene cation exchanger resin for enhanced removal of Cd(II) and Zn(II) ions from waters. The nano-hydroxyapatite particles (nHAp) had a sorption capacity of 1.17 mmol/g of Pb

Nanomaterials in DAE

Nanomaterials are being contemplated to play a role in Department of Atomic Energy (DAE) also. The most important application of these materials is in separation and recovery of valuable radio-isotopes from the nuclear waste stream. The preparation of sinter-active thorium based fuels is another prospective application of nanomaterials in DAE. Even targets materials for incorporating minor actinides for their transmutation using Accelerator Driven sub-critical Systems (ADSS) need to be highly sintered. Some of the proposed host lattices, like pyrochlores and zircon etc., are difficult to sinter to near theoretical densities. Here also, soft chemical routes, leading to sinter-active powders, are expected to play an important role. Likewise, carbon based materials in thin films forms are going to be used in Compact High Temperature Reactors (CHTR). Synthesis of Li_2TiO_3 is yet another example where soft-chemical methods are crucial as there is a Li-loss if this compound is prepared by a high temperature ceramic route.

However, in this article I will mainly discuss about the nanomaterials towards radio-nuclides applications. The most important component of the column chromatographic radionuclide generator system is the sorbent matrix. Owing to the difference in their K_d values, the parent and daughter radionuclides have different retention affinity towards the sorbent and can thus be easily separated. A particular sorbent for its application in radionuclide generators should have certain desired properties such as; a) Granularity and free flow characteristics, b) Sorption capacity for the parent radioisotope, c) Selectivity of sorption and elution, d) Radiation and chemical stability of the sorbent. Nanomaterials are expected to provide unprecedented opportunities in developing a new class of sorbents for chromatographic applications due to their unique morphological features. Due to their small dimensions, nanomaterials have extremely large surface area to volume ratio, which makes a large fraction of atoms of the materials to be the surface or interfacial atoms, resulting in more 'surface-dependent' material properties. These surface atoms are unsaturated, exhibit intrinsic surface reactivity and have a tendency to chemisorb charged species in aqueous solution in order to achieve surface stabilization.

$^{99\text{m}}\text{Tc}$ is the work-horse of diagnostic nuclear medicine. The column chromatographic generator using a bed of acidic alumina has emerged the most popular generator system world over. The capacity of alumina for taking up molybdate ions is limited ($2\text{-}20\text{ mg Mo per g}$ of alumina). Thus, an advanced sorbent material is desired that has got high sorption capacity for ^{99}Mo and better elution profile for the $^{99\text{m}}\text{Tc}$. Radiopharmaceuticals Division, BARC, in collaboration with Chemistry Division, has embarked upon development [40-43] of nano-sorbents for generator application. A new sorbent material, polymer embedded nano crystalline titania (Titanium Polymer-TiP) has been developed, from titanium (IV) chloride and isopropyl alcohol, for the adsorption of ^{99}Mo , which is a precursor to $^{99\text{m}}\text{Tc}$, a workhorse in radio-pharmaceuticals. The surface area of this polymer was $30\text{ m}^2/\text{g}$ with an average pore size of 40 nm. The average crystallite size of TiO_2 , embedded in polymer, was found to be 5nm. Potential of this adsorbent for the preparation of ^{99}Mo - $^{99\text{m}}\text{Tc}$ generator has been explored extensively. The feasibility of using nano-zirconia as an effective sorbent for developing a $^{99}\text{Mo}/^{99\text{m}}\text{Tc}$ chromatographic generator was also demonstrated. The structural characteristics of the sorbent matrix were

investigated by different analytical techniques such as XRD, BET surface area analysis, FT-IR and TEM etc. The material synthesized was nanocrystalline, in tetragonal phase with average particle size of ~7 nm and a large surface area of 340 m²/g. The sorption capacity of nano-zirconia is >250 mg Mo/g. Results of the studies indicate that ^{99m}Tc is both strongly and selectively retained by nano-zirconia at acidic pH and ^{99m}Tc could be readily eluted from it, using 0.9% NaCl. ^{99m}Tc could be eluted with >85% yield having acceptable radionuclidic, radiochemical and chemical purity for clinical applications. Nanostructured oxides of Ti and Zr have also been synthesized to evaluate their efficacy as sorbent matrices for the preparation of ¹⁸⁸W/¹⁸⁸Re generator. The performance of these materials, in the context of preparation of ¹⁸⁸W/¹⁸⁸Re generator was compared with respect to the adsorption capacity for ¹⁸⁸W, flow characteristics in the column, purity and quality of ¹⁸⁸Re for radiopharmaceuticals applications. The adsorption capacities of the nanocrystalline oxides of Ti and Zr were >300 mg W/g of the sorbent, which is much more than that of alumina. ¹⁸⁸Re could be eluted with normal (0.9%) saline solution with an elution yield of ~80% with high radionuclidic, radiochemical and chemical purity in an appreciably high radioactive concentration. Nanocrystalline γ -Al₂O₃ was synthesized by a mechanochemical method. It is a promising sorbent for the preparation of ¹⁸⁸W/¹⁸⁸Re generator. It showed significantly higher dynamic sorption capacity compared to the other reported materials. The generator performed consistently well with respect to the purity and elution yield of ¹⁸⁸Re over the period of 6 months.

Nanomaterials in sensor applications

Nanomaterials have shown tremendous potential in sensor applications also. Chemistry Division and Technical Physics Division, BARC are involved in development of sensor for various applications. Some of the specific examples are nanomaterials for sensing H₂S, NH₃, Lindane and various toxic metal ions. The sensing action is usually performed by picking the changes in resistivity or photoluminescence etc. Recently, a new inorganic-organic hybrid assay of Ag nanorod (AgNR)-Rhodamine 6G (R6G) was developed for the sensitive and selective determination of Pb²⁺ ions in aqueous solutions. The sensor could be used in conditions and the fluorescence intensity of the test solution reached maximum within 1 min and the system showed excellent stability at tested concentration of metal ions. This optical sensor showed [44] the lowest detection limit of 50

µg / L of Pb²⁺. Silver nanoparticle based optical assays have been developed that take advantage of the changes in the surface plasmon resonance of nanocrystals due to protein adsorption. Ultra thin films of SnO₂ developed by Langmuir-Blodgett deposition technique has shown ability to sense ammonia gas at room temperature [45,46]. Localised surface plasmon resonance based detection of model protein, bovine serum albumin (BSA) have been demonstrated using silver nanoparticle thin films prepared by LB technique. A significant change in peak position as well as the absorbance could be observed when these silver nanoparticles thin films were treated with BSA [47]. For quick, on site monitoring of biomolecules or environmental pollutants hand held biosensors based on electrical measurements would be preferred. Binding of specific target molecules to the immobilized probe molecules inside the pores can cause a measurable change in capacitance due to the change in the dielectric constant and thickness. The standardized protocols required for the fabrication and characterization of porous silicon based capacitive immunosensor that gives higher sensitivity compared to sensors fabricated on polished silicon for the same die area were reported recently [48]. Several semiconducting oxides such as SnO₂, CuO, WO₃, ZnO, In₂O₃ in nanocrystalline form are being used [49-51] as potential gas sensors based on the principle of their reversible change in electrical conductance (resistance) on exposure to redox gases. ZnO nanoparticles and nanowires showed selective and sensitive response to ppm level of H₂S gas, while CuO showed response to even sub-ppm level of the gas. In₂O₃ single crystal whiskers prepared by carbo-thermal method could sense 200 ppb of H₂S gas at room temperature. Te thin films are sensitive to both NH₃ and H₂S gases because of the native oxide layer on top. 1-D nanostructures of Te are sensitive to chlorine gases.

Conclusions

An attempt was made in this article to touch upon chemistry aspects and applications of various nanomaterials. However, this subject is too vast to be covered in a rather short article, which is not exhaustive due to space constraints. There are dedicated books [52, 53] for the chemistry aspects of nanomaterials. However, I am sure that from the foregoing one can easily get a flavor of this rapidly growing field of nanomaterials.

Acknowledgements

I acknowledge all the colleagues, students and collaborators (within and outside Chemistry Division, BARC)

who have contributed to the research on nanomaterials reported in this article. In particular I would like to place on records our collaboration with Dr. A. Dash of RPhD, BARC. I also wish to thank Dr. D. Das, Head, Chemistry Division, BARC and Dr. T. Mukherjee, Director, Chemistry Group, BARC for their keen interest in and support to this work.

References

1. A.A. Khaleel, Chem. Eur. J. 10 (2004) 925.
2. Q. Tang, Q. Zhang, P. Wang, Y. Wang and H. Wan, Chem. Mater. 16 (2004) 1967.
3. A. Murali, A. Barve, V.J. Leppert and S.H. Risbud, Nano Lett. 1 (2001) 287.
4. A. K. Tyagi, R. D. Purohit, S. V. Chavan and V. Bedekar, Encyclopedia of Nanoscience & Nanotechnology (ASP) (In Press), Ed. H. S. Nalwa.
5. J. D. Mackenzie, E. P. Bescher, Acc. Chem. Res. 40 (2007) 810.
6. Sriparna Chatterjee, O. D. Jayakumar, A. K Tyagi and Pushan Ayyub, J. Crystal Growth 312 (2010) 2714.
7. Dimple P. Dutta, J. Manjanna and A. K. Tyagi, J. Apply Phys. 106 (2009) 043915
8. Dimple P. Dutta, R. Ghildiyal and A. K. Tyagi, J. Phys. Chem. C 113 (2009) 16954
9. G. Yaswant, C. L. Prajapat, M. R. Singh, S. K. Gupta, G. Ravikumar, O. D. Jayakumar and A. K. Tyagi, Physica C 468 (2008) 944.
10. Ram Seshadri and C. N. R. Rao, Mater. Res. Bull. 29 (1994) 795.
11. Shalini Singh, M. C. Rath, A. K. Singh, T. Mukherjee, O. D. Jayakumar, A. K. Tyagi and S. K. Sarkar, Rad. Phys. Chem. 80 (2011) 736.
12. B. J. de Gans, P. C. Duineveld and U. S. Schubert, Adv. Mater. 16 (2004) 203.
13. C. M. Hong and S. Wagner, IEEE Electron Device Lett. 21 (2000) 384.
14. A. C. Small, J. H. Johnston and N. Clark, Eur. J. Inorg. Chem. 2 (2010) 242.
15. O. D. Jayakumar, A. K. Tyagi J. Mater. Chem. (2011) DOI: 10.1039/C1JM10836K.
16. V. Bansal, P. Poddar, A. Ahmad, M. Sastry, J. Am. Chem. Soc. 128 (2006) 11958.
17. P. Mukherjee, M. Roy, B. P. Mandal, G. K. Dey, P. K. Mukherjee, J. Ghatak, A. K. Tyagi, S. P. Kale, Nanotechnology 19 (2008) 075103
18. S. S. Shankar, A. Rai, B. Ankamwar, A. Singh, A. Ahmad, M. Sastry, Nat. Mater. 3 (2004) 482.
19. P. Yong, N. A. Rowson, J. P. G. Farr, I. R. Harris, L. E. Macaskie, Biotechnology, and Bioengineering 80 (2002) 369.
20. R. Wahl, M. Mertig, J. Raff, S. S. obell, W. Pompe, Adv. Mater. 13 (2001) 736.
21. A. Dutta, S. Patra, Vinila Bedekar, A.K. Tyagi and R. N. Basu, J. Nanosci & Nanotech. 9 (2009) 3075
22. Sathi R. Nair, R. D. Purohit, A. K. Tyagi, P. K. Sinha and B. P. Sharma, Mater Res. Bull. 43 (2008) 1573.
23. Sathi Nair, R. D. Purohit, A. K. Tyagi, P. K. Sinha and B. P. Sharma, J. Am. Ceram. Soc. 91 (2008) 88.
24. B. P. Mandal, S.K. Deshpande and A.K. Tyagi, J. Mater. Res. 23 (2008) 911.
25. B. P. Mandal, R. Shukla, S. N. Achary, A. K. Tyagi, Inorg. Chem. 49 (2010) 10415.
26. R. Shukla, A. Arya and A. K. Tyagi, Inorg. Chem. 49 (2010) 1152.
27. R. Shukla, J. Manjanna, A. K. Bera, S. M. Yusuf and A. K. Tyagi, Inorg. Chem. 48 (2009) 11691.
28. R. Shukla, A. Bera, S. M. Yusuf, S. K. Deshpande, A. K. Tyagi, W. Hermes, M. Eul, R. Pöttgen, J. Phys. Chem. C 113 (2009) 12663.
29. S. N. Achary, S. K. Sali, N. K. Kulkarni, P. S. R. Krishna, A. B. Shinde and A. K. Tyagi, Chem. Mater. 21 (2009) 125.
30. C. Pichot, Curr. Opin. Colloid Interface Sci. 9 (2004) 213.
31. T. Karir, P. A. Hassan, S. K. Kulshreshtha, G. Samuel, N. Sivaprasad, M. Ventakesh, Anal. Chem. 78 (2006) 3577.
32. A. J. Haes, W. P. Hall, L. Chang, W. L. Klein and R. P. Van Duyne, Nano Lett., 4 (2004) 1029.
33. O. D. Jayakumar, R. Ganguli, A. K. Tyagi, D. K. Chandrasekharan, C. K. K. Nair, J. Nanosci & Nanotech 9 (2009) 6344.
34. R Ghosh, L. Pradhan, Y. P. Devi, S. S. Meena, R. Tewari, A. Kumar, S. Sharma, N. S. Gajbhiye, R. K. Vatsa, Badri N. Pandey, R. S. Ningthoujam, J. Mater. Chem. (2011) DOI: 10.1039/c1jm10092k
35. S. Chatterjee, K. Bhattacharyya, P. Ayyub and A. K. Tyagi, J. Phys. Chem. C 114 (2010) 9424.
36. K. Bhattacharyya, S. Varma, A. K. Tripathi and A. K. Tyagi, J. Mater. Res. 25 (2010) 125.
37. K. Bhattacharyya, S. Varma, A. K. Tripathi, S. R. Bharadwaj and A. K. Tyagi, J. Phys. Chem. B 113 (2009) 5917.
38. K. Bhattacharyya, S. Varma, A. K. Tripathi, S. R. Bharadwaj and A. K. Tyagi, J. Phys. Chem. C 112 (2008) 19102.
39. R. Shukla, Jayshree Ramkumar and A. K. Tyagi, Int. J. Nanotechnology 7 (2010) 989.
40. R. Chakravarty, R. Shukla, S. Gandhi, R. Ram, A. Dash, M. Venkatesh, A. K. Tyagi, J. Nanosci. Nanotech. 8 (2008) 4447.
41. R. Chakravarty, R. Shukla, R. Ram, M. Venkatesh, A. Dash and A. K. Tyagi, ACS App. Mater. Interfaces, 2 (2010) 2069.
42. R. Chakravarty, R. Shukla, A. K. Tyagi, A. Dash and M. Venkatesh, App. Rad. Isot. 68 (2010) 229
43. R. Chakravarty, R. Shukla, R. Ram, M. Venkatesh, A. K. Tyagi and A. Dash, Anal. Chem. (2011) DOI: 10.1021/ac201232m.
44. A. K. Tyagi, J. Ramakumar and O. D. Jayakumar (Unpublished).

45. Sipra Choudhury, C.A. Betty, K.G. Girija and S.K. Kulshreshtha, *Applied Physics Letters*, 89 (2006) 071914
46. Sipra Choudhury, C.A. Betty, K.G. Girija, *Thin solid Films*, 517 (2008) 923.
47. G. Verma, S. Choudhury, P. A. Hassan, *AIP Conf. Proc.* 1313 (2010) 352.
48. C. A. Betty, R. Lal, J. V. Yakhmi, and S. K. Kulshreshtha, *Biosensors & Bioelectronics*, 22 (2007) 1027.
49. N. S. Ramgir, M. Ghosh, P. Veerender, N. Datta, M. Kaur, D. K. Aswal, S. K. Gupta, *Sensors and Actuators, B: Chemical* 156 (2011) 875.
50. M. Kaur, N. Jain, K. Sharma, S. Bhattacharya, M. Roy, A. K. Tyagi, S. K. Gupta, J. V. Yakhmi, *Sensors and Actuators, B: Chemical* 133 (2008) 456.
51. S. Sen, M. Sharma, V. Kumar, K. P. Muthe, P. V. Satyam, U. M. Bhatta, M. Roy, N. K. Gaur, S. K. Gupta, J. V. Yakhmi, *Talanta* 77 (2009) 1567.
52. C. N. R. Rao, P. J. Thomas and G. U. Kulkarni, *Nanocrystals: Synthesis, Properties and Applications*; Springer-Verlag, Berlin (2007).
53. C. N. R. Rao, A. Muller and A. K. Cheetham, *Recent Advances in the Chemistry of Nanomaterials*, Wiley-VCH Verlag GmbH & Co. (2004).



Dr. A. K. Tyagi is presently Head, Solid State Chemistry Section, Chemistry Division, Bhabha Atomic Research Centre (BARC), Mumbai and also a Professor (Chemistry) at Homi Bhabha National Institute (HBNI). He joined BARC, Mumbai in 1986 through BARC-Training School. Since then he has been working in the field of Chemistry of nanomaterials, functional materials and nuclear materials. He was a Max-Planck Fellow at MPI, Stuttgart, Germany during 1995-96. In recognition of his work, Dr. Tyagi has been conferred with several prestigious awards such as Homi Bhabha Science & Technology Award, Gold Medal of Indian Nuclear Society, MRSI Medal, CRSI Medal, Dr. Laxmi Award by ISCAS, Rheometric Scientific-ITAS Award, and IANCAS-Dr. Tarun Datta Memorial Award, Rajib Goyal Prize and DAE-SRC Outstanding Researcher Award. He is a Fellow of Royal Society of Chemistry, UK (FRSC), National Academy of Sciences, India (FNASc) and Maharashtra Academy of Sciences (FMASc).

Evaporation Induced Self Assembly of Nanoparticles by Spray Drying

D. Sen^{1*}, J. Bahadur¹, S. Mazumder¹, J.S. Melo², S.F. D' Souza²

¹Solid State Physics Division, ²Nuclear Agriculture and Bio-technology Division

Bhabha Atomic Research Centre, Mumbai-400085, India

*Corresponding author; e-mail: debasis@barc.gov.in

Abstract

Nanoparticles confined in drying droplets of less than a picoliter are forced to organize in sub-micrometric grains by capillary forces that arise due to solvent evaporation. To realize such evaporation induced self assembly, spray drying method has been utilized. Morphology of the assembled grains and inter-particle correlation of the assembled nanoparticles are significantly influenced by various physico-chemical conditions and interparticle interaction. Small-angle scattering in combination with electron microscopy can provide detail information about the mesoscopic structure of the grains and the hierarchical arrangement of the jammed nanoparticles in the grains. Such assembled grains can also be considered for various technological applications. Here we have described some of our recent results on synthesis and characterization of such assembled grains giving special emphasis on the effects of slower and faster drying on structure of the grains.

Keywords: self assembly, alumina and silica nanoparticles, spray drying, SANS study

Introduction

Spray drying is regarded as an indispensable industrial process [1] since long time because it has been widely used in various industries such as, food, pharmaceutical, ceramic, polymer, chemical and several other industries to obtain dry particles from solution phase. Recently, this method has embellished [2-9] itself in nano-science and nano-technology with an aim to realize evaporation induced self-assembly (EISA) of nanoparticles at various physicochemical and thermo-dynamical conditions apart from synthesizing various novel nano-composites, colloidal crystals, mesoporous materials, microcapsules etc..

In the spray drying process, liquid droplets are passed through a hot chamber where they get dried. During such drying process of micrometric colloidal droplets, shrinkage in droplet size and arrangement of nanoparticles inside a droplet is primarily driven by evaporation. The constituent particles get assembled by capillary forces that come into play because of the presence of wetting liquid between solid particles. At the end of the process, dried assembled grains are obtained.

At this juncture, it is worthy to mention that the morphology of the assembled grains and the internal arrangement of the nanoparticles in the grains depend strongly on: (i) the physico-chemical parameters of the

initial nanoparticle dispersion such as, concentration, size of nanoparticles and their interaction, viscosity, surface tension etc. and (ii) on the parameters related to drying such as, drying temperature and time, droplet size etc. It has been shown [5,8,9] that when the rate of drying is slow enough, a droplet containing stable dispersion of colloidal nanoparticles, shrinks in an isotropic fashion and the final assembled grains are spherical. Further, for such a situation, the final arrangements of the nanoparticles inside an assembled grain, corresponds to a packing due to random jamming of the constituent particles. If the constituent nanoparticles are spherical, in an ideal random jamming situation, the volume fraction of the particles in the grains corresponds to ~ 0.64 and the correlation may be considered as of hard sphere type. However, if the drying process is fast enough, depending on other physical parameters, various non-spherical morphologies of the dried grains, such as, doughnut, mushroom etc., are observed [6,7]. In a few cases, even crumpled and fractured grains have also been observed. It is to be mentioned that the origin of such complex morphological transition during EISA is not fully understood yet.

The fastness of a drying process is expressed quantitatively by Peclet number (P_e), a dimensionless number, which is represented by the ratio of τ_{mix} to τ_{dry} where τ_{mix} is the time of mixing, i.e., the average time taken

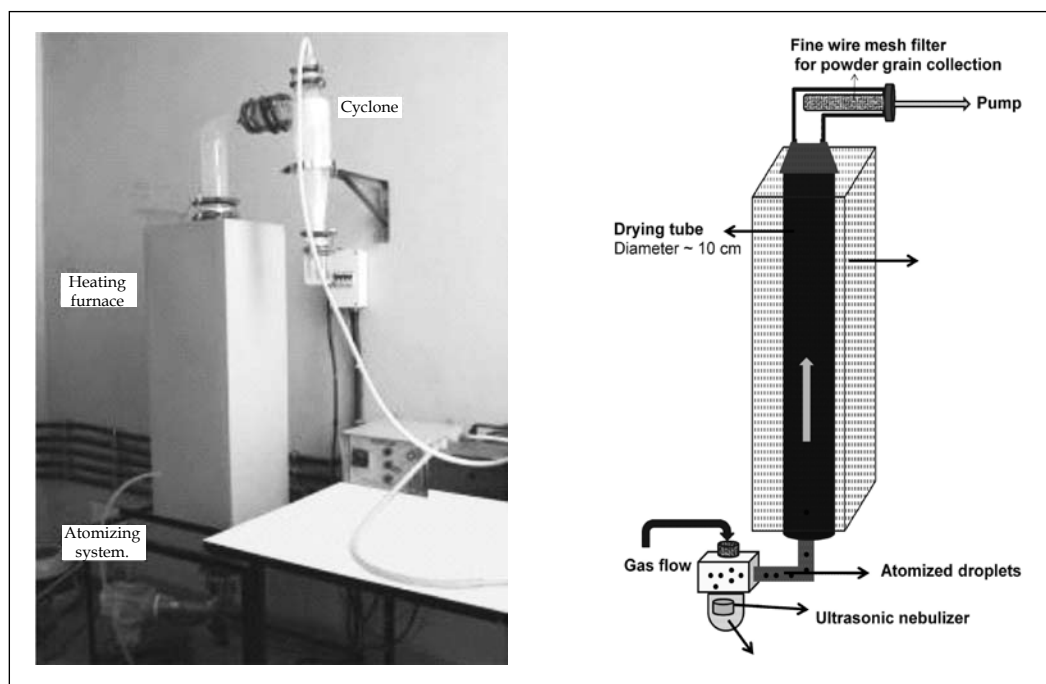


Fig. 1: (a) The spray dryer for slow drying rate developed at BARC. (b) Schematic diagram of the spray dryer.

by the colloidal particles to reach to the droplet centre from the boundary while performing Brownian motion and τ_{dry} is the drying time of the droplets. In fact, τ_{mix} can be estimated from the equation $\tau_{\text{mix}} = R_{\text{drop}}^2 / D$, where R_{drop} represents the radius of a droplet and D is the diffusion coefficient of the nanoparticles in the droplet. If $P_e \gg 1$, the drying process is regarded as a fast one and the formation of hollow grains or even morphological transformation of droplets may happen in such a case. A slow drying regime corresponds to a situation where $P_e \ll 1$ and in this case the drying process is isotropic as mentioned above.

In this article, we will describe how spray drying can be utilized to tailor the morphology of self assembled grains in micrometric length scale and the inter-particle correlation between the nanoparticles in the assembled grains.

Experimental

Spray drying

For spray drying experiments with slower drying rate, i.e., for $P_e \ll 1$, a simple spray dryer (SPD-1) has been developed [10] at BARC, Mumbai. It consists (Fig. 1) of three main stages: (i) droplet generator (either by multi-jet compressed air nebulizer or ultrasonic nebulizer), (ii) droplet dryer and (iii) dried particle collector (either by

wire mesh collector or cyclone separator). For faster drying case where $P_e \gg 1$, we have employed commercial spray dryer LU 220 and LU 228 from LABULTIMA, Mumbai. The residence time of the droplet in the drying chamber can be found from the geometry of the drying chamber and the flow rate of the carrier gas. The typical residence time of the droplet in the chamber in case of slow drying has been 7-10 sec. while that for the fast drying case remains as fraction of a second.

SANS and SEM

To characterize the mesoscopic structure of the assembled grains, small-angle neutron scattering (SANS) and scanning electron microscopy (SEM) have been used. For scattering measurements, SANS facilities [11, 12] at GT laboratory, Dhruva are used.

Results and discussion

On slow drying

When the rate of drying is slow enough, a droplet containing stable dispersion of colloidal nanoparticles, shrinks in an isotropic manner and in such a situation the final arrangements of the nanoparticles inside an assembled grain, corresponds to a packing due to random jamming of the constituent particles. However, such packing of

the constituent particles inside assembled grains can be modified by altering the physicochemical parameters of the self-assembly process. By doing so, one can also alter the available interfacial area inside the assembled grains, which may be an important parameter in any catalytic applications. The present study aimed at modification of internal structure [8] in such assembled grains by addition of electrolyte in the initial colloidal dispersion and thus by altering the jamming mechanism. Colloidal silica dispersion of 5% in weight was prepared from initial 40% colloidal silica dispersion (~10 nm) (Visa Chemical, Mumbai, India) by dilution with pure water (Milli-Q, Millipore). Sodium Chloride (NaCl) was added to the diluted silica dispersion. It was found that for NaCl concentration beyond 1.5 %, the dispersion became unstable and got phase separated. Thus, in our case the concentration of NaCl in the silica dispersion was kept below 1.5 wt % where there has been no phase separation. Silica dispersions (5%) with varying NaCl concentration have been prepared for further spray drying purpose. The feed was kept at ~ 50 ml/hr. The temperature of the oven was kept at 160 °C. The aspiration value was kept at 40 liter per minute. The dried micrometric/sub-micrometric powders ($P_{0.0}$, $P_{0.1}$, $P_{0.2}$, $P_{0.5}$, and $P_{1.0}$ for 0.0, 0.1, 0.2, 0.5 and 1.0 wt % NaCl, respectively) were collected at the end of the drying chamber using a wire mesh (400 mesh) filter. The collection efficiency was found to be nearly 50%. SEM micrograph of the grains for the samples $P_{0.0}$, $P_{0.5}$ and $P_{1.0}$ are shown in the Fig. 2. It is seen from the figure that the grains are spherical in shape. For highest electrolyte concentration few buckled particles are also seen.

SEM gives the external morphology of the grains and SANS can throw light about the correlation of the nanoparticles inside the grains. SANS data are plotted, in double logarithmic scale in Fig. 3 (a). It is evident from the figure that the profiles get modified significantly with addition of electrolyte. Particularly, the functionality of the profiles in the intermediate q region (~0.05 to 0.5 nm^{-1}) that primarily bears the signature of the correlation of the silica particles in the grain gets altered in a significant way. Scattering data have been analyzed in terms of two level structural model [8]. The differential scattering cross section per unit of solid volume may be given by

$$I(q) = \frac{(\phi_s \Delta \rho_s^2 I_s(q) + v_g \Delta \rho_g^2 P_g(q))}{\phi_s} \quad (1)$$

where ϕ_s is the volume fraction of silica nanoparticles in a grain of volume v_g . If ρ_s is the scattering length density

of silica, then $\Delta \rho_s = \rho_s - \rho_{\text{int}}$ (ρ_{int} being the scattering length density of interstices between silica nanoparticles). As interstices between silica nanoparticles is void (when electrolyte is removed), $\rho_{\text{int}} = 0$ and hence $\Delta \rho_s$ can be taken equal to ρ_s . $\Delta \rho_g^2$ represents the average scattering contrast of the grains hence $\Delta \rho_g = \phi_s \Delta \rho_s + \Delta \rho_{\text{int}}$. As the medium in which the grains are embedded and the medium of the interstices are both void/air in this case, $\Delta \rho_{\text{int}} = 0$ and thus $\Delta \rho_g = \phi_s \Delta \rho_s$. Here, $P_g(q)$ is the normalized form factor of the grains.

$$P_g(q) = \frac{\int_0^\infty f_g^2(q, r) v_g^2(r) D_g(r) dr}{\int_0^\infty D_g(r) dr} \quad (2)$$

where $f_g^2(q, R_{\text{grain}})$ represents the form factor of the grains of radius R_{grain} and is represented by

$$f_g(q, R_{\text{grain}}) = 3 \frac{[\sin(qR_{\text{grain}}) - qr \cos(qR_{\text{grain}})]}{(qR_{\text{grain}})^3} \quad (3)$$

$D_g(r)$ represents the size distribution of the assembled grains and is assumed as a lognormal distribution.

$$D_g(R) = \frac{1}{\sqrt{2\pi\sigma_g^2 R^2}} \exp\left[-\frac{[\ln(R/R_0^{\text{grain}})]^2}{2\sigma_g^2}\right] \quad (4)$$

The first term in the numerator of the equation -1 corresponds to the scattering from the colloidal particles in the grains. When the colloidal particles have a distribution in their size, then $I_s(q)$ may be represented as following under local monodisperse approximation.

$$I_s(q) = \frac{\int_0^\infty P_s(q, r_{\text{nano}}) D_s(r_{\text{nano}}) v^2(r_{\text{nano}}) S(q, r_{\text{nano}}) dr_{\text{nano}}}{\int_0^\infty v(r_{\text{nano}}) D_s(r_{\text{nano}}) dr_{\text{nano}}} \quad (5)$$

$S(q, r_{\text{nano}})$ is the inter-particle structure factor. $D_s(r_{\text{nano}})$ represents the size distribution of the nanoparticles. $P_s(q, r_{\text{nano}})$ represents the normalized form factor of nanoparticles with radius r_{nano} .

Analysis of scattering data [8] indicates that a sticky hard sphere type correlation, in case of silica alone, gets modified to a fractal like correlation when electrolyte is added prior to drying. The fit of the model to the data are shown in Fig. 3(b).

Experiments were also carried out [9] by varying the initial concentration (20%, 10%, 5% and 2.5%) of silica

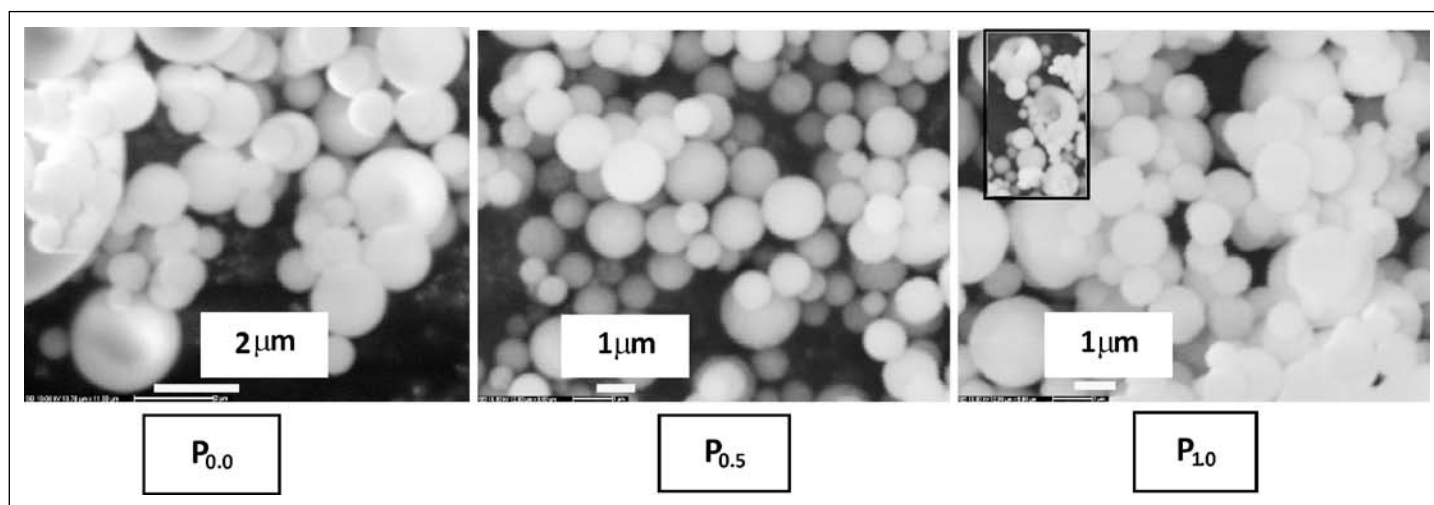


Fig. 2: The spherical spray dried grains of assembled silica nanoparticles are shown. For highest electrolyte concentration few buckled particles are also seen.

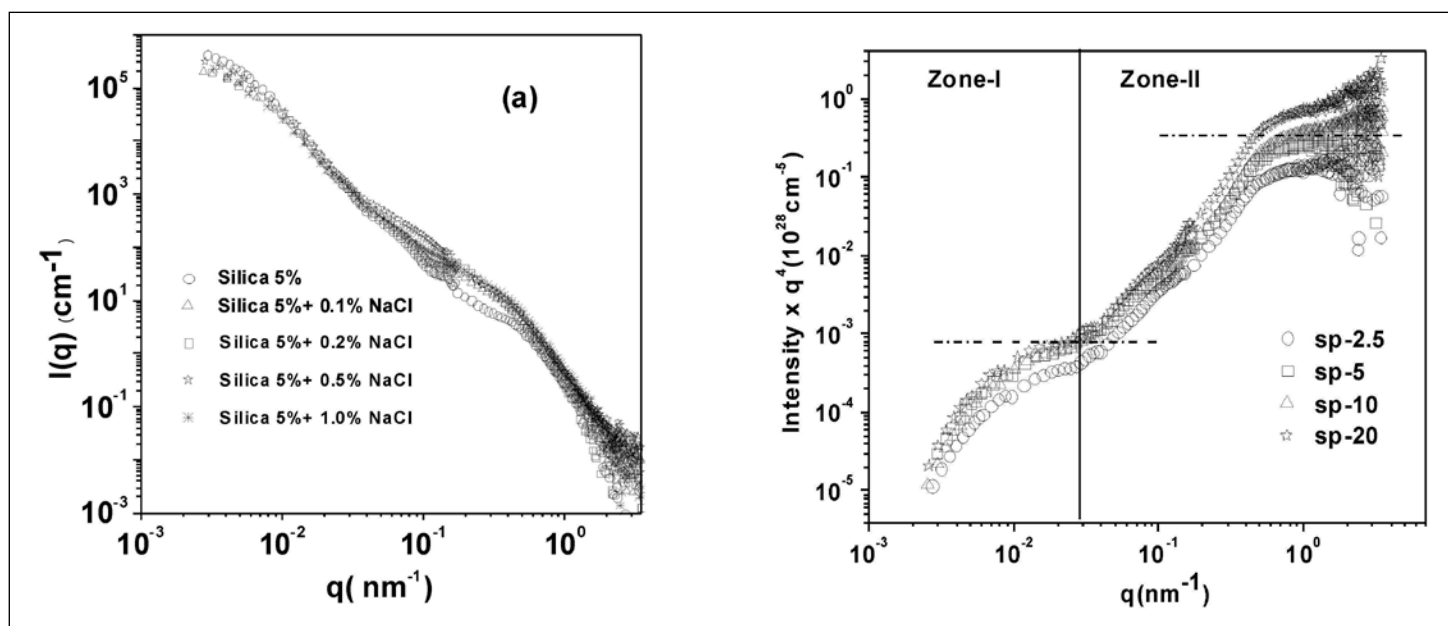


Fig. 3: (a) SANS profiles of the self-assembled samples are shown in double logarithmic scale. The presence of two length scales (individual nanoparticles) in this system is evident from the profiles. The profiles get modified, mainly in intermediate and high q regimes, with addition of electrolytes. (b). Solid line shows the fit of the model to the scattering data. The profiles are shifted vertically for clarity.

nanoparticles in the virgin dispersion prior to spray drying. For all the cases the grains remained spherical in shape. However, SANS (Fig. 4a) and Dynamic Light Scattering (Fig. 4b) (DLS) indicate that variation in grain size and the arrangement of the nanoparticles inside the grains with varying silica concentration in initial dispersion.

It has been found that average packing fraction of the nanoparticles in the grains reduces with increasing

concentration. Two distinct zones (Zone-1 and Zone-2) are visible from the SANS data. Zone-1 corresponds to the scattering signal due to overall grain while Zone-2 corresponds to the scattering from individual nanoparticles in the grains. Detail analysis of SANS data suggests that the packing of the nanoparticles, inside the assembled grains, is not uniform at higher colloidal concentration. For this case, a gradient in particle packing at higher concentration

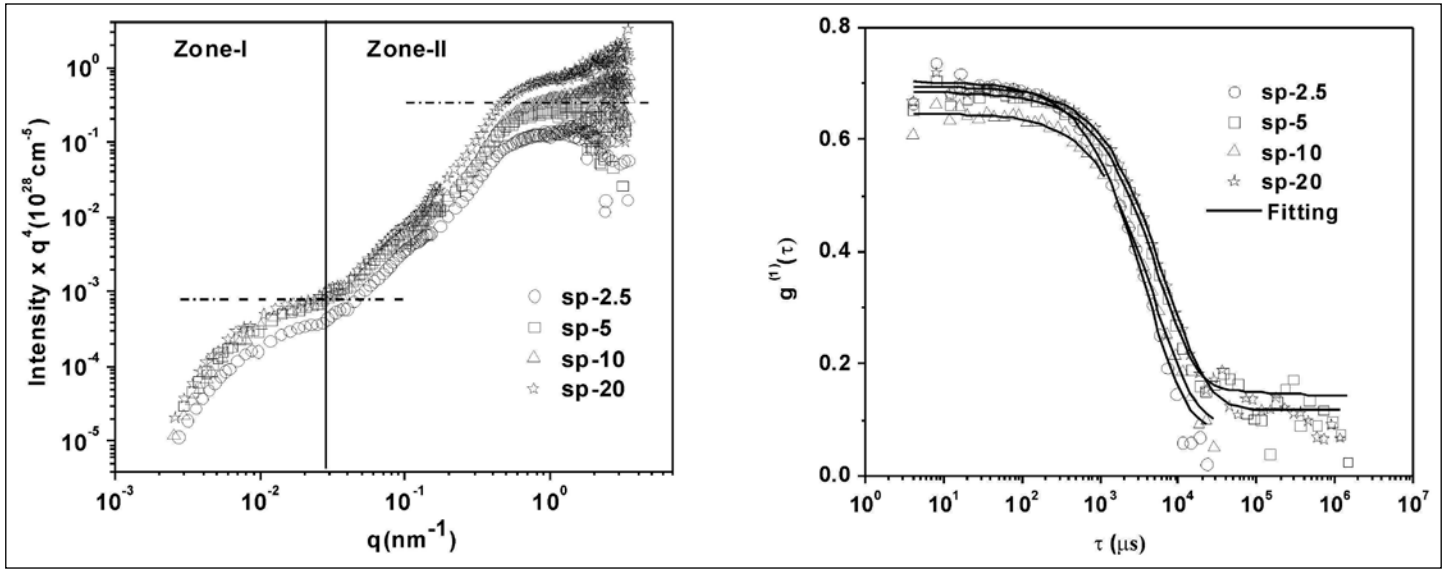


Fig. 4: (a) SANS profiles (in Porod representation) for the spray dried grains synthesized from dispersions with different silica volume fraction. (b) Dynamic light scattering data from the grains

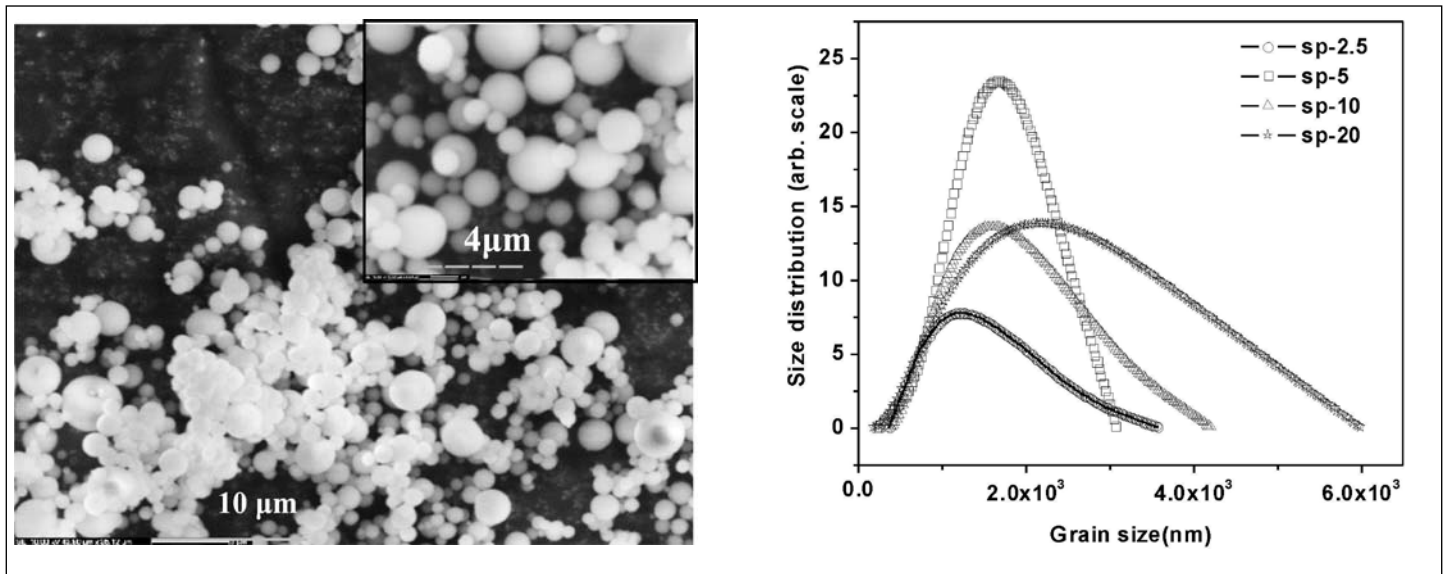


Fig.5: (a) SEM micrograph of spray dried grains for silica 2.5 % dispersion. (b) Size distribution of the grains as obtained from the dynamic light scattering data.

of silica is a possibility. in. Typical grain morphology for 2.5% dispersion is shown in Fig. 5(a). The variation in grain sizes with silica concentration, as obtained from DLS, is depicted in Fig 5(b).

On fast drying

As it is already mentioned earlier that when effective drying rate is fast enough i.e., $P_e \gg 1$, there exists a

possibility of morphological transformation during EISA. In such a situation, a spherical colloidal droplet while drying becomes initially viscous and a shell of nanoparticles forms due to capillary force at the air water interface. Eventually, such shell becomes elastic in nature and acts as a porous membrane through which water is transported out. If the stabilization forces between the nanoparticles overcome the attractive capillary force,

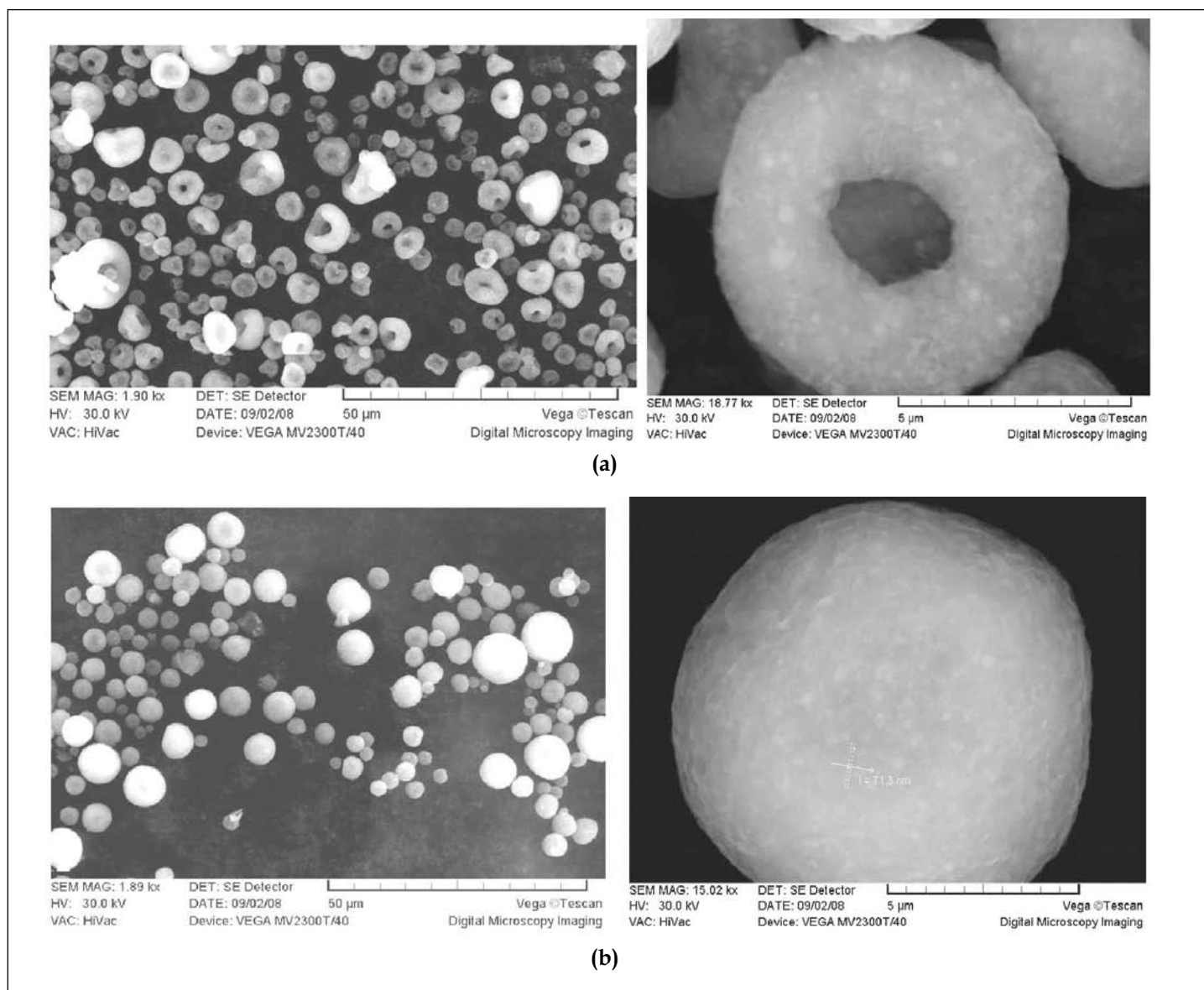


Fig.6: (a) SEM micrograph of doughnut like spray dried alumina colloids (2%). (b) SEM micrograph of spherical spray dried alumina colloids (5%).

then the nanoparticles can rearrange themselves in such a way that an overall shrinkage in the droplet volume occurs. However, if the stabilization force is not strong enough compared to the attractive capillary force, the rearrangement between the particles cannot occur and the overall size of the droplet cannot decrease after a certain time. In such a situation because of pressure difference across the shell, the droplet buckles. Of course, such buckling depends on the shell thickness and the effective elastic modulus of the shell.

Using spray dryers LU220 and LU228, LABULTIMA, we have performed several investigations related to the effect of various physico-chemical conditions on buckling. It has been found [6] that sphere to doughnut like morphological transformation occurs when the concentration of nanoparticles in the virgin dispersion is less but such transformation is hindered at higher nanoparticle concentration.

It is worthy to mention that spray drying technique can be used very efficiently in fast synthesis of porous grains by use of proper template materials and removal of such

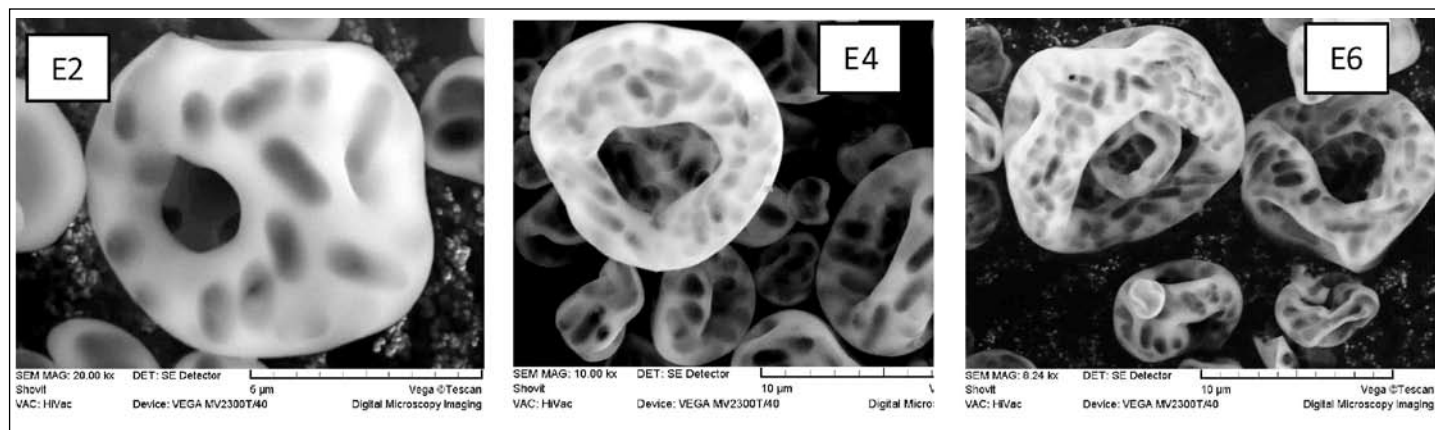


Fig. 7: *E. coli* templated porous grains of assembled silica nanoparticles for three different ratios of silica to *E. coli*. The ratio increases from left to right. Individual nanoparticles are not seen from SEM micrographs due to resolution constraints. However, their presence is evident from SANS profile.

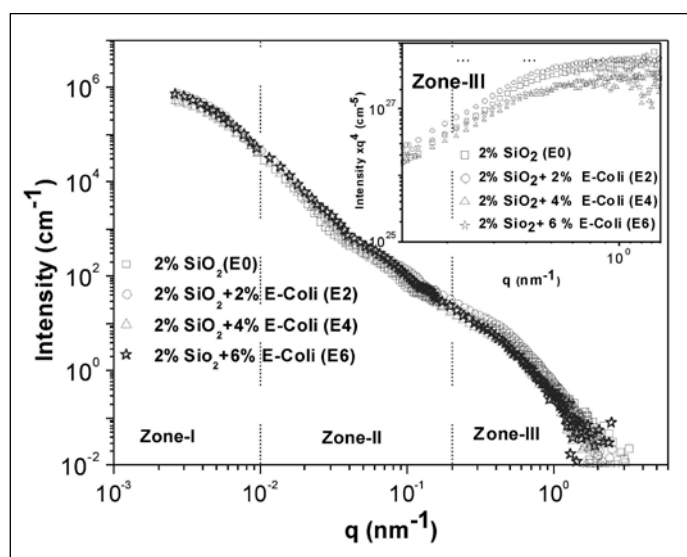


Fig. 8: SANS profiles from the *E. coli* templated porous grains of assembled silica grains.

template materials after EISA. We have used [7] *E. coli* bacteria as template for two reasons, firstly to see the effect of soft material particles on the morphological transformation and buckling phenomenon during EISA and secondly to synthesize porous grains of nanoparticle assembly with cylindrical pores. It is worthy to mention that column of such porous grains has found [13] potential applications in water purification from *E. coli* contaminated water. Such *E. coli* templated porous grains consisting of silica nanoparticles are shown in Fig. 7. In the virgin suspension before drying the amount of silica nanoparticles was 2wt % and the amount wet *E. coli* was varied as 2, 4 and 6 wt %. From the SEM micrographs, individual nanoparticles are

not visible because of resolution constraint. However, their presence is evident from the Zone-III of the SANS profiles as shown in Fig. 8. Zone-I corresponds to the scattering from overall grains and Zone-II primarily bears the signature of the scattering from the pores as templated by *E. coli*. The specific surface area of the grains were estimated from the Porod level of SANS data and were found to be 40, 20 and 18 m²/gm for E2, E4 and E6 samples. It has recently been found that such morphological deformation [7] and buckling [14] can be arrested [15] by proper tuning of surface charge and other physico-chemical conditions.

It is observed from the SEM micrographs that the buckling becomes more vigorous as *E. coli* fraction is increased. From the observations it seems that the size, shape and elastic modulus of the assembling particles in the droplets are important factors as far as these buckling deformations are concerned. As the Peclet number is more for bigger particles, the deformation, during buckling, is more when *E. coli* is present. Further, it is much softer (Longitudinal Young's modulus ~25 Mpa and circumferential Young's modulus ~75 MPa density ~1.1 gm/cm³) than silica (~75000 MPa, density ~2.5 gm/cm³). Thus the incorporation of the bacterial component results in decrease in the elastic constants vis-à-vis the enhancement of the buckling probability of the formed shell of the jammed particles at the boundary of the drying droplets. This facilitates in relatively easier buckling. Further, the non spherical shape of the particles (as in the present case for *E. coli*), causes somewhat anisotropic variation of the capillary forces at different zones of the grains, which gives rise to multi invagination zone on the surface of the droplet. This enhances the deformation during buckling and the grains

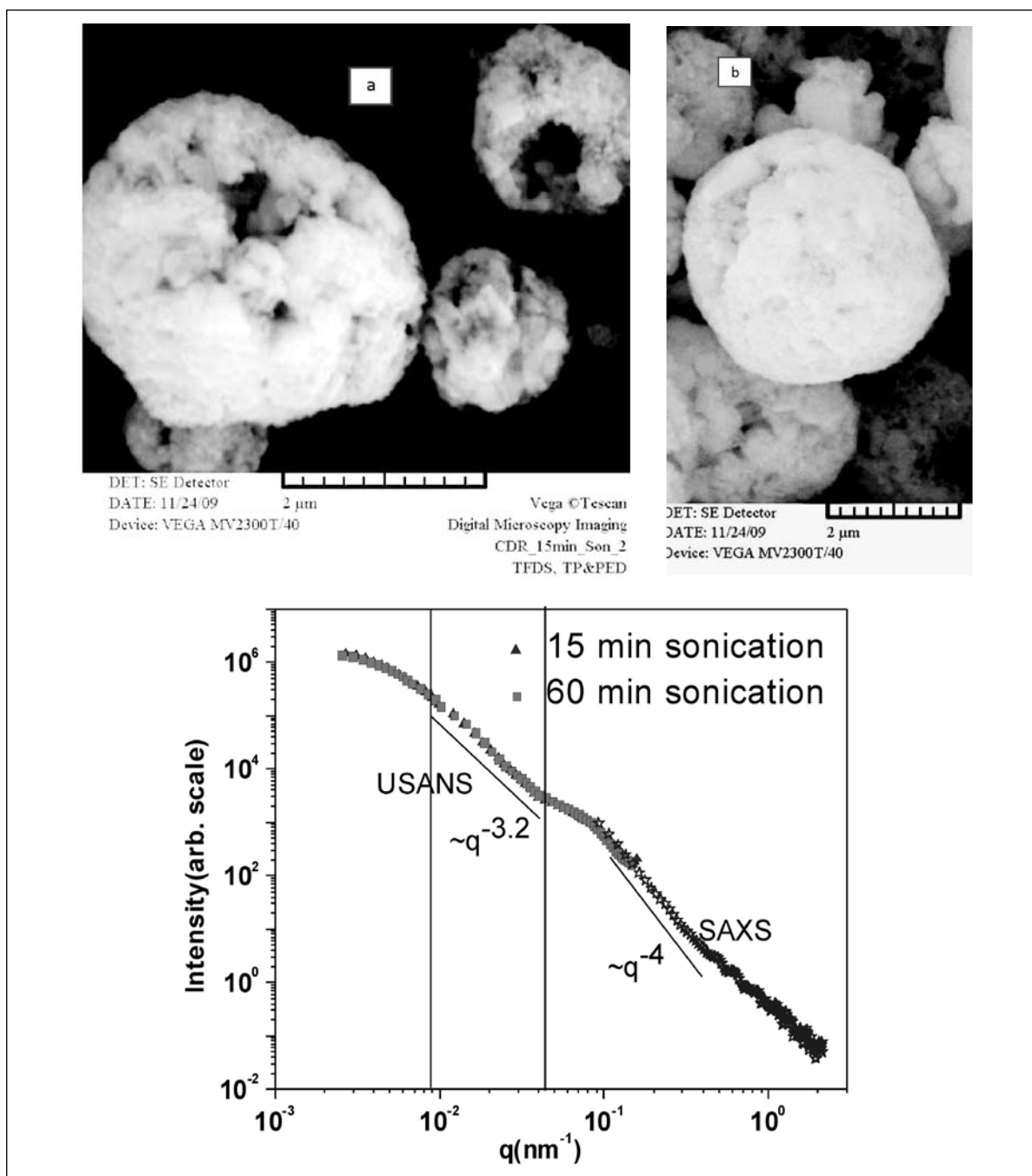


Figure 9: (a) SEM micrographs of the spray dried ceria grains (15 min. sonication). (b) 60 min. sonication Pores are evident from the micrograph. Individual nanoparticles are not visible due to resolution constraint. (c) SANS profiles for the grains. No significant change with sonication time is observed as far as small-angle scattering data are concerned.

with dimpled multi-faced deformed doughnut shape are realized (Fig. 7). From the SEM micrographs it is quite evident that the deformation gets amplified with increase in the volume fraction of the E. coli in the droplets.

Ceria is one of the most important catalytic materials that can play multiple roles owing to its ability to release and uptake oxygen under catalytic reaction conditions and thus has potential for the treatment of emissions from

automobiles. In this connection, synthesis of meso/macro porous ceria grains attracts a great deal of attention. Aqueous dispersion of ceria nanoparticles (M/S. Cottor industries, Mumbai) was sonicated for 15 min. and 60 min. prior to the spray drying. The porous nature of the powder grains is evident from the SEM images (Fig. 9). The mesoscopic structure of the assembled grains and the interaction of the ceria nanoparticles within the grains were probed by small-angle scattering. Normally, template materials are used to template pores in such grains. However, the synthesized grains, in the present, case are highly porous in nature without any addition of templates. This is attributed to the fact that agglomerates of nanoparticles get locked suddenly during the fast drying process. It is needless to mention that such pores effectively increase the available surface area for any catalytic reaction. Unlike, the spray drying of a stable dispersion as mentioned earlier, the colloidal droplets in the present situation do not shrink in an isotropic fashion and the interlocking of various agglomerates within a droplet gives rise to such pores. A slope of -3.2 of the scattering profiles in log-log scale supports the agglomerate nature within the grains. Multi level structure of the grains is evident from the profiles.

Conclusions

It has been demonstrated that evaporation induced self assembly of nanoparticles can be realized by spray drying. Spherical grains of assembled nanoparticles are realized because of isotropic compression of the spray droplets during drying. By varying physico-chemical conditions, it is possible to synthesize assembled grains with non-spherical shapes like doughnut or multifaceted doughnut etc. Such micrometric grains with interesting pore morphology can also be synthesized by addition of template or by tuning the agglomeration behavior. While the overall morphology of the assembled grains can be obtained by electron microscopy, small-angle scattering can provide the hierarchical structural information in the grains. Such micrometric assembled grains with definite pore structure may be considered as potential candidates for various applications such as filtration application, drug delivery, catalysis, nuclear waste management etc.

Acknowledgement

DS would like to thank Dr. Shovit Bhattacharya, TPD, BARC for SEM measurements and also to Mr. Arshad Khan, RPAD, BARC for his active help towards the development of the spray dryer with slower drying rate.

References

1. K. Masters, *Spray Drying Handbook*, 5th Edition, Longman Scientific & Technical, England, 1991.
2. F. Iskandar, L. Gradon, K. Okuyama, *J. Colloid and Interface Sci.*, **265**, 296-303 (2003).
3. N. Tsapis, E.R. Dufresne, S.S. Sinha, C.S. Riera, J.W. Hutchinson, L. Mahadevan, L. D.A. Weitz, D. A. *Phys. Rev. Lett.* **94**, 018302 (2005).
4. D. Sen, O. Spalla, L. Belloni, T. Charpentier, A. Thill, *Langmuir*, **22**, 3798-3806 (2006).
5. D. Sen, O. Spalla, O. Taché, P. Haltebourg, A. Thill, *Langmuir*, **23**, 4296-4302 (2007).
6. D. Sen, S. Mazumder, J.S. Melo, A. Khan, S. Bhattacharya, S.F. D'Souza, *Langmuir*, **25** (12) 6690-6695 (2009).
7. D. Sen, J.S. Melo, J. Bahadur, S. Mazumder, S. Bhattacharya, G. Ghosh, D. Dutta and S.F. D'Souza, *European Physical Journal-E*, **31**, (2010), 393-402
8. D. Sen, Arshad Khan; J. Bahadur; S. Mazumder; B.K. Sapra, *J. Colloid & Interface Science*, **347**, (2010) 25-30
9. J. Bahadur, D. Sen, S. Mazumder, Bhaskar Pal, Arshad Khan, G. Ghosh *J. Colloid and Interface Sci.* 351 357-364 (2010)
10. Arshad Khan, D. Sen, B.K. Sapra and S. Mazumder; *Proceedings of the 54th DAE SSPS* (2009), pp-445-446.
11. S. Mazumder, D. Sen, T. Saravanan, P.R. Vijayaraghavan, *J. Neutron Research*, **9**, 39 (2001).
12. V.K. Aswal and P.S. Goyal, *Curr. Sci.* 2001, **79**, 947.
13. J.S. Melo, D. Sen, S. Mazumder and S.F. D'Souza. *In proceedings of the Indian Desalination Association and Asia Pacific Desalination Association Conference on desalination and water purification held at Chennai, India* pp 411-417, 2010.
14. J. Bahadur, D. Sen, S. Mazumder, S. Bhattacharya, H. Frielinghaus, G. Goerigk *Langmuir* **2011**, 27 (13), pp 8404-8414
15. Debais Sen, Jose Savio Melo, Jitendra Bahadur, Subhasish Mazumder, Shovit Bhattacharya, Stanislaus Francis D' Souza, Henrich Frielinghaus, Günter Goerigk, Rudolf Loidl *Soft Matter* **7** 5423-5429 (2011)

	<p>D. Sen has joined the Solid State Physics Division, Bhabha Atomic Research Centre, Mumbai, India in 1996 after completion of 39th batch of BARC training school from Physics discipline. He obtained his Ph.D. degree in Physics from Mumbai University in 2004. He has worked extensively on mesoscopic structural properties in several technologically important materials using small-angle neutron and x-ray scattering. His current field of interest is evaporation induced self-assembly of nanoparticles and porous media. He has to his credit more than seventy publications in international journals.</p>
	<p>J. Bahadur obtained his M.Sc. in Physics in 2005 from the University of Allahabad. He joined the 49th batch of BARC Training School and was awarded the Homi Bhabha prize for standing first in his discipline. On completion of training, he joined Solid State Physics Division of BARC, Mumbai, India. He is currently working in the field of small angle neutron and x-ray scattering on nano-ceramic and nano-composite materials. His research interests include sintering behaviour of nano-ceramics and evaporation driven self-assembly of colloids.</p>
	<p>S. Mazumder is a senior scientific officer at the Solid State Physics Division, BARC, Mumbai, India. He is from 27th batch of BARC training school and has interest in scattering techniques for material investigation. His current field of interests includes evolution of structure during cement hydration.</p>
	<p>J. S. Melo obtained a M.Sc. in Biochemistry in 1984 and Ph.D. degree in Biochemistry in 1990 from Mumbai University. Currently he is a senior scientific officer of the Nuclear Agriculture & Biotechnology Division at Bhabha Atomic Research Centre, Mumbai, India, and is also an Associate Professor at the Homi Bhabha National Institute. In the field of bioprocessing, he has developed a number of novel techniques for immobilization of enzymes, cells and preparation of coimmobilizates. His current field of interest is bioremediation, nanoscience and sensors. He has to his credit several publications in International Journals, Symposia and Workshops.</p>
	<p>S. F. D'Souza is currently the Associate Director of the Biomedical Group and also Head, Nuclear Agriculture and Biotechnology Division, at Bhabha Atomic Research Centre. Mumbai, India, wherein he coordinates institutional programs on food agriculture and biotechnology. He is also Senior Professor at the Homi Bhabha National Institute. He has a Ph.D in Biochemistry and his major research interest has been in the field of enzyme and microbial technology with special reference to immobilized cells for use in bioprocessing, biosensors, bioremediation and nanotechnology. He has to his credit over 200 scientific papers and invited reviews in reputed International Journals.</p>

Light absorption and emission in gold nanoplates assembled in small groups via poly(vinylidene fluoride) molecules

B. Susrutha, A.D. Phule and S. Ram*

Materials Science Centre, Indian Institute of Technology, Kharagpur- 721302, India

*Corresponding author: E-mail: sram@matsc.iitkgp.ernet.in

Abstract

A simple in-situ chemical reduction of a gold salt by using poly(vinylidene fluoride) (PVF₂) molecules in DMF with ultrasonics in hot conditions is explored to prepare Au-nanoparticles (Au-NPs) in form of a nanofluid. It is shown that PVF₂ molecules bond primary Au-NPs (usually plates with 120-180 nm width and 10-15 nm thickness) one another in small assemblies in a spherical shape (~ 920 nm diameter). A nanofluid containing Au-NPs as small as 0.5 wt % exhibits an intense optical absorption, in the range 330-760 nm, in three well-separated band-groups at 385 nm, 540 nm, and 675 nm. The 540 nm band has the maximum peak intensity, showing a molar extinction coefficient $1.105 \times 10^4 \text{ L/mol-cm}$. A different spectrum occurs in the emission with a prominent band at 476 nm. Here, PVF₂ molecules immobilize Au-NPs so that the surface stabilized Au-NPs assemble in a specific spherical shape in minimizing the total surface energy. This is modeled assuming a preferably linear PVF₂ structure of a bonded layer on the nascent Au-NPs. The bonded layer confines a localized distribution of the surface plasmons in the interface regime and in turn controls the light absorption and emission in a complex function of the surface bridging and the local dielectric field.

Keywords: Au-PVF₂ nanoassemblies, optical absorption, photoluminescence, nanofluids

Introduction

Noble metal nanostructures have drawn considerable interest in recent years because of their wide applications in catalysis, biosensing, optics, and medical diagnostics [1-4]. In particular, it is known since far long that optical properties of gold-nanoparticles (Au-NPs) are strongly influenced by the shape, size and surface topology as well as the local environments [5, 6]. Several methods have been developed to fabricate shape controlled Au-NPs with functional properties [7-9]. Two-dimensional (2D) shapes such as nanodisks, nanoplates, and nanobelts are highly sensitive in tailoring such properties [10, 11]. These geometrical attributes are especially useful in cancer hyperthermia and other medical applications because the surface plasmon resonance (SPR) band can be tuned easily from the visible to near infrared region [12, 13]. Limited studies have been carried out on submicrometer or micrometer-sized plates that are not so stable in a solution phase, and thus lose colloidal properties [14-16]. Within the last one decade [17-20], our group synthesized different nanofluids containing silver or gold of different sizes and shapes using reactive polymer molecules of poly(vinyl alcohol) (PVA), poly(vinyl pyrrolidone) (PVP), or poly(vinylidene fluoride) (PVF₂) in a single step of in-

situ reaction at moderate temperature. In addition to (i) a model reductant and (ii) a model surface stabilizer, these polymer molecules serve as a template when growing a 2D-metallic structure in a solution. Au-nanoplatelets (0.5-1.0 wt %) embedded in PVA molecules and cast as films exhibit two SPR bands near 570-595 nm and 820-830 nm [18]. Au-nanoplates (30-140 nm width and 6-10 nm thickness) obtained using cetyltrimethyl ammonium bromide has two bands of 760 nm and 1055 nm useful for biomedical applications [21].

In this article, we report on light absorption and emission in Au-nanoplates which are assembled in small groups via PVF₂ molecules. Peculiarly, a sharp absorption band of symmetric shape arises with average peak position at 540 nm at a specific Au-content of 0.5 wt %. PVF₂ molecules bond Au-NPs in this specific shape of a sphere in minimizing the total surface energy. A rather different band occurs in the emission with average position ~ 476 nm from a surface interface.

Experimental

A nanofluid Au-PVF₂ was prepared in a single step of a reaction $\text{Au}^{3+} \rightarrow \text{Au}$ that was carried out using (i) a gold salt $\text{HAuCl}_4 \cdot 3\text{H}_2\text{O}$ (99.99% pure from Merck chemicals), (ii) PVF₂

of weight average molecular weight $\sim 40,000$ (spectroscopic grade from Alfa Aesar), and (iii) triethanol amine (TEA) in a dilute solution in *N,N*-dimethyl formamide (DMF) in hot conditions. The TEA was used to serve not only as a surface stabilizer to produce Au-NPs in small assemblies but also a modest reductant to monitor a controlled $\text{Au}^{3+} \rightarrow \text{Au}$ reaction in a rheological fluid in presence of the PVF_2 molecules. It has been observed that when adding drop wise (1-2% volume wise), TEA promotes the $\text{Au}^{3+} \rightarrow \text{Au}$ reaction, showing a distinct visible color from surface stabilized Au-NPs and dispersed through the PVF_2 molecules. A typical reaction batch carried out used 0.1 ml of a HAuCl_4 solution (0.075 M concentration), 5 ml of a 0.3 g/L PVF_2 and 0.01 ml TEA in a total 5.11 ml volume. To begin the reaction, the HAuCl_4 solution was added to the PVF_2 solution drop wise by ultrasonication at 50-60°C. 10 min heating at this temperature in presence of ultrasonication followed by 20-30 min normal heating onto a magnetic stirrer results in an intense bluish violet colored nanofluid mostly free from byproduct volatile impurities.

Morphology and size distribution of the Au-NPs in a nanofluid were studied by using a field emission scanning electron microscope (FESEM) of SUPRA-40 with an accelerated voltage 2-30 kV. The optical absorption spectrum (200-800 nm) of the nanofluid was measured (against the parent PVF_2 solution) with a Perkin Elmer absorption spectrophotometer of Lambda 750. A Perkin Elmer (Model-LS 55) luminescence spectrometer was used with a red sensitive PMT detector (RS928) and a pulsed xenon lamp (20 kW power for 8 μs) to study emission of the same sample.

Results and Discussion

Typical FESEM images measured from an Au- PVF_2 nanofluid at three selective magnifications in order to illustrate the microstructural features that incur at different length scales are shown in Fig. 1 (a-c). All these images were taken from the same sample which contained 0.5 wt% Au in form of a basic structure of nanoplates (Fig.1c). As mentioned above, this specific sample has been studied in detail because it presents a prominent absorption band of a symmetric shape in the green region 540 nm along with a weak band in the red region 675 nm and a weak band in the violet region 385 nm. These three separated absorption bands can be explored to tailor light emission over a wide range 300-800 nm for different applications. In Fig. 1a, the FESEM images when taken at a rather low magnification present distinct assemblies of near spherical shapes,

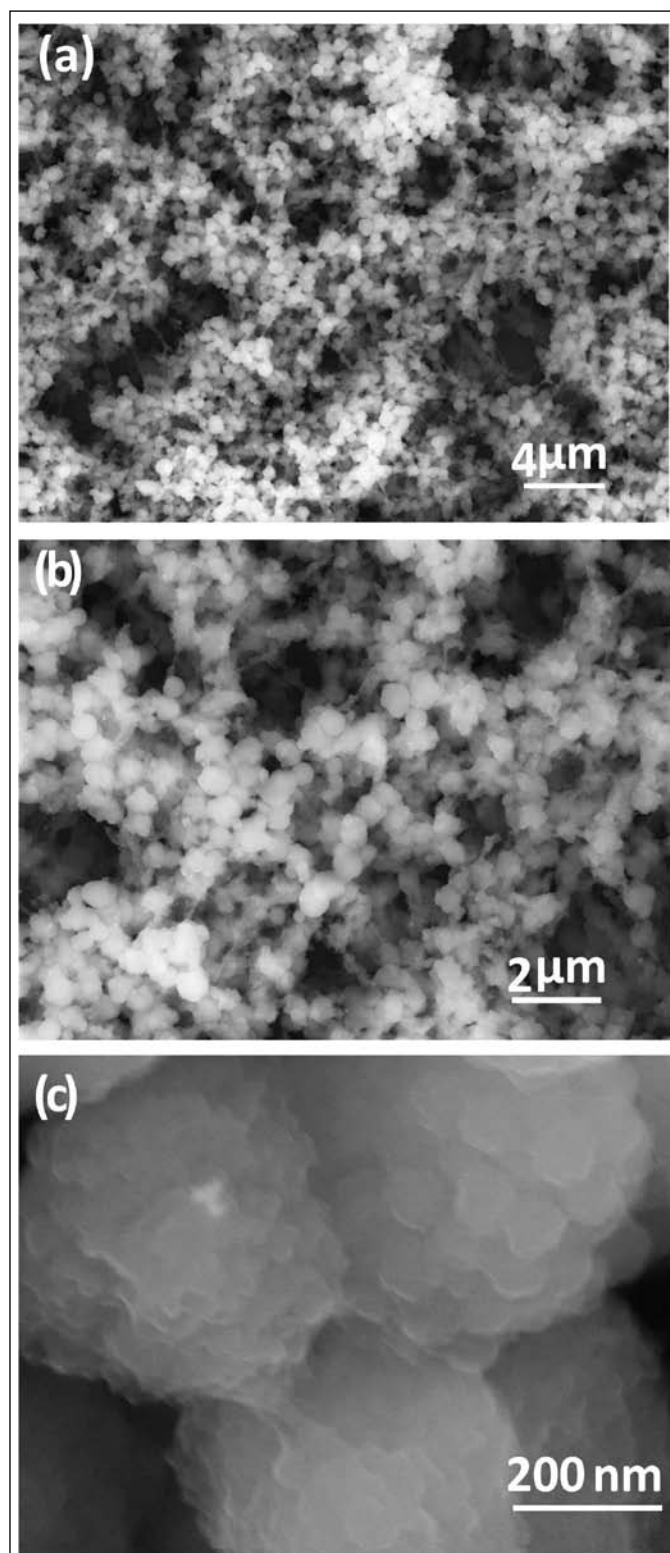


Fig. 1: FESEM images (a-c) of Au-NPs (0.5 wt%) embedded in PVF_2 from a nanofluid in an organic medium of DMF, showing that PVF_2 molecules bond Au-NPs in clusters.

showing a fairly sharp size distribution with an average 920 nm diameter. As can be seen from magnified FESEM images in Fig.1b, the PVF₂ molecules are interbridging small Au-NPs in stable assemblies. Within an assembly, the PVF₂ molecules bond primary Au-NPs, mostly thin plates with 120-180 nm width and 10-15 nm thickness. This is demonstrated well with high resolution FESEM images in Fig. 1c.

Fig. 2 presents absorption spectrum of an Au-PVF₂ nanofluid, containing 0.5 wt% Au-NPs, measured in the range 330-760 nm. As expected, the Au-nanoplates reveal two distinct transverse (T) and longitudinal (L) modes of the absorption in the localized SPs on the metallic surface upon a tightly bonded polymer surface layer. The T-mode reflects in a prominent band at 540 nm while the L-mode assumes a rather poor intensity by an order of magnitude with average position lying at 675 nm. Both of these bands have a doublet structure as can be seen with their deconvolutions. As a result, two bands of 534 nm and 553 nm comprise the T-mode while those of 658 nm and 682 nm comprise the L-mode {see the inset (a) in Fig. 2}. The red-shifted band components arise from the Au-SPs which bond the surface polymer layer while the main band components arise from the regular Au-SPs in the surface modified Au-nanoplates and coalesced in spherical assemblies as shown in the FESEM images. As given in Table-1, a molar extinction coefficient $\epsilon_{\max} = 1.105 \times 10^4$ L/mol-cm is obtained for the 540 nm bandgroup. This specific value is an order of larger magnitude when comparing to a value $\epsilon_{\max} = 1 \times 10^3$ L/mol-cm observed in an absorption band at 562 nm in 0.5 wt % Au-NPs embedded in PVP molecules in form of a nanofluid in water [17].

Furthermore, an order of lower ϵ_{\max} -value is observed in the 675 nm band, or in another similarly weak band shown at shorter wavelength over 340-440 nm in Fig. 2. Table-1 also includes the values for the oscillator strength (f_{osc}) in the three major bandgroups observed at 385 nm, 540 nm, and 675 nm in Fig. 2.

The f_{osc} -value has been calculated from the integrated area in a bandgroup by using the standard relation [22],

$$f_{\text{osc}} = 4.314 \times 10^{-9} \int_{-\infty}^{\infty} \epsilon d\nu, \quad (1)$$

where the ϵ -value (the molar extinction coefficient) is taken per unit concentration of Au-NPs in mol/L and $\nu = \lambda^{-1}$ expresses the band in an energy scale.

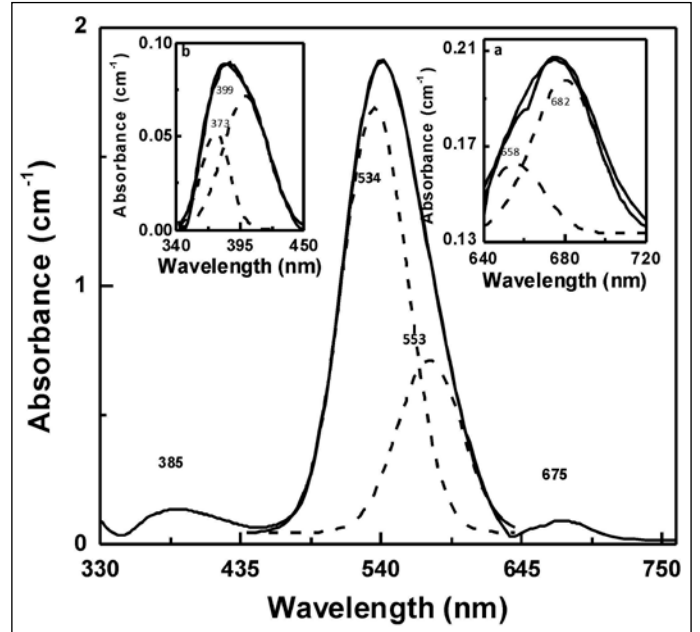


Fig. 2: Optical absorption spectrum in a nanofluid containing 0.5 wt% Au-NPs embedded in PVF₂ in DMF, with deconvolution of the weak bands (a) 680 nm and (b) 385 nm in the inset.

Table 1: SPR bands observed in absorption spectrum in a 0.5 wt % Au-PVF₂ nanofluid

Band position λ_{\max} (nm)	ϵ_{\max} -value (L/mol-cm)	f_{osc} -value
385	0.13×10^4	0.26
540	1.11×10^4	0.33
675	0.11×10^4	0.12

The reaction was carried out with 0.594 mM HAuCl₄ in 0.3 g/L PVF₂ in DMF.

In Au-PVF₂ assemblies in a nanofluid, a short wavelength absorption observed over 340-440 nm is a new bandgroup for Au-NPs. In all possible experimental shapes, Au-NPs are known to absorb only above 450 nm in a usual SPs structure [1-5]. Also this bandgroup (Fig. 2b) consists of two band components of 373 nm and 399 nm in a similar sequence of band intensities as those shown in the 675 nm bandgroup assigned to the L-mode of the Au-SPs in Au-nanoplates modified by a bonded surface PVF₂ layer. Considering a close similarity with the L-mode of the Au-SPs in the absorption profile, this specific bandgroup arises possibly when the L-mode is coupled to the T-mode in the localized Au-SPs on the Au-nanoplates mediated

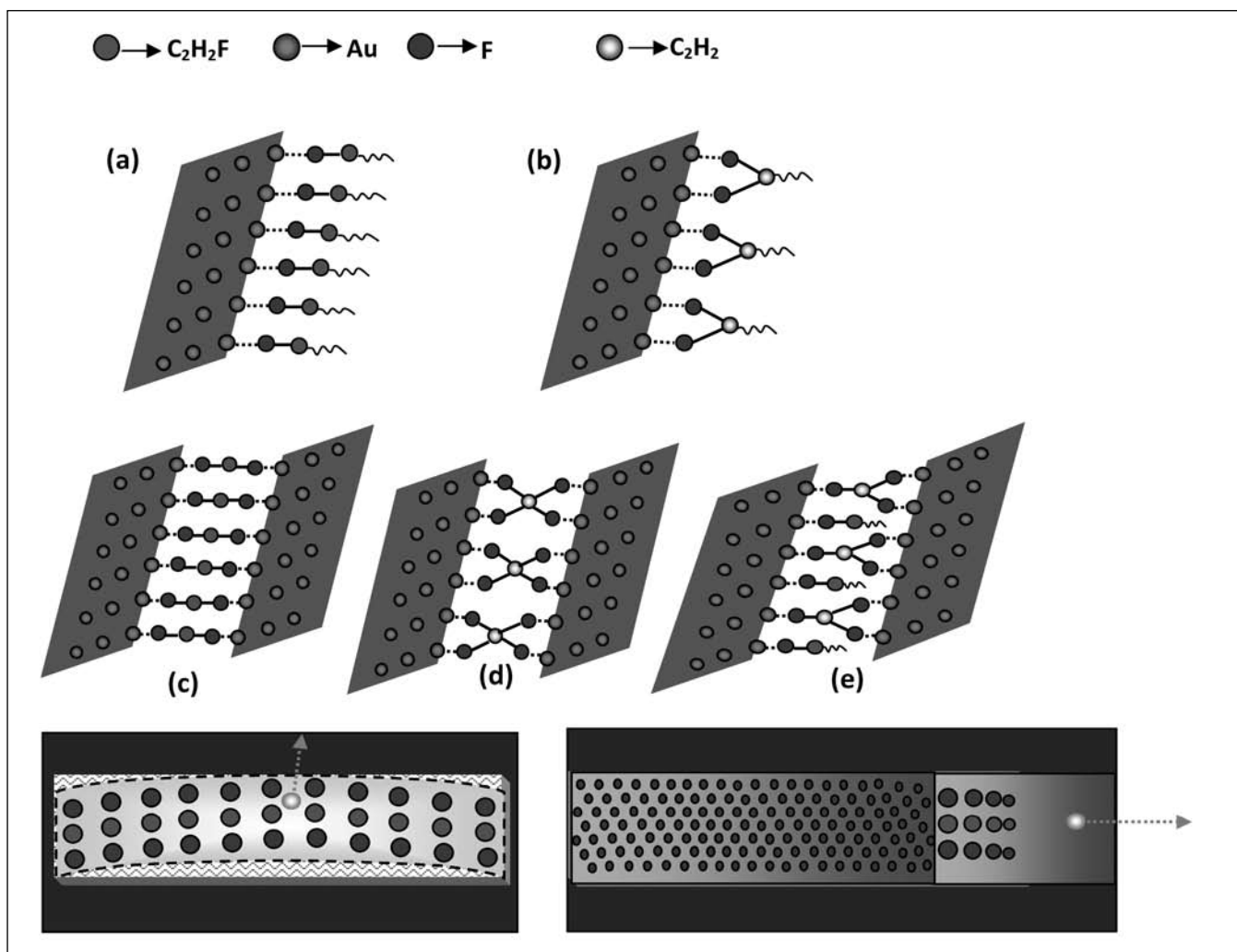


Fig. 3: A model chemical bonding of PVF₂ molecules on a gold surface; (a) a linear molecular bridging and (b) a molecule adjoining two Au-atoms, and (c-e) polymer molecules interbridging two Au-particles in three different local bonding from the two basic structures. Model displacements of the bonded surface layer (f) perpendicular and (g) along the sample surface.

through the bonded surface PVF₂ molecules. For example, a combination of a T-band observed at 534 nm and an L-band at 658 nm can generate a new band of 339 nm, which is not very far off a deconvoluted band at 373 nm if adding a small energy loss of 0.033 eV. Considering a similar energy-loss in interaction with the surroundings during the absorption of the photons describes the other absorption band component shown at 399 nm in a combination of the two distinct bands observed at 553 nm (T) and 682 nm (L) in Fig. 2. This result confers that a bonded polymer PVF₂ surface layer on the Au-NPs causes desirably not only a localized structure of the Au-SPs on the Au-NPs but also mediates an exchange coupling between the two modes of the Au-SPs.

As expected, it modifies the local dielectric field around a surface modified Au-nanoplate in the assemblies so that the field modulates electronic transitions in the localized SPs in an exchange coupled composite system.

Considering the FESEM images (Fig.1) in correlation to the absorption bands (Fig. 2) implies that the PVF₂ molecules very efficiently immobilizing Au-NPs in the shape of nanoplates so that a surface stabilized sample coalesces in a specific spherical shape in minimizing the total surface energy. Formation of a molecular PVF₂ bonding through Au-atoms from the surface of a model Au-nanoplate is demonstrated in Fig. 3.(a-e). A model structure in Fig. 3a describes a linear molecular PVF₂ bridging which adjoins a

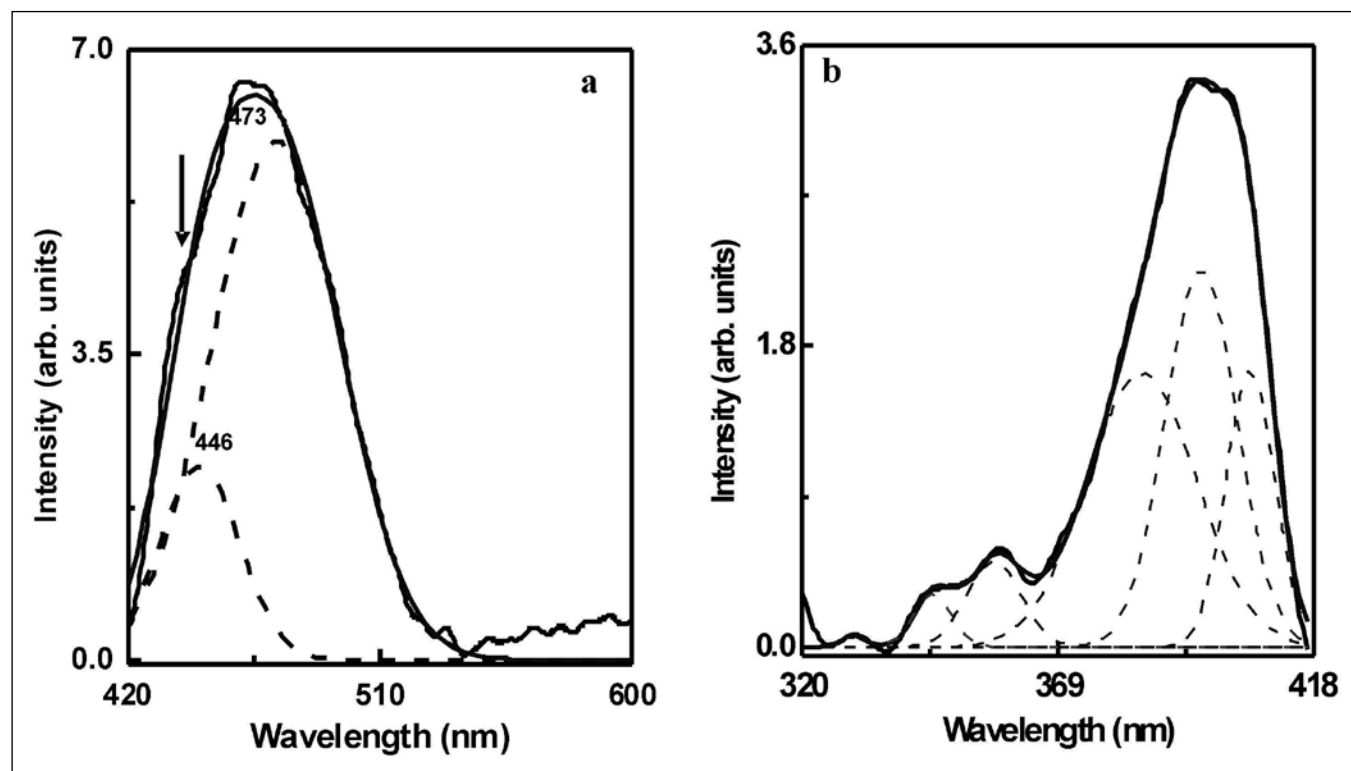


Fig. 4: (a) Emission ($\lambda_{ex} = 390$ nm) and (b) excitation ($\lambda_{em} = 440$ nm) spectra in a nanofluid containing 0.5 wt% Au-NPs embedded in PVF₂ in DMF.

single Au-atom from the sample whereas a PVF₂ molecule in a model structure in Fig. 3b adjoins two different Au-atoms. Other three configurations proposed in Fig. 3 (c-e) are derived just by bridging the above two basic configurations side-to-side. All these three configurations bond a fluorine rich interface layer with the surface Au-atoms from a nanoplate. Although average number density of fluorine atoms does not change in these configurations, they differ one from another in terms of the local site symmetry in the fluorine atoms. From geometrical stability point of view, the configuration (d) made-up of a binary combination of two basic structures (b) would be rather more rigid and stable in interbonding two Au-NPs. Obviously, this represents the most preferred interface configuration in a stable assembly of Au-NPs. The configuration (e), i.e., a binary combination of two different basic structures (a, b) may be more useful in ordering a non-centrosymmetric configuration of the electric dipoles of the fluorine atoms, useful to modulate the local electric field in a nanofluid. Evidently, model displacements of a bonded PVF₂ surface layer perpendicular to the interface (Fig. 3f) and along the interface (Fig.3g) would affect the T-mode and L-mode

oscillations of the Au-SPs bounded by a surface layer. The local electric field from a bonded surface charge layer, which confines Au-SPs in the interface, induces mixing between the T- and L-modes in the confined Au-SPs.

We also studied light-emission in the Au-PVF₂ nanofluid having 0.5 wt% Au-NPs by exciting the specimen at different wavelengths (λ_{ex}) by a pulse xenon source. Fig. 4a shows a typical emission spectrum when measured over 420-600 nm by exciting at a specific value of the excitation maximum. $\lambda_{ex} \sim 390$ nm. It consists of two bands of peak positions 466 nm and 473 nm which are not shown in the absorption spectrum in Fig.2. It arises from the surface-interface in the Au-NPs on a bonded PVF₂ layer. The λ_{ex} -value has been chosen to measure the light emission in Fig. 4a as per the excitation spectrum as given in Fig. 4b. As expected, this excitation spectrum contain several bands over 320-420 nm when PVF₂ surface modified Au-NPs coalesce in assemblies in from of a hybrid composite.

Conclusions

The Au-nanoplates (120-180 nm width and 10-15 nm thickness) when embedded in PVF₂ molecules following an




in-situ chemical reduction reaction $\text{Au}^{3+} \rightarrow \text{Au}$ in presence of PVF₂ molecules in a liquid such as DMF coalesce in small assemblies. The product is a stable rheological nanofluid at Au-NPs contents below 5.0 Wt%. A specific composition, which contained 0.5 wt% Au-NPs, presents uniquely an intense absorption band of symmetric shape with average peak position lying at 540 nm. A symmetric absorption is characteristic of a sharp size distribution of Au-NPs and that is feasible only on immobilized Au-NPs with a stable surface layer. Two weak bandgroups 340-440 nm and 600-740 nm share the spectrum. A different spectrum incurs in the emission, with average position lying at 476 nm, from the surface-interface, which is modeled assuming a preferably linear PVF₂ bonded layer on the nascent Au-NPs. A bonded layer confines a localized distribution of the Au-SPs in the interface so that it controls the light absorption and emission in a composite structure.

Acknowledgement

This work is supported by a research grant DAE-BRNS, Governments of India.

References:

1. J. F. Wang, M. S. Gudiksen, X. F. Duan, Y. Cui, and C. M. Liber, *Science*, 293 (2001) 1455.
2. R. Jin, Y. Cao, E. Hao, G. S. Meraux, G. C. Schatz, and C. A. Mirkin, *Nature (London)*, 425 (2003) 487.
3. J. U. Kim, S. H. Cha, K. Shin, J. Y. Jho, and J. C. Lee, *Adv. Mater.*, 16 (2004) 459.
4. D. J. Milliron, S. M. Hughes, Y. Cui, L. Manna, J. B. Li, L. W. Wang, and A. P. Alivisatos, *Nature*, 430 (2004) 190.
5. M. A. El-Sayed, *Acc. Chem. Res.*, 34 (2001) 257.
6. Y. Xia, Y. J. Xiong, B. Lim, and S. E. Skrabalak, *Angew Chem. Int. Edn.*, 48 (2009) 60.
7. F. Kim, J. H. Song, and P. Yang, *J. Am. Chem. Soc.*, 124 (2002) 14316.
8. C. J. Murphy and N. R. Jana, *Adv. Mater.*, 14 (2002) 80.
9. M. M. Steven, N. T. Flynn, C. Wang, D. A. Tirrell, and R. Langer, *Adv. Mater.*, 16 (2004) 915.
10. Z. W. Pan, Z. R. Dai, and Z. L. Wang, *Science*, 291 (2001) 1947.
11. M. Maillard, S. Giorgio, and M. P. Pileni, *Adv. Mater.*, 14 (2002) 1084.
12. T. J. Norman, Jr., C. D. Grant, D. Magana, J. Z. Zhang, J. Lu, D. Cao, F. Bridges, and A. V. Buuren, *J. Phys. Chem. B*, 106 (2002) 7005.
13. E. S. Day, J. G. Morton, and J. L. West, *J. Biomech. Eng.*, 131 (2009) 074001-5.
14. S. S. Shankar, A. Rai, B. Ankamwar, A. Singh, A. Ahmad, and M. Sastry, *Nature Materials.*, 3 (2004) 482.
15. Z. R. Guo, Y. Zhang, L. Huang, M. Wang, J. Wang, J. F. Sun, L. N. Xu, and N. Gu, *J. Colloid Interface Sci.*, 309 (2007) 518.
16. Z. R. Guo, Y. Zhang, A. Q. Xu, M. Wang, L. Huang, K. Xu, and N. Gu, *J. Phys. Chem. C*, 112 (2008) 12638.
17. A. Gautam, P. Tripathy, and S. Ram, *J. Mater. Sci.*, 41 (2006) 3007.
18. S. Ram, P. Tripathy, and H. -J. Fecht, *J. Nanosci. Nanotechnol.*, 7 (2007) 1.
19. A. Mishra, S. Ram, and G. Ghosh, *J. Phys. Chem. C*, 113 (2009) 6976.
20. S. Ram, A.D. Phule, and A.K. Tyagi, *Phil. Mag. Lett.*, 90 (2010) 781.
21. X. Fan, Z. R. Guo, J. M. Hong, Y. Zhang, J. N. Zhang, and N. Gu, *Nanotechnology*, 21 (2010) 105602.
22. E. B. Wilson, J. C. Decius, P. C. Cross, *Molecular vibration*, McGraw-Hill, New York, (1995) 466.

	<p>B. Susrutha studied M. Sc. (Analytical Chemistry) at Osmania University during 2004-06. She is currently doing Ph. D. at Materials Science Centre, IIT Kharagpur, under the supervision of Prof. S. Ram (IIT Kharagpur) and Prof. A. K. Taygi (BARC, Mumbai). Her research area includes synthesis of nanofluids and ceramic composites with a dielectric or ferroelectric host for efficient light emission, energy transfer, and other functional properties for biological and other applications.</p>
	<p>A. D. Phule received his M. Sc. (Organic Chemistry) from Pune University during 2005-07. At present he is a Ph. D. scholar at Materials Science Centre, IIT Kharagpur, jointly under the supervision of Prof. S. Ram (IIT Kharagpur) and Prof. A. K. Taygi (BARC, Mumbai). His area of research interest includes development of nanofluids and hybrid nanocomposites with polymeric hosts for optical sensor, barcodes, light emitters, and different biological and drug applications.</p>
	<p>Dr. S. Ram received his M. Sc. (Physics) and Ph. D. (Physics) degrees From Banaras Hindu University in 1978 and 1982 successively. He has received several awards including the Alexander Humboldt Fellowship-1994-96, 2004 (Germany), CNRS Fellow-1989 (France), and MRSI (India) medal-2003. He was visiting Scientist/Professor at McMaster University-1988-89 (Canada), Domain University-1989-92 (France), and Ulm University-2005, 06, 07, 08 (Germany). He joined Materials Science Centre, Indian Institute of Technology at Kharagpur, as an assistant professor in 1996, and presently Professor in this Centre. Till date, he has published over 210 peer-reviewed papers, 11 patents, 07 Book chapters, supervised 12 Ph.D., 33 M. Tech., and 21 B. Tech. theses, and carried out about 10 sponsored projects on nanomaterials, biomaterials and applications. His research interest includes glasses, magnetoceramics, intermetallics, nanofluids, magneto-optic materials of garnets, cermets, high-energy-density magnets, ferroics, superconductors, magnetic sensors, GMR, GMS and GMC materials, hydrogen energy storage materials, solid fuels, nanostructured solids, fibres and composites, photonics</p>

Preparation and Characterization of Collagen-based Liposome Nanoparticles Composite Matrix

Krishnamoorthy Ganesan*, Praveen Kumar Sehgal, Asit Baran Mandal and Sadulla Sayeed

*Bioproducts Laboratory-Biomaterial Development Division,
Central Leather Research Institute (Council of Scientific & Industrial Research),
Adyar, Chennai-600 020, Tamil Nadu, India*

**Corresponding author: email: krishnamoorthyganesan@yahoo.com*

Abstract

The mineralized collagen-cholesterol (CH)-free liposome nanoparticle (LNP) composite matrix has been prepared and characterized for use as tissue engineering applications. The CH-free LNP was prepared by heating method under the N₂ atmosphere and this above composite matrix was prepared by incubation of bovine Achilles tendon collagen with preformed Ca²⁺ and P_i loaded LNP. The particle size analysis showed that this LNP was in the various size ranges between 20-300 nm. The results from Thermo mechanical (TMA), Differential Scanning calorimetric (DSC) and Thermo gravimetric (TGA) analysis of the collagen matrix also indicates an increase in the tensile strength (TS), denaturation temperature (T_D) and significantly decreases the weight loss. The cell viability assay showed more than 90% fibroblast viability (NIH 3T3) 96 h. This composite matrix demonstrates a higher resistance to collagenolytic activity. This matrix could be useful to bone, dental implant and dura matter.

Keywords: Biomaterial; Collagen; Liposome nanoparticles; Mineralized collagen matrix

Introduction

The combination of polymeric biomaterials such as chitosan, alginate, dextran, fibrin, gelatin and collagen with liposomes could revolutionize the current state of drug delivery and tissue engineering technology [1,2]. The combination of collagen and liposomes based technologies for drug delivery system has been long achieved [3,4]. In this case, drugs and other bioactive agents were firstly, encapsulated in the liposomes and then embedded inside a depot composed of collagen-based systems, including scaffolds and injectable gels [5]. The combination of this two biomaterial (i.e., collagen and liposomes-based system) has improved storage stability, prolonged the drug release rate, and increased the therapeutic efficacy [6,7]. Though CH increasing the stability of liposomes, it unfortunately, creates certain problems when used in human pharmaceuticals, very difficult to atherosclerosis conditions in the cardiovascular system, readily oxidized and creating stability problems. As an alternative methodology, a number of researches have been performed to design and characterize the CH-free LNP to pharmaceuticals application. To date, little is known about the application of CH-free LNPs for retention of entrapped solutes and these reasons, alone, were sufficient to propose that CH-free LNPs may be relevant carriers for agents that

are not currently retained in conventional formulations. While in most cases natural and synthetic phospholipids are the major component, different types of biocompatible plant extract can be employed for improving the stability and drug delivery efficiency of conventional LNP [8]. In addition, a study was conducted that temperature sensitive liposomes and collagen may thermally trigger the release of Ca²⁺ and P_i [9]. The collagen-based biomaterial composite matrix with liposome for tissue engineering applications such as hard tissue replacement is currently not available.

Recent studies also demonstrate mineralized collagen composite for tissue engineering application [9]. The nucleation of new mineral phase in embryonic bone and rapidly mineralizing skeletal tissues takes place through the presence of matrix vesicles rich in calcium binding phospholipids. The possibility that short chains of hydrophobic groups can serve as anchors for collagen onto liposomes, was demonstrated [10]. In view of this, collagen can attach to the LNP surface in a stable way, and form the mineralized collagen matrix protecting structured shells, thus improving their stability. Among the many biomolecules involved in the bone mineralization processes, phospholipids play an important role because of their ability to bind Ca²⁺/P_i. This Ca²⁺-binding phospholipids

as a coating material for implant osteo integration has studied [11]. The collagen molecules interact with the alkyl chains of phospholipids with the hydrophobic residues on the collagen molecule surface [12,13]. Recent evidence suggesting that non-collagenous material associated with collagen serve as the mineral nucleation site [14]. Role of phospholipids in bone repair and its technological exploitation was studied [15,16]. Blending of the biomaterial with lecithins to improve hydrophobicity and biocompatibility has studied [17-19].

In this study, we used phenolic glycosides for preparation of CH-free LNP. The obtained CH-free LNP combine with collagen for composite matrix formation in an attempt to develop a novel biomaterial.

Experimental

Preparation of CH-free LNP

The LNP was prepared by the following method [20]. A known amount of liposome ingredients (phosphatidylcholine (PC):CH, PC:Phenolic glycoside) were added to a preheated (60 °C, 5 min) glycerol (final concentration 3%, v/v) with aqueous CaCl₂ (0.2M) or Na₂HPO₄ (0.2M). The mixture was further heated (60 °C) while stirring (approx. 1000 rpm) on a hotplate stirrer for a period of 45–60 min under nitrogen atmosphere. For the preparation of CH-containing formulations, CH was first dissolved in the aqueous phase of Milli Q water (autoclaved) at elevated temperatures (c. 120 °C) while stirring (approx. 6500-24000 rpm) for a period of 15–30 min under nitrogen atmosphere before adding the other components mentioned above. After preparation of the LNP samples, they were left at room temperature under N₂ for 30 min to stabilize. The CH-free LNP was produced by passing the emulsion repeatedly through a polycarbonate membrane having pores 400 and 200 nm in diameter. The diameter of the LNP is determined by the pore size of the membrane used during the extrusion method. The LNP produced using these methods are unilamellar. The residual solvent is removed by subjecting the LNP film to a high vacuum on a good lyophilizer for 90-120 min. The particle size, shape and zeta potential were analyzed by Dynamic light scattering (DLS).

Preparation of collagen-LNP composite matrix

A known amount of isolated collagen [21] in 0.05M acetic acid with pH 7.4 (1N NaOH in the presence of 10x HEPES buffer with a final concentration of 0.5x) was prepared. The gelling mixture was placed inside an ice

water bath at 4 °C to slow down the polymerization rate for 5 min. LNP was added to the mixture and thoroughly mixed well. A mixture of olive oil and silicon oil at a ratio of 1:1 was laid down on the aqueous gelling mixture at a volume ratio of 6:1. A nonionic surfactant, Tween 20, was added to the aqueous phase before emulsification. The mixture was homogenized at a maximal speed (6,500-24,000 rpm) for 30 min. The emulsions formed were then placed in a 37 °C water bath to speed up the polymerization. During the process, the solution became a white milky suspension. The mixture was incubated for 30 min until equilibrium. The mixture was centrifuged briefly at 10,000 rpm for 10 min to separate the solid matrix from the liquid phase, including an aqueous and an oil phase. After discarding the oil and the liquid phases, this composite matrix was rinsed twice with Millipore water and ready for further characterizations.

Characterization of collagen-LNP composite matrix

The TMA ((TMA, Instron series II Automated Materials Testing System), DSC (DSC, TA-DSC Q 200) and TGA (TGA, TA-TGA Q 50) were used for analysis of mechanical and thermal stability of this composite matrix. The water-uptake and swelling studies ratio was obtained by incubation of the samples (W_0 and S_0 respectively) in water at room temperature for 2 h. The water-uptake ratio is defined as $(W_t - W_0)/(W_0)$. The swelling ratio is defined as $(S_t - S_0)/(S_0)$. FT-IR (Perkin Elmer spectrometer) spectra were used for analysis of structural elicitation of this matrix. The SEM (SEM, FEI-Quanta 200) were used to observe the size and surface morphology of this matrix. Biodegradation of collagen composite matrix was analyzed by following modified method [22].

Results & Discussion

The analyses of the size distribution of Ca²⁺ and P_i loaded LNP were revealed by DLS. The particle sizes were more preferably from 20 to 900 nm, most preferably 100-250 nm ranges and zeta potential observed 30 to -60 mV. Therefore, zeta potential of LNP observed 30 to -60 mV were sufficiently high for electrostatic stabilization probably because of the charges of phenolic glycosides in LNP. Tensile strength of the collagen matrix increased with the presence of mineral on collagen matrix. The % elongation, on the other hand, showed a same trend. Furthermore, mineralization leads to a significantly improve tensile strength compared to the collagen matrix.

The T_D of the native, collagen-LNP and mineralized collagen were shown at 69.89, 84.04 and 108.87 °C for

Table 1 : TS, %E, T_D, T_g, % Degradation and % cell viability mineralized collagen.

Process	TS (Mpa)	%E	T _D (°C)	% T _g	% Water uptake	% Swelling	% Degradation	% Cell viability
Native collagen matrix	11.13	20.04	69.89	54.06	85	8	93	100
Collagen-LNP matrix	13.28	24.71	84.04	59.46	40	4	42	95
Mineralized collagen matrix	17.78	22.34	108.87	70.64	20	2	11	98

all collagen respectively. Mineralized collagen exhibits an increase in the denaturation temperature (T_D) when compared to native collagen. From this data, it can be observed that an initial thermal transitional change occurs between the temperature range of 200-500 °C for all the collagen, with maximum percentage glass transitional (T_g) weight loss at 54.06, 59.46 and 70.64 % for all treated collagen respectively. When collagen/ Ca²⁺ and P_i loaded LNP weight ratio is 2:1, the coating of collagen onto this LNP can remarkably improve their in vitro stability because it has basically no effect on the fluidity of this LNP.

The mineralized collagen matrix was resulting from thermally triggered self-assembly of collagen fibril and liposome mineralization. Heating of the precursor fluid to 37 °C induces collagen monomers to self-assemble into a collagen, into which mineral crystals are deposited. Water-uptake and swelling ratio of the collagen, collagen-LNP and mineralized collagen composite matrix were 85, 40 and 20 % and 8, 4 and 2 % at pH 7.4 respectively. Generally, the water-uptake ratio is controlled by hydrophilicity and water maintenance of the matrix. Although the formation of Ca²⁺ and P_i loaded LNP particles may decrease more or less the amount of hydrophilic groups of the collagen.

The mineralized collagen matrices presented lower swelling ratio. This composite matrix exhibited 42 and 11% degradation of collagen as against 93% degradation in the case of the native collagen matrix at 96 h period of incubation. The stability of this composite matrix against ChC would have been prevented by the LNP with collagen network, which links microfibrils, shielding in collagen helices. Small and larger LNP (100-200nm) on collagen matrix were detected in the SEM image [Fig. 1]. The surfaces of both as observed by SEM were spherical and smooth. In addition, collagen is a hydrophobic protein and the composite matrix prepared from it has a more

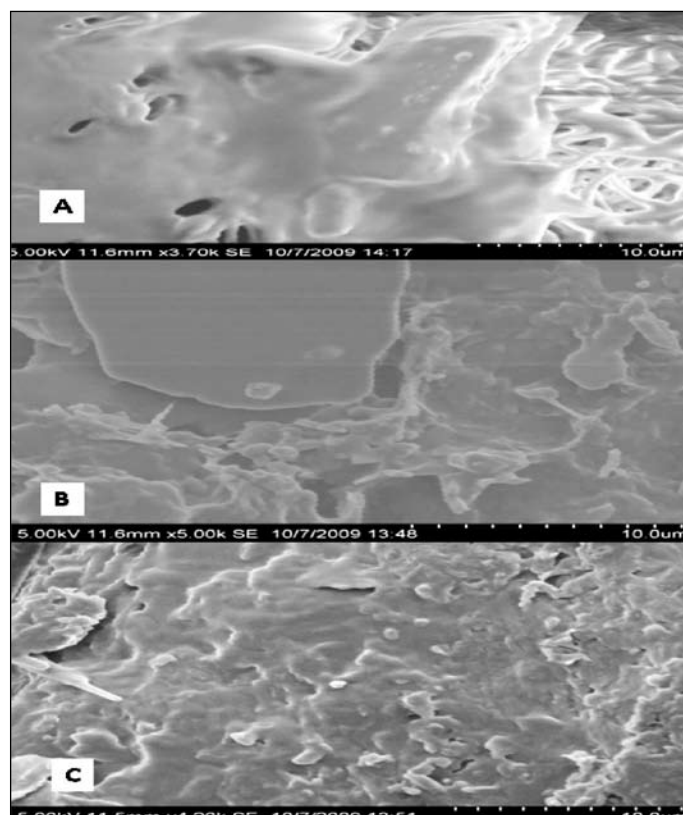


Fig 1: SEM analysis of A) collagen, B) collagen-LNP and C) mineralized collagen matrix

hydrophobic. These matrices exhibited more than 90% fibroblast viability (NIH 3T3) at 96 h [Fig. 2]. Mineralized collagen composite matrix with LNP, suggesting the high degree of biocompatibility evidenced that collagen matrix may be of potential use in tissue engineering.

In current studies, the in vitro biocompatibility efficacy of the collagen matrix to support cell proliferation and viability was assessed by growing NIH 3T3 fibroblast and were found to be grown uniformly with normal



Fig.2: Cell viability analysis of A) collagen, B) collagen-LNP and C) mineralized collagen matrix

may have the ability to nucleate mineral growth under these above conditions. The practical significance of this finding is that it suggests that in situ liposomal mineralization of the collagen matrix may provide a route for the formation of the mineral/collagen composite biomaterials with significant interaction between the mineral and collagen phases. In addition, LNP also promote mineralization. Lipids are present in the extracellular matrix at sites of the mineralization and are associated with the mineral phase such as regulating the growth of preformed mineral crystal. However, for this approaches to be practical will require a significant increase the mechanical stability into a range more suitable for repair of hard tissue. Further experiments will be necessary to investigate the possibility of significantly increasing the mineralization capacity of LNP. This collagen composite matrix may represent materials of choice for a new generation of biomaterials for hard tissue replacement.

Conclusions





Toward an ultimate goal of bone regeneration, we have introduced LNP as a modifying additive in the collagen matrix, based on which a series of novel collagen/LNP-Ca²⁺ and P_i composite matrix is developed. This composite matrix was successfully prepared through interactions between collagen with Ca²⁺ and P_i loaded LNP. Triggered mineral release from temperature sensitive LNP was combined with thermal collagen gelation to form a mineralized collagen matrix, thereby mimicking the processes that occur during natural mineralized tissue formation. This strategy takes advantage of liposomal encapsulation of minerals and their release into a collagen matrix formed by thermally triggered

self-assembly of acid-soluble type I collagen. The approach is designed to yield an injectable collagen-LNP composite precursor useful for minimally invasive reconstruction of bone, dental tissue and dura matter. Biomimetic composite matrix may represent materials of choice for a new generation of rapidly osteointegrating materials.

References

1. K. Y. Lee and S. H. Yuk. *Prog. Polym. Sci.* 32 (2007) 669.
2. M. S. Mufamadi, V. Pillay, Y. E. Choonara, L. C. Du Toit, G. Modi, D. Naidoo and V. M. K. Ndesendo. *J. Drug Deliv.* 2011 (2011) 1.
3. H. Wang, P. Zhao, W. Su, S. Wang, Z. Liao, R. Niu and J. Chang. *Biomaterials* 31 (2010) 8741.
4. P. S. Nunes, R. L. Albuquerque-Júnior, D. R. Cavalcante, M. D. Dantas, J. C. Cardoso, M. S. Bezerra, J. C. Souza, M. R. Serafini, L. J. Quitans, L. R. Bonjardim and A. A. Araujo. *J. Biomed. Biotechnol.* 9 (2011).
5. L. Weiner, S.S. Carpenter-Green and E.C. Soehngen. *J. Pharm. Sci.* 74 (1985) 922.
6. X. Shi, W. Ma, C. Sun and S. Wu. *Biomaterials* 22 (2001) 1627.
7. R. Nair, M. Sevukarajan, T. Mohammed, Badivaddin and C. K. Ashok Kumar. *J. Innov Trends. Pharm. Sci.* 1 (2010) 288.
8. D. B. Fenske and P. R. Cullis. *Exp. Opin. Drug Deliv.* 5 (2008) 25.
9. A. W. Pederson, J. W. Ruberti and P. B. Messersmith. *Biomaterials* 24 (2003) 4881.
10. J. Pokorny, J. Davidek, V. Chocholata, J. Panek, H. Bulantova, W. Janitz, H. Valentova and M. Vierecklova. *Nahrung.* 34 (1990) 159.
11. M. Santin, W. Rhys-Williams, J. O'Reilly, M. C. Davies, K. Shakesheff, W. G. Love, W. A. Lloyd and S. P. Denyer. *J. R. Soc. Interface* 3 (2006) 277.

12. J. Filipovic-Grcic, N. Skalko-Basnet and I. Jalsenjak. *J. Microencapsul.* 18 (2001) 3.
13. M. J. Fonseca, M. A. Alsina and F. Reig. *Biochim. Biophys. Acta (BBA)-Biomembr.* 1279 (1996) 259.
14. H. P. Wiesmann, U. Meyer, U. Plate and H. J. Hohling. *Int. Rev. Cytol.* 242 (2005) 121.
15. A. Merolli and M. Santin. *Molecules* 14 (2009) 5367.
16. J. H. Collier and P. B. Messersmith. *Annu. Rev. Mater. Res.* 31(2001) 237.
17. Y. Wang, F. Z. Cui, Y. P. Jiao, K. Hu and D. D. Fan. *Biomed. Mater.* 3 (2008)
18. R. Nirmala, H. M. Park, R. Navamathavan, H. S. Kang, M. H. El-Newehy and H. Y. Kim. *Mater. Sci. Engine. C.* 31 (2011) 486.
19. X. Shi, Y. Wang, L. Ren, W. Huang and D. A. Wang. *Int. J. Pharm.* 373 (2009) 85.
20. **G. Krishnamoorthy, P. Stephen, M. Prabhu, P. K. Sehgal and S. Sadulla.** *AIP conf. Proc.* 1276 (2010) 163.
21. P. K. Sehgal, M. R. Ahmed, R. Jayakumar and R. Sripriya. A process for the preparation of transparent soft collagen film. *Indian Patent.* DEL 2001, p. 201.
22. G. Krishnamoorthy, B. Madhan, S. Sadulla, J. Raghava Rao and W. Mathulatha. *J. Appli. Polym. Sci.*108 (2008) 199.

	<p>Mr. Ganesan Krishnamoorthy obtained his MSc degree in Biochemistry from Bharathidasan University, Tiruchirappalli and currently pursuing PhD in Biotechnology at Anna University, Chennai. Major objectives of his research work are Green chemistry approach to stabilization of collagen based biomaterials and coating of liposome nanoparticles on collagen matrix for biomedical applications (Drug delivery, Tissue engineering and Regenerative medicine).</p>
	<p>Dr. Praveen Kumar Sehgal obtained his PhD degree in Chemistry from Madras University, Chennai. He is presently scientist G, CSIR-CLRI, Chennai. Major objectives of his R & D work are better utilization of slaughter by-products and biomedical application of animal tissues (Drug delivery and Tissue engineering applications).</p>
	<p>Prof. Dr. Asit Baran Mandal obtained his PhD degree in Chemistry from Jadavpur University, Kolkata. He is a fellow of the Academy of Saint Cecilia (FASc) and Royal Society of Chemistry (FRSC), UK. He is presently Director of CSIR-CLRI, Chennai. Major objectives of his current research work are development of methodologies and physico-chemical techniques for the characterization of micellar and reverse micellar systems involving collagen, peptides, drugs, synthetic and vegetable tanning materials and polymeric surfactants.</p>
	<p>Prof. Dr. Sayeed Sadulla obtained his M.Tech degree in Leather Technology from Madras University and PhD from Anna University, Chennai. He has more than 35 years of experience in R & D in Leather Technology, Education and Training & Science and Technology Management. He had a distinguished career as a scientist and educationist at CSIR-CLRI, Chennai from 1975 to 2007 and superannuated as Director Grade Scientist. His current research interest/activities include Green Chemistry (Leather processing) and Collagen based biomaterials for industrial and biomedical applications.</p>

Application of Nanophosphors in Solid State White Light Generation

Dimple P. Dutta

Chemistry Division, Bhabha Atomic Research Centre, Mumbai 400 085

e-mail : dimpled@barc.gov.in

Abstract

Solid-state lighting (SSL) is emerging as a highly competent field and a possible alternative to existing lighting technologies. Phosphor converted light emitting diodes (pc-LED) form an integral part of this genre of research. In this manuscript, the potential of different rare earth/transition metal doped host materials have been discussed. The host materials studied were gadolinia, zinc aluminate and zinc phosphate. The effect of dopant ion concentration as well as that of the synthesis technique employed, on the resultant CIE coordinates of the phosphors have been studied. The nanophosphors were synthesized through sonochemical process or polyol method and characterized by using X-ray diffraction (XRD), transmission electron microscopy (TEM) and photoluminescence (PL) spectrophotometry. The results of XRD and TEM show that resultant nanoparticles are single phase and have spherical shape. The doped samples showed multi color emission on single wavelength excitation. Energy transfer was observed from host to the dopant ions. Characteristic blue and yellow emission from Dy³⁺ ions, green from Tb³⁺ ions and red from Eu³⁺ ions were observed. However, the Mn²⁺ ions in zinc gallate host yielded red emission which has been assigned to charge-transfer deexcitation associated with Mn²⁺ ion.

Keywords: Gadolinia, Zinc gallate, Zinc aluminate, Nanoparticles, Photoluminescence

The emphasis on research on SSL has gained tremendous momentum in the past decade due to their inherent advantages of high light efficiency, low energy consumption and long service lifetime compared to conventional light sources [1-5]. There are various approaches to get efficient solid state sources for white light generation. We can directly mix light from three (or more) monochromatic sources, red, green and blue (RGB), to produce a white source matching with the RGB sensors in the human eye. Another method is to use a blue LED to pump one or more visible light-emitting phosphors that has been integrated into the phosphor-converted LED (pc-LED) package. The pc-LED is designed to leak some of the blue light beyond the phosphor to generate the blue portion of the spectrum, while phosphor converts the remainder of the blue light into the red and green portions of the spectrum. We can also use an ultraviolet LED to pump a combination of red, green and blue phosphors in such a way that none of the pump LED light is allowed to escape.

Each of these approaches has potential advantages and clear technical challenges. Mixing the emission from red, blue and green colored LEDs is most advantageous since there is no quantum deficit arising from Stokes shift and hence offers infinitely graduated color and white point control. However, this form requires independent output power control on each LEDs, there is a gap in the

operating voltage between them and both these factors makes the operation quite cumbersome. In 1996, the white LEDs fabricated from blue LED chips combined with yellow phosphors Ce³⁺(YAG) were commercialized [6]. This phosphor-conversion white LED represented an innovation in solid-state lighting, because they were small, lightweight, had a long lifetime and was easy to operate. However, they were inherently less efficient than an RGB source because of the unavoidable energy loss concomitant with the wavelength-conversion of a photon from wavelength λ_1 to λ_2 with $\lambda_2 > \lambda_1$. The energy loss is particularly large for wavelength-conversion processes from the UV (400 nm) to the red (625 nm) where the loss is 36%. The third approach is to have UV-LEDs. In this case the UV light is completely adsorbed by the phosphors and the mixed RGB output appears white. The quantum deficit between the UV pump and the phosphors, especially the low-energy red phosphor, dissipates significant energy and makes this approach inherently less efficient than either the RGB or the pc-LED schemes for generating white light. However, the UV-LED approach has the advantage that color can be controlled by the phosphor mix at least at one point in time and at one temperature and hence the color rendering should be excellent.

The use of phosphors by man probably started more than 2000 years ago when they were used in fireworks to

modify the colour output. However, the importance of LED phosphors for white and coloured light generation must be considered an important market driver in the future. Phosphors are usually made from a suitable host material, to which an activator is added. They are composed of an inert host lattice (silicate/phosphate/oxide/fluoride/sulfide) and an optically excited activator, typically a 3d or 4f electron metal ion, which is capable of exhibiting high photoluminescence efficiency, stability and high absorption cross-section [7]. Oxide phosphors offer potential advantage over the commonly used sulfide phosphors, due to their superior chemical and photo-stability and excellent luminescent properties [8,9]. The unique luminescent properties of rare-earth elements hosted in different matrices find technologically important applications in optoelectronic devices such as plasma panels, flat panel displays, luminescent lighting, IR windows etc [7,10]. Phosphors are now critical to the long-term performance of LED lighting, and the ideal phosphor material should have a broad excitation spectrum in the desired spectral region, narrow emission bands centered on suitable wavelengths, high quantum efficiency (>90%), high levels of absorption at the excitation wavelength, high temperature stability of emission spectra and quantum efficiency along with a suitable morphology. The quality of the white light is determined from its CIE coordinates along with correlated color temperature (CCT). CCT is the temperature of an equivalent blackbody radiator that has a color which most closely matches the emission from a non blackbody radiator. For high quality white light, sources with CIE coordinates in the range $x = 0.28$ to 0.35 and $y = 0.30$ to 0.37 with a CCT between 2500 and 6500 K are required [11,12]. The CCT range signifies how warm or cool the white light is, viz, a warmer (i.e., lower temperature) light is often used in public areas to promote relaxation, while a cooler, whiter light is used in offices.

Conventional phosphors are in micrometer scale, light scattering at grain boundaries is strong and decreases light output. Conventional phosphors obtained by solid state sintering method has lower concentration quenching threshold due to non-uniform doping. Nanophosphors in size from tens to hundreds of nanometers that are smaller than the light wavelength can reduce scattering. Soft chemical routes to synthesize these nanophosphors can improve uniformity of doping and lift the concentration quenching threshold. Some soft chemical techniques are also capable for massive production at low cost. In this

have been synthesized using soft chemical techniques like sonochemical method or polyol route. Sonochemical synthesis is based on acoustic cavitation resulting from the continuous formation, growth and implosive collapse of the bubbles in a liquid [13,14].

Gadolinium oxide (Gd_2O_3), a rare earth sesquioxide, has unique properties which can be utilized in a wide range of technological applications. Gadolinium oxide (Gd_2O_3) is an attractive host lattice for several lanthanide ions to produce efficient phosphors emitting a variety of colors. Recently, $Gd_2O_3:Eu^{3+}$ phosphor has been considered as one of the better phosphor candidate for flat panel displays (FPDs) owing to its good color purity [15-17]. The red-emitting Eu-doped Gd_2O_3 phosphor is gaining importance due to its favorable low thermal expansion, phase stability, high melting point [18]. It has been widely used as X-ray scintillator materials, high definition projection televisions, flat panel displays, and photoelectronic apparatus [19]. Over the past decade, Eu^{3+} and Tb^{3+} activated Gd_2O_3 phosphors had been investigated extensively [17,20-22]. Tb^{3+} , Dy^{3+} and Eu^{3+} ions doped Gd_2O_3 particles have got potential application in immunoassays [23].

Recently, we have reported the sonochemical synthesis of a novel nano-crystalline $Gd_2O_3:RE$ ($RE = Dy^{3+}, Tb^{3+}$) phosphor which simultaneously emits blue and yellow light from its active region on exciting the host and consequently is expected to have tremendous applications in white light

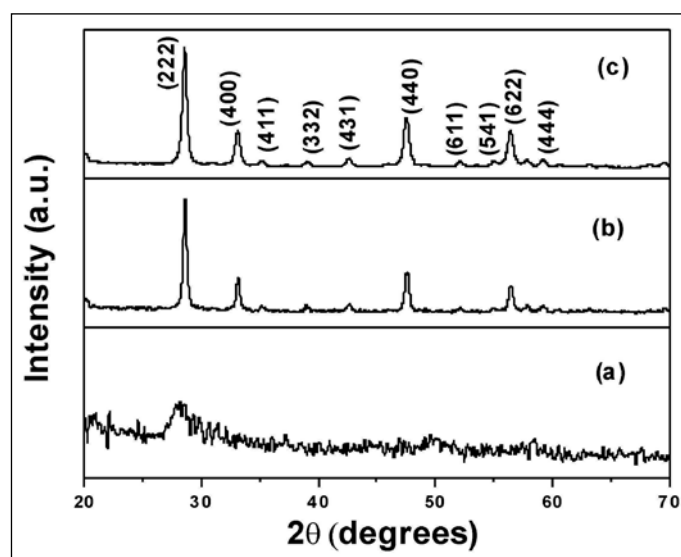


Fig. 1: XRD patterns of Gd_2O_3 nano powders (a) as prepared (b) annealed (c) doped with rare-earth ions.

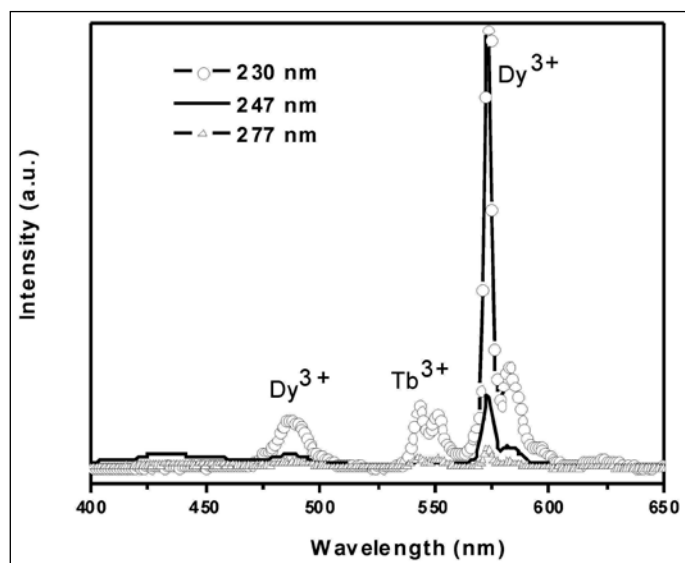


Fig. 2: Emission spectrum of $Gd_2O_3:Tb^{3+}:Dy^{3+}$ ($Tb = 0.05\%$ and $Dy = 1.95\%$) nano particles obtained after excitation at 230 nm, 247 nm and 277 nm.

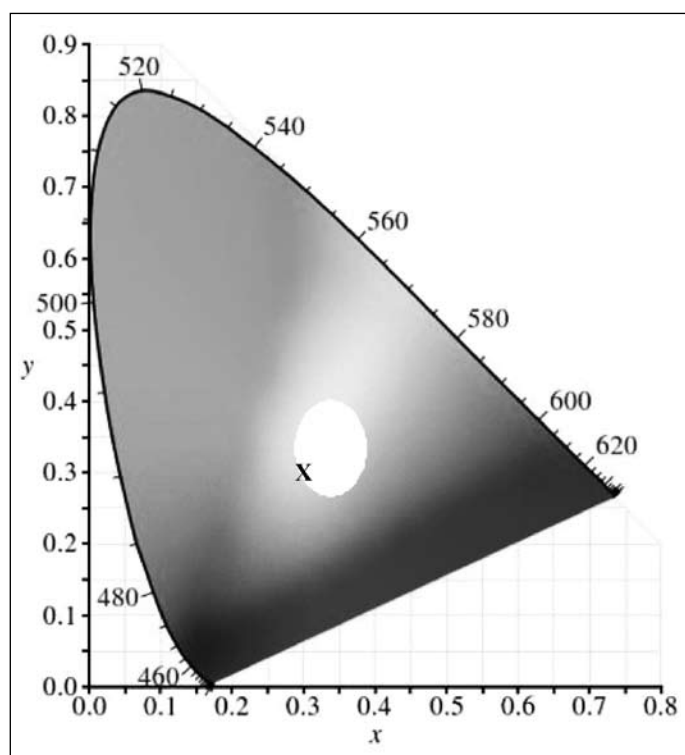


Fig. 3: CIE chromaticity diagram for $Gd_2O_3:Dy^{3+}(1.95\%):Tb^{3+}(0.05\%)$ nanoparticles at $\lambda_{exc} = 247nm$.

article, we report the work done on nanophosphors like $Gd_2O_3:RE$ ($RE = Eu, Dy, Tb$), $ZnAl_2O_4:M$ and $ZnGa_2O_4:M$ (where $M = Dy^{3+}, Tb^{3+}, Eu^{3+}$ and Mn^{2+}). The nanophosphors



Fig. 4: Photographs of $Gd_2O_3:Dy^{3+}(2\%)$ film on quartz under ultraviolet light with room lights switched off. Bright white emission is observed with the ultraviolet excitation.

emitting deep UV-LEDs [24]. Figure 1 (a, b) illustrates the diffraction patterns of the as prepared and annealed Gd_2O_3 nano particles, respectively. It is evident from the XRD patterns that the structure-less features detected for the as prepared samples were due to the amorphous nature of the product. On annealing the powder at 500 °C for 1 h, diffraction peaks were observed which matched with the reported data for Gd_2O_3 (PC-PDF card #76-0155). In the case of Eu^{3+} and Dy^{3+} doped Gd_2O_3 samples, annealing at 500 °C yielded crystalline nano particles; whereas for Tb^{3+} doped Gd_2O_3 , the annealing temperature required was 800 °C. The XRD patterns of the single, double and triple doped Gd_2O_3 nano particles, obtained after annealing at 800 °C, are similar and one such representative pattern is shown in Figure 1c. The emission spectra of $Gd_2O_3:Dy^{3+}(1.95\%):Tb^{3+}(0.05\%)$ on excitation at 230 nm, 247 nm and 277 nm is illustrated in Figure 2. It showed the presence of characteristic yellow, blue and green emissions due to Dy^{3+} and Tb^{3+} ions, respectively. As seen in the spectrum, on excitation at the main host site (230 nm), there is an efficient energy transfer from host to Dy^{3+} dopant, and hence maximum emission is observed at 575 nm. However, on exciting the sample at 247 nm, the intensity of emission at 575 nm reduces considerably, though it is still higher than that observed for excitation at 277 nm. This can be attributed to the fact that as the energy associated with higher wavelength excitation is lower, the probability of energy transfer from host to all the dopants is comparatively reduced. The CIE chromaticity coordinates calculated from

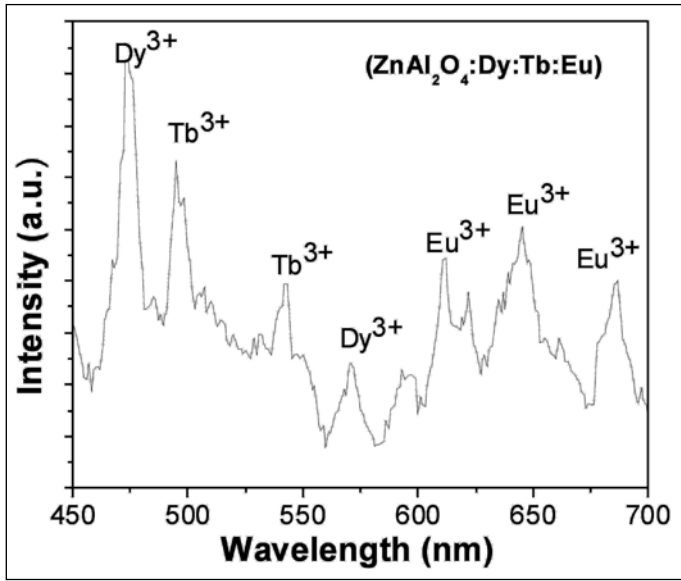


Fig. 5: PL emission spectra monitored at $\lambda_{exc} = 380\text{nm}$ for $\text{ZnGa}_2\text{O}_4:\text{Dy}^{3+}(1.5\%):\text{Tb}^{3+}(0.25\%):\text{Eu}^{3+}(0.25\%)$ nanoparticles.

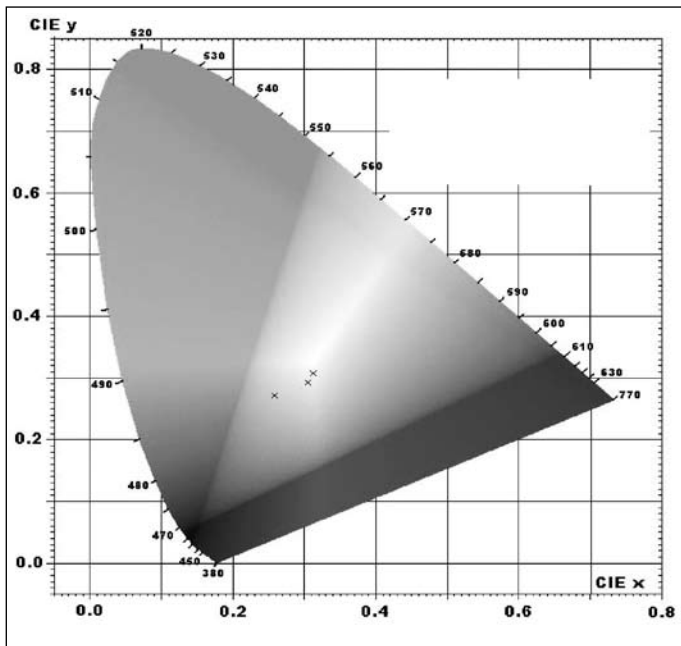


Fig. 6 : Chromaticity diagram for $\text{ZnAl}_2\text{O}_4:\text{Dy}^{3+}(1.5\%):\text{Tb}^{3+}(0.25\%):\text{Eu}^{3+}(0.25\%)$ nanoparticles with $\lambda_{exc} A = 380\text{nm}$, $B = 364\text{nm}$, $C = 396\text{nm}$

the emission curve of $\text{Gd}_2\text{O}_3:\text{Dy}^{3+}(1.95\%):\text{Tb}^{3+}(0.05\%)$ for 247 nm excitation were $x = 0.315$ and $y = 0.316$ (Figure 3). These values correspond almost exactly to the CIE coordinates of the balanced white light region of the chromaticity diagram where $x = 0.33$, $y = 0.33$. The corresponding CCT value was found to be 6508K. CIE standard illuminant D_{65} has a CCT of

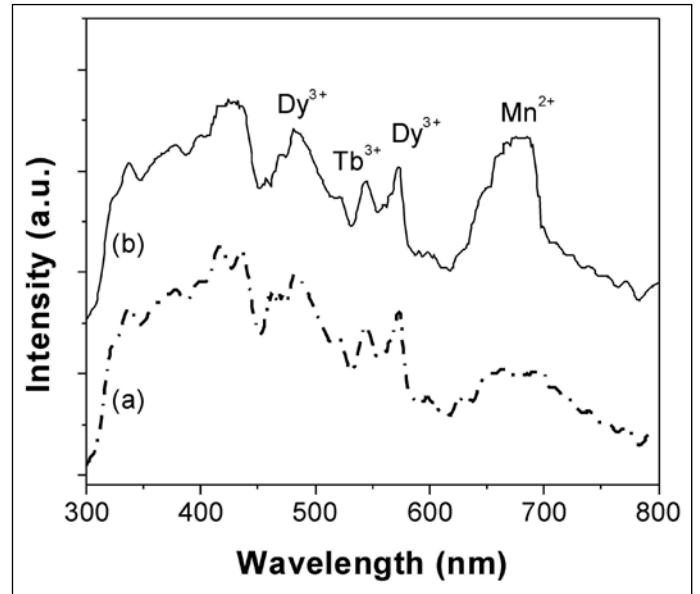


Fig. 7: Emission spectra monitored at $\lambda_{exc} = 340\text{nm}$ for (a) $\text{ZnGa}_2\text{O}_4:\text{Dy}^{3+}(2\%):\text{Tb}^{3+}(0.5\%):\text{Mn}^{2+}(1.5\%)$ and (b) $\text{ZnGa}_2\text{O}_4:\text{Dy}^{3+}(2\%):\text{Tb}^{3+}(0.5\%):\text{Mn}^{2+}(2.5\%)$ nanoparticles.

6500K which represents standard daylight. For this double doped sample, an excitation at 247 nm resulted in a CCT of 6508K which was extremely close to that of D_{65} . Due to the non dispersibility of the sonochemically-synthesized $\text{Gd}_2\text{O}_3:\text{Tb}^{3+}:\text{Dy}^{3+}$ nano particle in aqueous/organic solvent, polyol method of synthesis was explored [25]. The CIE chromaticity coordinates ($x = 0.270$, $y = 0.328$) and the CCT value (9157 K) of the $\text{Gd}_2\text{O}_3:\text{Dy}^{3+}(1.95\%):\text{Tb}^{3+}(0.05\%)$ phosphor synthesized by polyol route was distant from that of the D_{65} point (6500 K). This proves that method of synthesis plays a major role in optical properties of nanomaterials. Dispersible $\text{Gd}_2\text{O}_3:\text{Dy}^{3+}(2\%)$ phosphor was then synthesized using polyol technique. The phosphor showed white luminescence in solid form, as aqueous solution and also when spin coated on quartz substrate. For the spin coated sample CIE coordinates were $x = 0.313$ and $y = 0.296$ and the correlated color temperature was 6815 K. The photograph in Figure 4 show a spin coated $\text{Gd}_2\text{O}_3:\text{Dy}^{3+}(2\%)$ phosphor film on a quartz slide substrate, and the bright white luminescence of this film observed under ultraviolet light with $\lambda_{exc} = 310\text{nm}$. This demonstrates that $\text{Gd}_2\text{O}_3:\text{Dy}^{3+}(2\%)$ films are good candidate materials for new lighting devices.

Recently, ZnAl_2O_4 and ZnGa_2O_4 have attracted attention as an important phosphor host material for applications in thin film electroluminescent displays, mechano-optical stress

sensors, and stress imaging devices [26-30]. The optical band gap of polycrystalline ZnAl_2O_4 semiconductors is 3.8eV, which indicates that zinc aluminate in the polycrystalline form is transparent for light possessing wavelengths >320 nm [31]. The optical bandgap of ZnGa_2O_4 is approximately 4.4eV. Like other wide bandgap semiconductors, ZnGa_2O_4 exhibits a blue emission under excitation by both ultraviolet light and low-voltage electrons [32]. Activation with Mn^{2+} , Eu^{3+} , Tb^{3+} ions shifts the emission to green or red.

We have reported the synthesis of nanocrystalline single, double and triple doped $\text{ZnAl}_2\text{O}_4:\text{M}$ ($\text{M} = \text{Dy}^{3+}$, Tb^{3+} and Eu^{3+}) and $\text{ZnGa}_2\text{O}_4:\text{M}$ ($\text{M} = \text{Dy}^{3+}$, Tb^{3+} and $\text{Eu}^{3+}/\text{Mn}^{2+}$), by sonochemical method [33]. In our study, Dy^{3+} , Tb^{3+} and $\text{Eu}^{3+}/\text{Mn}^{2+}$ ions were single, double and triple doped in ZnAl_2O_4 and ZnGa_2O_4 host lattice using sonochemical technique. By altering the individual doping concentrations in the triple doped samples, the desired photoluminescence emission at selected wavelength could be obtained. The highlight of the work is the synthesis of a novel composition of nanocrystalline $\text{ZnAl}_2\text{O}_4:\text{Dy}^{3+}:\text{Tb}^{3+}:\text{Eu}^{3+}$ and $\text{ZnGa}_2\text{O}_4:\text{Dy}^{3+}:\text{Tb}^{3+}:\text{Mn}^{2+}$ phosphors which simultaneously emits blue, green, yellow and red light from its active region on exciting the host and have very impressive CIE and CCT values.

The PL emission spectrum of $\text{ZnAl}_2\text{O}_4:\text{Dy}^{3+}(1.5\%):\text{Tb}^{3+}(0.25\%):\text{Eu}^{3+}(0.25\%)$ sample at λ_{exc} of 380nm is shown in Figure 5. It is possible to distinguish four emission bands centered at ~595, 611, 644 and 686nm which correspond to $^5\text{D}_0 \rightarrow ^7\text{F}_1$, $^5\text{D}_0 \rightarrow ^7\text{F}_2$, $^5\text{D}_0 \rightarrow ^7\text{F}_3$ and $^5\text{D}_0 \rightarrow ^7\text{F}_4$ transitions of Eu^{3+} ions, respectively. The emissions from Dy^{3+} ions centered at 480nm ($^4\text{F}_{9/2} \rightarrow ^6\text{H}_{15/2}$) and a less strong one in the yellow region centered at 571nm ($^4\text{F}_{9/2} \rightarrow ^6\text{H}_{13/2}$) are also clearly discernible. The emission bands observed at 495 and 543 nm are due to the $^5\text{D}_4 \rightarrow ^7\text{F}_6$ and $^5\text{D}_4 \rightarrow ^7\text{F}_5$ transitions of Tb^{3+} ions. The broad band at ~506nm is due to the intrinsic luminescence of the host lattice. The color emission of the $\text{ZnAl}_2\text{O}_4:\text{Dy}^{3+}(1.5\%):\text{Tb}^{3+}(0.25\%):\text{Eu}^{3+}(0.25\%)$ nanoparticles was evaluated. CIE coordinates with corresponding CCT for different λ_{exc} is shown in Table 1. The chromaticity diagram shown in Figure 6 indicates that all the emissions with $\lambda_{\text{exc}} = 364$ and 380nm lie predominantly in the white region. From the diagram it is evident that closest to white light region is the emission obtained from the $\text{ZnAl}_2\text{O}_4:\text{Dy}^{3+}(1.5\%):\text{Tb}^{3+}(0.25\%):\text{Eu}^{3+}(0.25\%)$ nanoparticles with $\lambda_{\text{exc}} = 380\text{nm}$ and its CCT value (6689K) is also close to that of noon daylight (6500K, commonly known as D65 point).

Table 1: CIE and CCT values of $\text{ZnAl}_2\text{O}_4:\text{Dy}^{3+}(1.5\%):\text{Tb}^{3+}(0.25\%):\text{Eu}^{3+}(0.25\%)$ nanoparticles for various λ_{exc}

Excitation wavelength (nm)	X	y	CCT(K)
364	0.305	0.293	7475
380	0.312	0.307	6689
396	0.259	0.272	15329

Similarly, in an effort to get white light from zinc gallate phosphor, we codoped the $\text{ZnGa}_2\text{O}_4:\text{Dy}^{3+}(2\%)$ nanoparticles with Tb^{3+} and Mn^{2+} ions. The emission spectra obtained from the $\text{ZnGa}_2\text{O}_4:\text{Dy}^{3+}(2%):\text{Tb}^{3+}(0.5%):\text{Mn}^{2+}(1.5\%)$ and $\text{ZnGa}_2\text{O}_4:\text{Dy}^{3+}(2%):\text{Tb}^{3+}(0.5%):\text{Mn}^{2+}(2.5\%)$ nanoparticles on excitation at 340nm are shown in Figure 7. Apart from emissions from the host (in the blue region) and Dy^{3+} ions, strong broad red emissions from Mn^{2+} dopants have been observed between 650 to 700 nm. A very weak green emission was also seen at 519nm which originates from the $^4\text{T}_1 \rightarrow ^6\text{A}_1$ transition of Mn^{2+} . The emission at 544nm is due to the transition between the excited $^5\text{D}_4$ state and the $^7\text{F}_5$ ground state of Tb^{3+} ion. The CIE coordinates for $\text{ZnGa}_2\text{O}_4:\text{Dy}^{3+}(2%):\text{Tb}^{3+}(0.5%):\text{Mn}^{2+}(1.5\%)$ and $\text{ZnGa}_2\text{O}_4:\text{Dy}^{3+}(2%):\text{Tb}^{3+}(0.5%):\text{Mn}^{2+}(2.5\%)$ nanoparticles was found to be $x = 0.265$, $y = 0.285$ and $x = 0.304$, $y = 0.310$, respectively with CCT values of 12298K and 7251K.

The highlight of the work is the synthesis of novel compositions of nanocrystalline $\text{Gd}_2\text{O}_3:\text{Dy}^{3+}(1.95%):\text{Tb}^{3+}(0.05\%)$, $\text{ZnAl}_2\text{O}_4:\text{Dy}^{3+}:\text{Tb}^{3+}:\text{Eu}^{3+}$ and $\text{ZnGa}_2\text{O}_4:\text{Dy}^{3+}:\text{Tb}^{3+}:\text{Mn}^{2+}$ phosphors which simultaneously emits blue, green, yellow and red light from its active region on exciting the host and have very impressive CIE and CCT values. Such co-doped nanocrystalline phosphors are expected to have tremendous applications as tunable multi color displays and in white light emitting UV-LEDs. The results thus provide a practical basis for the design of white light illumination sources by blending this kind of phosphors with an appropriate UV emitter.

References

1. S. Nakamura, Appl. Phys. Lett., 64 (1994) 1687.
2. S. Aanegola, J. Petroski and E. Radkov, SPIE 10 (2003) 16.
3. Y. Narukawa, Optics & Photonics News, 4 (2004) 25.
4. L. S. Rohwer, A. M. Srivastava: Electrochem. Soc. Interface, 12 (2003) 36.

5. J. Y. Taso: Ed. Light Emitting Diodes (LEDs) for General Illumination Update 2002; Optoelectronics Industry Development Association: Washington, DC, (2002).
6. K. Bando, K. Sakano, Y. Noguchi, and Y. Shimizu, J. Light Vis. Environ., 22 (1998) 2.
7. J. McKittrick, L. E. Shea, C. F. Bacalski and E. J. Bosze, Displays, 19 (1999) 169.
8. M. Flynn and A.H. Kitai, J. Electrochem. Soc., 148 (2001) H149.
9. M. Yu, J. Lin, Y. H. Zhou and S. B. Wang, Mater. Lett., 56 (2002) 1007.
10. Justel T, Nikol H and Ronda C Angew. Chem. Int. Ed., 37 (1998) 3084.
11. B.W. D'Andrade and S.R. Forrest, Adv. Mater., 16 (2004)1585.
12. J. McKittrick, L. E. Shea, C. F. Bacalski and E. J. Bosze, Displays, 19 (1999)169.
13. S. SundarManoharan and M. Rao Encyclopedia of Nanoscience and Nanotechnology ed Nalwa H S (U.S.A.: American Scientific Publishers) (2004) 67.
14. K. S. Suslick, Science, 247 (1990) 1439
15. J. C. Park, H. K. Moon, D. K. Kim, S. H. Byeon, B. C. Kim and K. S. Suh, Appl. Phys. Lett., 77 (2000) 2162
16. Y. C. Kang, S. B. Park, I. W. Lenggoro and K. Okuyama, J. Phys. Chem. Solids, 60 (1999) 379.
17. B. Mercier, C. Dujardin, G. Ledoux, C. Louis and O. Tillement, J. Appl. Phys., 96 (2004) 650.
18. H. Guo, N. Dong, M. Yin, W. Zhang, L. Lou and S. Xia, J. Phys. Chem. B, 108 (2004) 19205-19209.
19. A. Brill and W. L. Wanmaker, Journal of Electrochemistry Society, 111, (1964) 1363-1368.
20. Y. Li, G. Liu and G. Hong, Journal of Rare Earths, 22 (2004) 70-74.
21. G.-X. Liu, G.-Y. Hong, and D.-X. Sun, Chinese Journal of Inorganic Chemistry, 20 (2004) 1367-1370 (Chinese).
22. G.-X. Liu, J.-X. Wang, X.-T. Dong, and G.-Y. Hong, Journal of Inorganic Materials, 22 (2007) 803-806, (Chinese).
23. W. O. Gordon, J. A. Carter and B. M. Tissue, J. Lumin., 108 (2004) 339.
24. V. Bedekar, D. P. Dutta, M. Mohapatra, S. V. Godbole, R. Ghildiyal and A. K. Tyagi, Nanotechnology, 20 (2009) 125707 (9pp)
25. V. Bedekar, D. P. Dutta and A. K. Tyagi, J. Nanoscience Nanotech., 10 (2010) 8234-8238.
26. T. Minami, Y. Kuroi, T. Miyata, H. Yamada and S. Takata, J. Lumines., 72 (1997) 997.
27. J. S. Kim, S. G. Lee, H. L. Park, J. Y. Park and S. D. Han, Mater. Lett., 58 (2004) 1354.
28. H. Matsui, C. N. Xu and H. Tateyama, Appl. Phys. Lett., 78 (2001) 1068.
29. E. Martinez-Sanchez, M. Garcia-Hipolito, J. Guzman, F. Ramos-Brito, J. Santoyo Salazar, R. Martinez-Martinez, O. Alvarez-Fregoso, M. I. Ramos-Cortes, J. J. Mendez-Delgado and C. Falcony, Phys. Status Solidi a, 202 (2005) 102.
30. Z. Lou, J. Hao, Appl. Phys. A, 80 (2005) 151.
31. S. K. Sampath, J. F. Cordor, J. Am. Ceram. Soc., 81 (1998) 649.
32. I.K. Jeong, H. L. Park, S. Mho, Solid State Commun., 105 (1997) 179.
33. D. P. Dutta, R. Ghildiyal and A. K. Tyagi, J. Phys. Chem. C, 113 (2009) 16954-16961.



Dr. Dimple P. Dutta joined the BARC Training School in 1996 after obtaining her M.Sc. in Chemistry from IIT Kanpur. Subsequently, she joined the Chemistry Division and has worked on design and development of Group III metal organic compounds as single source precursors for III-VI materials like gallium and indium chalcogenides. She was a postdoctoral Fellow at University of Heidelberg, Germany, during the period 2001-2002. Her major area of research includes synthesis of optical and magnetic nanoparticles using soft chemical techniques and studying their properties. She has an impressive list of publications to her credit and has presented her research work at several forums. Dr. Dutta also serves as reviewer for many journals of international repute.

Photocatalytic Properties of mixed oxides of BaCrO₄ and TiO₂

Tanmay K. Ghorai*, Chirantan Roy Chaudhry, Suman Biswas, Mukut Chakraborty, Ranjan Das, Jhimli Sengupta

Department of Chemistry, West Bengal State University, Barasat, North 24 Pgs, Kolkata-700126, India

*Corresponding author: E-mail: tanmay_ghorai@yahoo.co.in

Abstract

Mixed oxides of TiO₂ and BaCrO₄ (upto 5 mol %) have been synthesized by mechanical alloying method. Initially BaCrO₄ were prepared by co-precipitation technique. BaCrO₄/TiO₂ oxides were characterized by powder X-ray diffraction, BET, EDAX, SEM, ESR and photocatalytic activity measurements by UV-VIS absorption spectroscopy. The results show that the solid solution of TiO₂ with 1 mole percent of BaCrO₄ (BCT1) exhibit photocatalytic activity 3-5 times higher than that of P25 TiO₂ for oxidation of various dyes (RB, TB, MO and BG) under UV light irradiation ($\lambda > 420$ nm). Among the all dyes the oxidation of RB is faster. Due to the smaller ionic radius of the barium cation and the special electronic structures of BaCrO₄ the 1 mol % of BaCrO₄ in TiO₂ (BCT1) shows highest photocatalytic activity. The average crystallite sizes of BCT1 were found to be ~12 nm measured from XRD and grain size about 100±5 nm measured from SEM which also gave the morphology of the compounds. The EPR spectrum of BCT1 indicates that the ejection of electron helps to degrade the dye molecule faster.

Keywords: TiO₂ and BaCrO₄, Characterization; Photocatalyst; Photo oxidation.

Introduction

Most of the textile dyes and other industrial dyestuffs constitute a large group of organic compounds which are hazardous for the environment. Due to the large number of aromatic groups present in dye molecules and the stability of modern dyes, traditional and conventional techniques are ineffective for discoloration and degradation of dyes, and just transfer organic compounds from water to another phase. This is the reason for investigating the new methods which should conduct complete decomposition of dyes [1].

Titania is a very versatile material with attractive applications as pigment in paintings, in the production of electrochemistry electrodes, capacitors, solar cells, catalysis and photocatalysis. Regarding the latter application, purification of contaminated waters through complete mineralization of pollutants has extensively been used [2-7].

However, its wide band-gap energy (ca. 3.0 eV for rutile and 3.2 eV for anatase) means that only 5% of solar spectrum is used. Moreover, TiO₂ presents a relatively high electron-hole recombination rate which is detrimental to its photoactivity. In this sense, doping with metals or metal oxides could make a double effect: firstly, it could reduce the band gap energy, thus shifting the absorption band to the visible region. Secondly, metals could provoke a decrease in electron-hole recombination rate, acting as electron traps.

Therefore, there are some examples in the literature of the doping of titania with metals such as Ni (II) [8], Cu (II) [9], Nb (V) [10], Cr (III) [11-12], Fe (III) [13-16], and metal molybdates [17]. These were reported to improve the photocatalytic properties with enhanced absorption of visible/ultraviolet light.

The photocatalytic property of a multicomponent system is strongly influenced by the composition and the preparation procedure. In recent years, the application of heterogeneous photocatalysis on the removal of contaminants in air and wastewater has fetched some interest [18-19]. Due to the high photocatalytic activity and stability of titanium dioxide, it is generally used as a photocatalyst for the removal of organic pollutants from water or air [20-22].

Therefore, binary metal oxides such as TiO₂/WO₃, TiO₂/MoO₃, TiO₂/SiO₂ and TiO₂/ZrO₂ have been widely studied for their unique chemical, physical and photocatalytic properties [23-26]. Jiang Yin et al shows that MCrO₄ (Ba, Sr) has photocatalytic properties [27] but so far no studies have been reported on photocatalytic properties of BaCrO₄/TiO₂ mixed oxides.

Furthermore, photoactivity is highly dependent on surface area, crystallinity or crystal size which, in turn, are influenced by the method of synthesis. As far as such methods are concerned, the catalytic properties

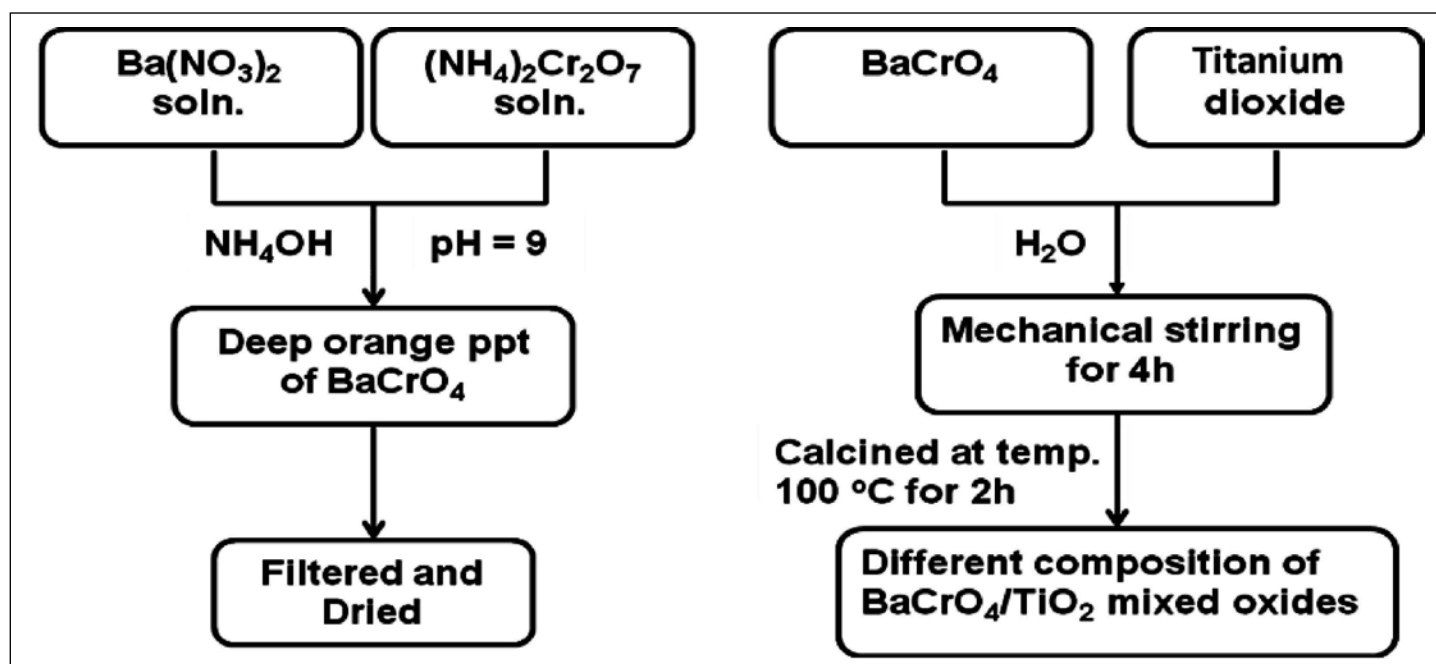


Fig.1 : Flow-chart synthesis for the different compositions of $\text{BaCrO}_4/\text{TiO}_2$ mixed oxides

are closely related to their structure and depend on the method of preparation and on the thermal treatment. The $\text{BaCrO}_4/\text{TiO}_2$ mixed oxides in taken in different mole ratios and subjected to mechanical milling method (using a ball mill) and their photocatalytic activities were evaluated by the photooxidations of different dyes like Rhodamine B (RB), Methyl orange (MO), thymol blue (TB) and Bromocresol green (BG) under UV light (400-W Hg lamp; $\lambda > 420$ nm) irradiation. This work deals with mechanochemical activation of BaCrO_4 and TiO_2 , in order to obtain nanocrystalline and single-phase products. The advantages of this approach are that the use of voluminous solutions and complicated operations as well as the sintering of the final product can be avoided.

Experimental

Synthesis of $\text{BaCrO}_4/\text{TiO}_2$ photocatalysts

The total synthesis of BaCrO_4 and TiO_2 in different mole ratio has been performed by two steps. In the first step, the starting material of barium chromate was prepared. Barium chromates were synthesized by co-precipitation method. Equimolar amount of barium nitrate and ammonium dichromate solutions were taken in a beaker. Then the aqueous ammonia was added dropwise via vigorous stirring to the above solution to adjust pH

to about 9 and a light orange amorphous precipitate was formed. The synthesis procedure is presented in Fig. 1.

In the second step the stoichiometric mixture BaCrO_4 and TiO_2 powders with different mole ratios (barium chromate in TiO_2 is 1 mol%, 3 mol% and 5 mol%) were ground and mixed thoroughly in water and subjected to mechanical grinding in a planetary ball mill. This mechanical milling was allowed for 4 h for complete mixing of the oxides forming a solid solution. The milling was performed in Fritsch Pulverisette No. 6 planetary ball mill, using a rotational speed of 250 rpm at a constant rotation direction and a ball to powder weight ratio of 10:1. The both container and balls were made of aluminium oxide. The prepared samples were dried at 100 °C for 15 h in an oven and photocatalytic activity was studied. The total procedure is presented in Fig. 1. The samples, when heat treated above 200°C, showed poor photocatalytic activity.

Rhodamine B (RB), Methyl orange (MO), Thymol blue (TB), Bromocresol green (BG) and 4-nitrophenol (4-NP) were A.R. reagents procured from MERCK India.

Photocatalytic experiment

Photocatalytic experiments were conducted using nanophotocatalysts in presence of different photocatalytically

degradable dyes in water solution. The photocatalytic reaction was carried out under UV light irradiation with slow stirring (using magnetic stirrer) of the solution mixture and BaCrO₄/TiO₂ photocatalysts. The light source was a 400-W Hg lamp (PHILIPS-HPL-N, G/74/2, MBF-400) and wave length is λ>280 nm. The container consists of a Petri dish of volume 200ml. The reactions were performed by adding nano powder of each photocatalyst (0.1 g) into each set of a 100 ml of different solution of dyes.

Analytical methods

A small volume (1ml) of reactant liquid was siphoned out at regular interval of time for analysis. It was then centrifuged at 1100 rpm for 15 min, filtered through a 0.2μm-millipore filter to remove the suspended catalyst particles and concentration of dye was measured by absorption spectrometry using UV-VIS spectrometer (UV-1601, SHIMADZU) at its wavelength of maximum absorption.

Characterization

The crystal structure of the prepared samples was determined by the X-ray diffractometer (XRD) (Model: Philips PW 1710) equipped with a Cu Kα radiation. The accelerating voltage and current used were 40 kV and 20 mA, respectively. The 2θ ranged from 15 to 70 °.

Crystallite sizes (D) of the obtained powders were calculated by the X-ray line broadening technique performed on the direction of lattice using computer software (APD 1800, Philips Research Laboratories) based on Scherer's formula [28].

$$D = \frac{0.89 \lambda}{\beta \cos \theta} \quad (1)$$

Where D is the Crystallite size, λ is the X-ray wavelength, θ is the Bragg's angle and β is full width at half maxima. The stoichiometry of BaCrO₄/TiO₂ alloys have been examined by energy dispersive X-ray spectroscopy (EDX) (GEOL JMS-5800) which is consistent with the amount taken of BaCrO₄ and TiO₂ during synthesis.

BET surface area measurements were carried out using a BECKMAN COULTER SA3100 through nitrogen adsorption-desorption isotherm at 77K. The average sizes of nanoparticles were measured in the scanning electron microscopy (SEM) (JEOL JMS-5800). The ESR spectrum

was obtained by BURCKER ER083CS model at room temperature (ca. 298 K). The UV-VIS diffuse reflectance spectra of the prepared powders were obtained by a UV-VIS spectrophotometer (UV-1601 Shimadzu) at room temperature.

After leaching the BaCrO₄/TiO₂ solid solution through filtration with whatman-42, the reaction solution (after reaction) was subjected to inductively coupled plasma (ICP) analysis in order to measure the amount of leached BaCrO₄/TiO₂ solid solution.

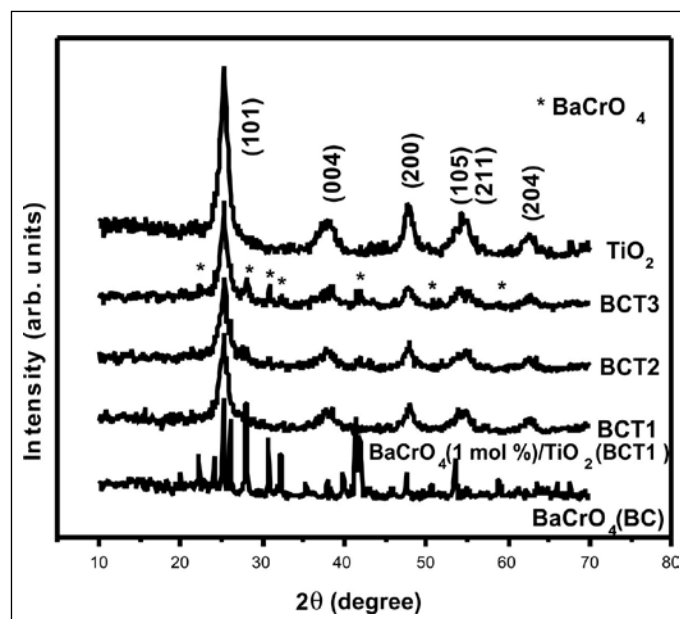


Fig. 2. XRD of BaCrO₄, BaCrO₄/TiO₂ mixed oxides (BCT1, BCT2, BCT3) and TiO₂ at 100 °C for 15 h

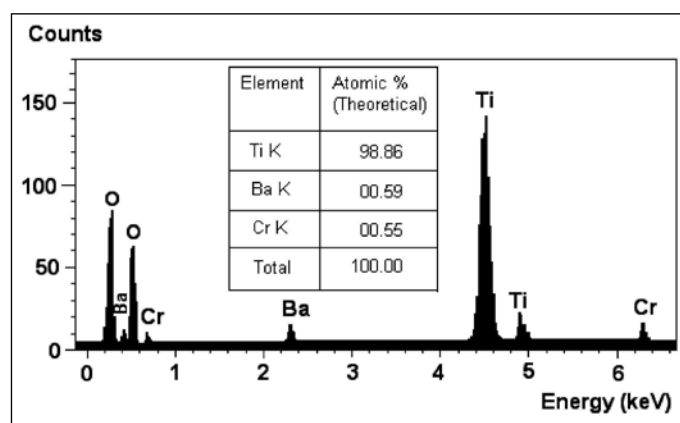


Fig. 3: EDAX of BaCrO₄ (1 mol %)/TiO₂ (BCT1)

Results and discussion

XRD analysis

The XRD pattern of the different compositions of BaCrO₄/TiO₂ heat treatment at 100 °C for 15 h in air atmosphere was shown in Fig. 2. It has been revealed that the phases prepared at different molar ratios of mixed oxides BaCrO₄ and TiO₂ [BaCrO₄ (1 mol%)/TiO₂ (BCT1), BaCrO₄ (3 mol%)/TiO₂ (BCT2), BaCrO₄ (5 mol%)/TiO₂ (BCT3), and TiO₂] have anatase phase up to 1 mol% of BaCrO₄ (as per JCPDS No. 72-0746). After that increase the BaCrO₄ concentrations in TiO₂ lattice the BaCrO₄ peaks are appear, which shown in the XRD of BCT3, because BaCrO₄ did not resolved in TiO₂ lattice and photocatalytic activity is decrease. The XRD pattern at TiO₂ sample shows distinct peaks of the anatase phases, without any indication of rutile phases. Average crystallite sizes of the prepared photocatalysts were calculated according to Scherer's formula and indicated that the crystallite sizes of the samples were ~12 nm. The atomic level dispersion BaCrO₄ in TiO₂ have been presented in Fig. 3 through energy dispersive X-ray spectroscopy.

Specific surface area (BET) analysis

The BET surface area of BaCrO₄/TiO₂ (BCT1) composites calcined at 100 °C was 55.4m²/g, while the surface area of P25 is 49.1m²/g and the surface area of other prepared photocatalysts are presented in Table 1. Though surface area of BCT2, BCT3 and Degussa P25 are comparable, but photocatalytic activity of BCT1 is 5 times greater than P25 TiO₂. Therefore, among all the prepared photocatalyst the BCT1 is more photoactive for faster degradation of different dyes like RB, MO, TB and BG under UV light (400-W Hg lamp; λ>280 nm).

Reaction rate constant measured after 50% degradation of Rhodamine B under UV light and catalyst; BET surface area measured by dinitrogen adsorption desorption isotherm at 100 °C; Crystallite size in nm calculated from Scherer equation; Photodegradation efficiency; RB: Rhodamine B; TB: Thymol Blue; MO: Methyl Orange; BG: Bromocresol Green; p-NP: pare Nitro Phenol .

Scanning electron microscopy (SEM) analysis

Fig. 4 shows scanning electron microscopy of BCT1. The grains separated by well-defined grain boundaries are visible which are uniformly distributed and shape of the particle is not determined precisely. The average grain size of BCT1 sample is about 100±5 nm. The grain sizes calculated from the micrographs using UTI image tool software (version 2.0).

EPR spectrum study

Fig. 5 illustrates the ESR spectrum of the BaCrO₄/TiO₂ recorded at 298 K. The characteristic feature of this spectrum is a signal at a g-tensor value of 2.001, indicating the presence of Ba²⁺/Cr³⁺ on irradiated TiO₂. Due to absence of any hyperfine line in ESR spectra, it can be suggested that Ba²⁺/Cr³⁺ cations are well separated. No EPR signal was detected on pure TiO₂ or BaCrO₄ species. The EPR signal of BaCrO₄/TiO₂ indicates that the ejection of an electron is the crucial role for photooxidation of RB under UV light.

Photocatalytic activity of the prepared samples

The photooxidation of different coloured dyes solution like RB, MO, TB, BG and 4-nitrophenil to colourless solution using the prepared photocatalysts and UV light (400-W Hg lamp; λ>280 nm) irradiation is shown in Fig. 6. UV-VIS spectra of RB, MO, TB, BG and 4-NP taken after the irradiation with BaCrO₄/TiO₂ (BCT1) BaCrO₄/

Table 1 : Resultant properties of BCT1, BCT2, BCT3, P25 TiO₂ and BaCrO₄ composites

Sample	Reaction rate Constant k(h ⁻¹)	S _{BET} (m ² /g)	Crystallite size (nm)	Photo degradation efficiency (%)				
				RB	TB	MO	BG	p-NP
BCT1	7.77	55.4	12.03	99.8	61.8	49.9	18.6	7.9
BCT2	5.41	49.5	12.35	94.3				
BCT3	2.83	39.1	12.55	70.6				
P25 TiO ₂	4.98	49.1	12.42	95.7				
BaCrO ₄	0.36	1.3	18.21	7.9				

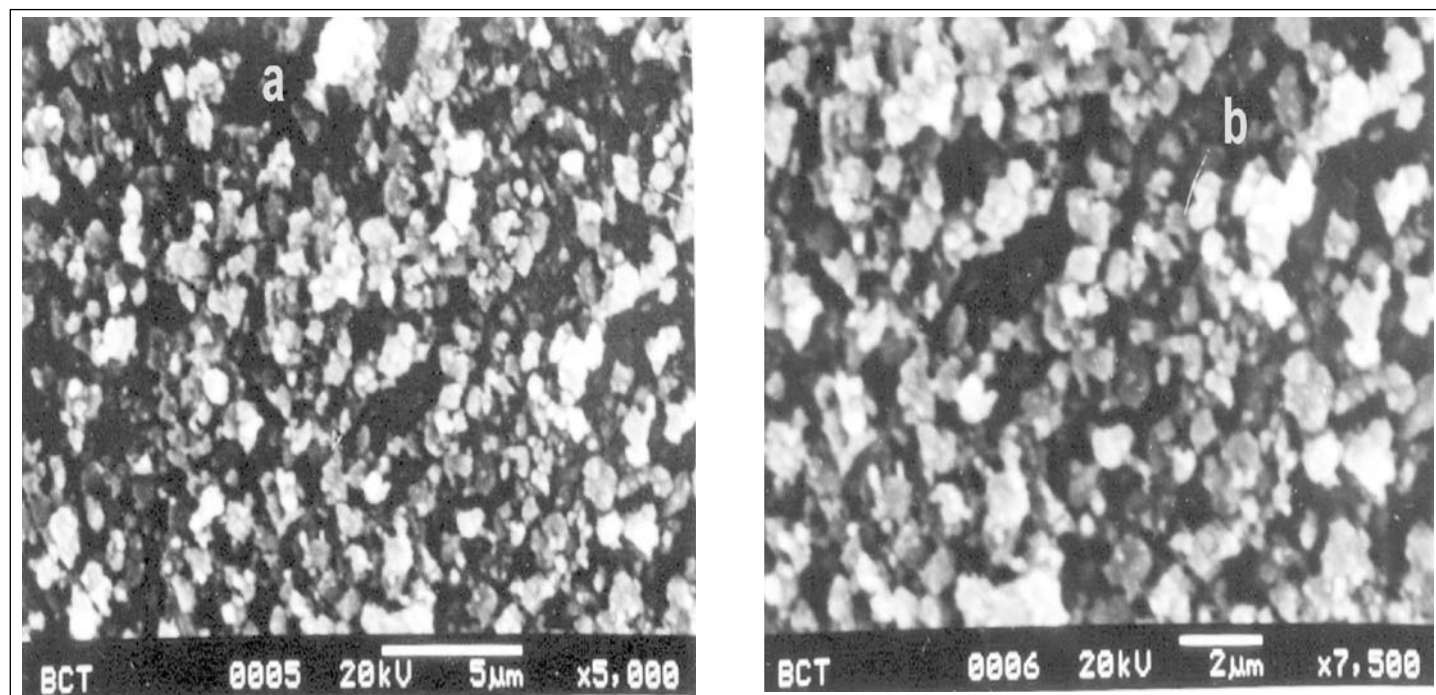


Fig. 4: Scanning electron microscopy (SEM) of BCT1 calcined at 100 °C for 2 h at resolution a) 5000 and b) 7500.

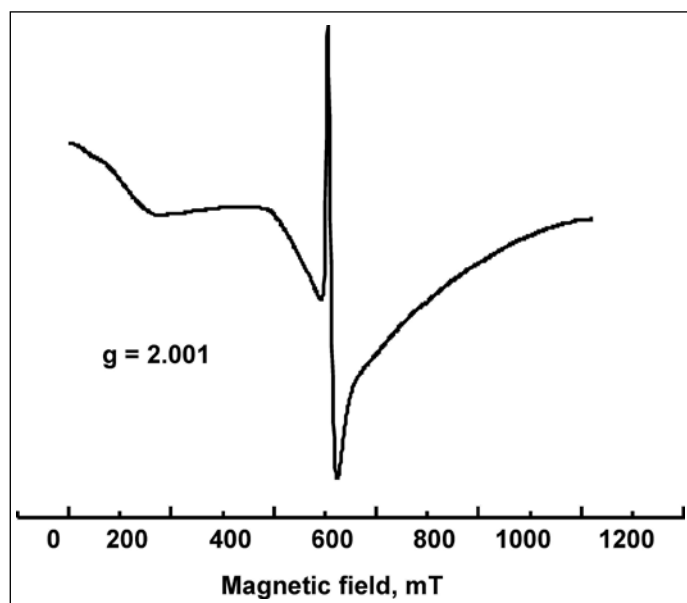


Fig. 5: ESR spectra of BaCrO₄/TiO₂ mixed oxides at room temperature

TiO₂ (BCT2), BaCrO₄/TiO₂ (BCT3), TiO₂ and BaCrO₄/TiO₂ (BC) compositions, were measured and corresponding absorbance of dyes were found at 554, 464, 597 and 616 nm respectively. Among all the four dyes including 4-NP the rate of degradation of Rhodamine B is faster in the presence

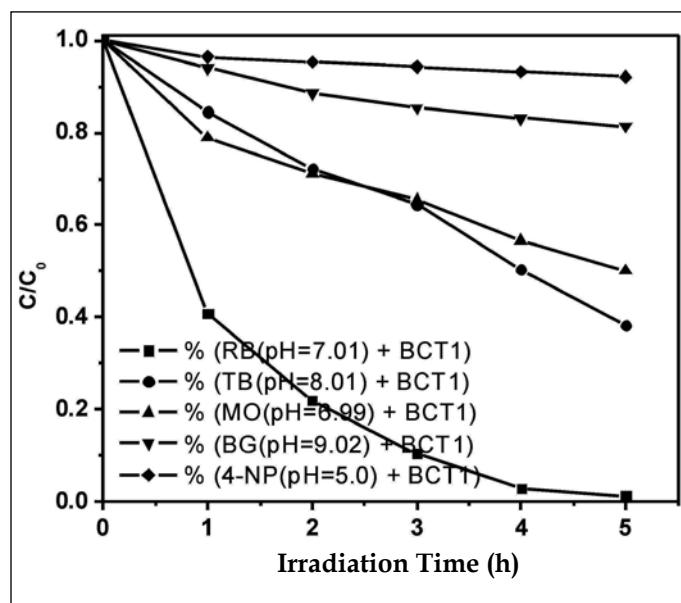


Fig. 6: Effect of BCT1 on diff. dyes under UV light

of BCT1 and UV light. The time required for completely decolorization of RB is 5 h. For all the cases the catalysts were taken at 1 g/l and different dye concentration was about 10 mM. Fig. 7 shows the photooxidation of RB in presence of different catalyst (BCT1, BCT2, BCT3, P25 TiO₂,

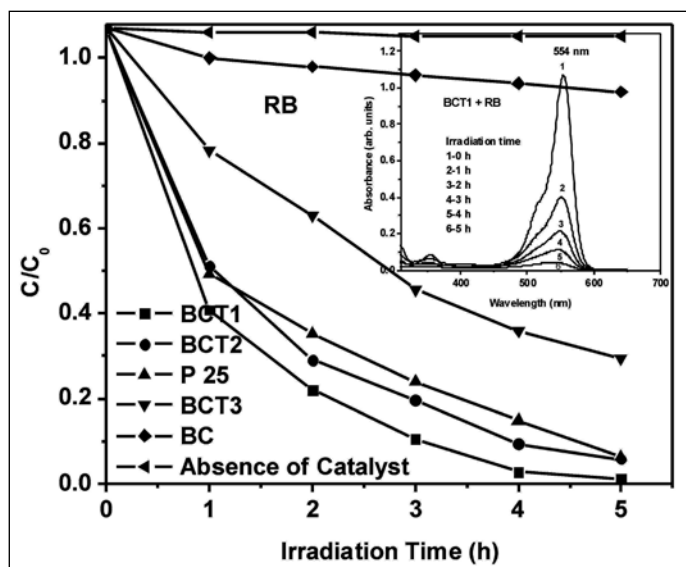


Fig. 7: The changes in concentrations of RB solution at 554 nm in the presence of BCT1, BCT2, P25 TiO₂, BCT3, BC and absence of catalyst, the catalyst concentration is C_{catalysts} = 1 g/l. Rhodamine B concentration is C_{RB} = 10 mM, 400-W Hg lamp (λ > 280 nm).

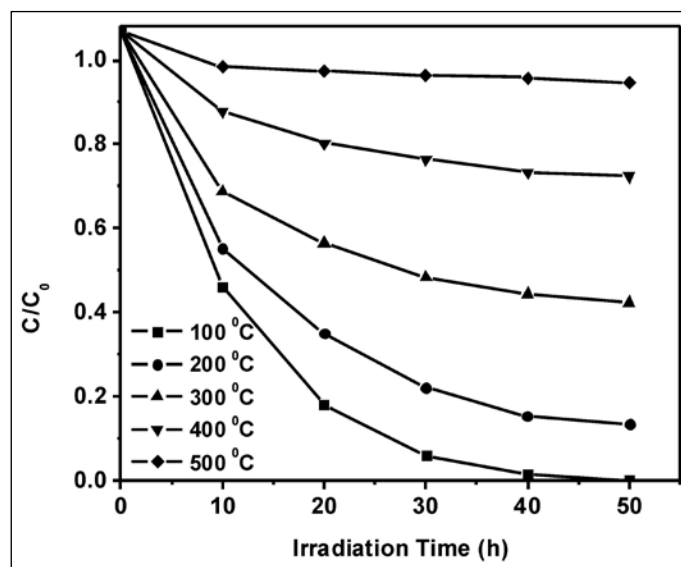


Fig. 9: The effect of calcinations temperature for 15 h for 100 °C, 200 °C and other temperature is for 2 h on the photocatalytic activity of BCT1, the catalyst concentration is C_{catalysts} = 1 g/l. Rhodamine B concentration is C_{RB} = 10 mM, 400-W Hg lamp (λ > 280 nm).

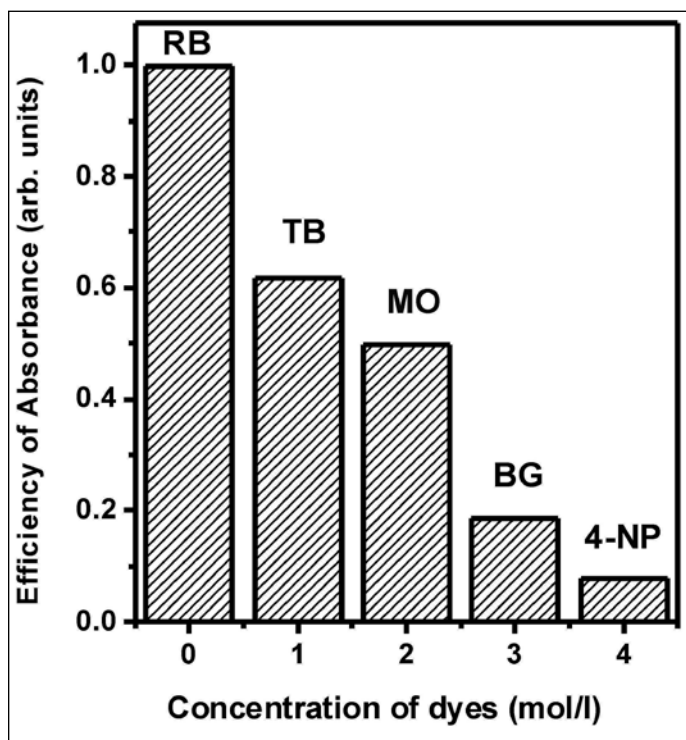


Fig. 8: Catalytic efficiency of BCT1 on Different dyes under UV light

BC and absence of catalyst) and UV light. Under UV light irradiation, the alloy BaCrO₄/TiO₂ (BCT1) exhibited highest photocatalytic activity than that of other compositions of

BaCrO₄/TiO₂ mixed oxides, P25 TiO₂, and barium chromate (BC). It is also observed that in absence of catalyst the degradation of dyes is not possible under UV light (shown in Fig. 6). The BCT1 composites have shown five times higher photocatalytic activity than that of P25 TiO₂ in case of Rhodamine B. The increment of BaCrO₄ concentration beyond 1 mole % led to lower photocatalytic activity. The degradation rate constant (k) for RB, MO, TB and BG using BCT1, BCT2, BCT3, P25 TiO₂, BC photocatalysts have been presented as the time required for 50 % decolourization of dyes solutions in Table 1. The catalytic efficiency of BCT1 on Different dyes under UV light was shown in Fig. 8. The photooxidation efficiency of RB is highest among all other dyes and p-NP in presence of catalyst and UV light.

Effect of heat-treatment temperatures

The effect of heat-treating temperature of the solid solution or composites on the photocatalytic activity was also investigated. Fig. 9 shows the profiles of the photooxidations of Rhodamine B under UV light (λ > 280 nm) irradiation using BCT1 solid solution calcined at 100 °C, 200 °C, 300 °C, 400 °C and 500 °C. The samples calcined at 100 °C showed highest photocatalytic activity. It seems that the increase of the calcination temperature decreases the defect-states on the surface. Above 100 °C the activity of catalyst decreases with rise of crystallite sizes of solid solution. It is also observed that adsorption of dye (RB,

TB, MO, and BG) decreases with increase of heat treatment temperature of the catalyst. This is probably due to decrease of defect-structure on the surface of solid catalyst. Thus defect structure signifies its crucial role for photocatalytic activity.

Conclusions

Synthesis of nano-sized composites or solid solution of BaCrO₄ and TiO₂ with high photocatalytic activity for oxidative degradation of different dyes was successfully obtained through mechanochemical synthesis. XRD data shows the formation of mixed oxides having anatase structure with no free BaCrO₄ upto 1 mole % of BaCrO₄/TiO₂. BaCrO₄/TiO₂ catalyst have crystallite size about 12 nm measured from XRD and grain size about 100±5 nm measured from SEM. The maximum solubility of BaCrO₄ in TiO₂ is 1 mol percent and this composition has highest photocatalytic activity that is 5 times higher than P25 TiO₂ for the oxidation of RB. We also observed that the rate of degradation of Rhodamine B is fastest among all the four dyes with the prepared catalyst in visible light.

Acknowledgements

This work was supported by the Department of Scientific and Technology, India. The authors are grateful for its financial support.

References

1. I.K. Konstantinou, T.A. Albanis, *Appl. Catal. B. Environ.* 49 (2004) 1-14.
2. C. Guillard, J. Disdier, C. Monnet, J. Dussaud, S. Malato, J. Blanco, M.I. Maldonado, J.M. Herrmann, *Appl. Catal. B* 46 (2003) 319.
3. S. Malato, J. Blanco, A. Campos, J. Ca´ceres, C. Guillard, J.M. Herrmann, A.R. Fern´andez-Alba, *Appl. Catal. B* 42 (2003) 349.
4. P. Pichat, in: M.A. Tarr (Ed.), *Chemical Degradation Methods for Wastes and Pollutants: Environmental and Industrial Applications*, Marcel Dekker Inc., New York, Basel, 2003, pp. 77-119.
5. M.A. Aramendi´a, A. Marinas, J.M. Marinas, J.M. Moreno, F.J. Urbano, *Catal. Today* 101 (2005) 187.
6. C.E. Taylor, *Catal. Today* 84 (2003) 9. On the other hand, the possibility of carrying out selective photooxidations in nonaqueous media is very interesting in the context of Green

Chemistry.

7. K.I. Shimizu, H. Akahane, T. Kodama, Y. Kitayama, *Appl. Catal. A* 269 (2004) 75.
8. D. Jing, Y. Zhang, L. Guo, *Chem. Phys. Lett.* 415 (2005) 74-78.
9. G. Colon, M. Maicu, M. C. Hidalgo, J. A. Navio, *Appl. Catal. B: Environ.* 67 (2006) 41-51.
10. K. Tennakone, J. Bandara, *Sol. Energy Mater. Sol. Cells* 60 (2000) 361.
11. N. Serpone, D. Lawless, *Langmuir* 10 (1994) 643.
12. J. C. Yu, G. Li, X. Wang, X. Hu, C. W. Leung, Z. Zhang, *Chem. Commun.* (2006) 2717-2719.
13. J. Zhu, W. Zheng, B. He, J. Zhang, M. Anpo, *J. Mol. Catal. A: Chem.* 216 (2004) 35-43.
14. T. K. Ghorai, S. K. Biswas, P. Pramanik, *Appl. Surf. Sci.* 254 (2008) 7498-7504.
15. M. I. Litter, J. A. Navio, *J. Photochem. Photobiol. A: Chem.* 98 (1996) 171-181.
16. J. Feng, R. S. K. Wong, X. Hu, P. L. Yue, *Catal. Today* 98 (2004) 441-446.
17. T. K. Ghorai, D. Dhak, S. K. Biswas, S. Dalai, P. Pramanik, *J. Mol. Catal. A: Chem.* 273 (2007) 224-229.
18. J-Chuan Xu, Y-Li Shi, J-Er Huang, B. Wang, H-Lin Li, *J. Mol. Catal. A: Chem.* 219 (2004) 351-355.
19. M. A. Hasnat, M. M. Uddin, A. J. F. Samed, S. S. Alam, S. Hossain, *J. Hazardous Mater.* 147 (2007) 471-477.
20. A. Fuerte, M. D. Hernandez-Alonso, A. J. Maira, A. Martinez-Arias, M. Fernandez-Garcia, J. C. Conesa and J. Soria, *Chem. Commun.*, 2001, 2718-2719.
21. Y. Chen, K. Wang, L. Lou, *J. Photochem. Photobiol. A: Chem.* 163 (2004) 281-287.
22. J. C. Colmenares, M. A. Aramendia, A. Marinas, J. M. Marinas, F. J. Urbano, *Appl. Catal. A: Gen.*, 306 (2006) 120-127.
23. Y. R. Do, W. Lee, K. Dwight, A. Wold, *J. Solid State Chem.* 108 (1994) 198.
24. J. Papp, S. Soled, K. Dwight, A. Wold, *Chem. Mater.* 6 (1994) 496.
25. X. Fu, L. A. Clark, Q. Yang, M. A. Anderson, *Environ. Sci. Tech.* 30 (1996) 647.
26. Z. Liu, J. Davis, *J. Phys. Chem.* 98 (1994) 1253.
27. Jiang Yin, Zhigang Zou, Jinhua Ye, *Chemical Physics Letters* 378 (2003) 24-28.
28. P. Klug, L. E. Alexander, *Direction Procedures for Polycrystalline and Amorphous Materials*, Wiley, New York, 1954.

	<p>Dr. Tanmay Kumar Ghorai is presently working at Department of Chemistry in the West Bengal State University as an Assistant Professor since 2009. He received the Young Scientist Award (2010) from the Department of Science & Technology (DST) in the Fast Track Scheme, Govt. of India. He also received the prestigious fellowship BOYSCAST from DST in the year 2010-11, Govt. of India. He is involved in the complete synthesis procedure, characterization and study of the photocatalytic application of BaCrO₄ and TiO₂ mixed oxide synthesized by mechanical alloying.</p>
	<p>Dr. Chirantan Roy Choudhury is presently working at Department of Chemistry in the West Bengal State University as an Assistant Professor since 2009. He is involved in the synthesis of BaCrO₄ and TiO₂ mixed oxide in different mole ratio by mechanical alloying.</p>
	<p>Dr. Suman Biswas is a permanent faculty at Department of Chemistry in the West Bengal State University as an Assistant Professor since 2009. He is basically an organic chemist. His contribution is mainly the synthesis and study of the catalytic application of BaCrO₄ and TiO₂ mixed oxide in different mole ratio by mechanical alloying.</p>
	<p>Dr. Mukut Chakraborty is a permanent faculty at Department of Chemistry in the West Bengal State University as a Reader since 2009. He is the recipient of Convention Award for Young Scientists by Indian Chemical Society in the year 1999. His current research work is Conducting Polymer, Nanocomposites synthesis and characterization of polymeric nanomaterials. His main role is the write up of SEM and ESR characterization of BaCrO₄ and TiO₂ mixed oxide synthesis.</p>
	<p>Dr. Ranjan Das is working at Department of Chemistry in the West Bengal State University as an Associate Professor since 2010. He worked as an Associate Research Scientist of CNRS in Institut Gilbert Laustriat - UMR 7175, Strasbourg in 2007-08. In 2010, he was nominated to the position of Invited Professor in the Laboratoire de Biophotonique et de Pharmacologie, University de Strasbourg, France. His current research interests are in photophysics of charge-transfer dyes, core-shell nanoparticles, dye encapsulated nanomaterials. His main function in the manuscript is correcting the grammatical error and helping to response to the reviewer comments</p>
	<p>Dr. Jhimli Sengupta is presently working at Department of Chemistry in the West Bengal State University as an Assistant Professor since 2009. She received the Young Scientist Award (2010) from the Department of Science & Technology (DST) in the Fast Track Scheme, Govt. of India. Her main activity in this manuscript is the systematic study of the catalytic activity of oxidation of different organic dyes under UV light</p>

News and Forthcoming Events

Year 2011 is being celebrated as International Chemistry Year throughout the world.

Some of the International Conferences being organised in INDIA, in the year 2011 are:

1. International Conference on Vistas in Chemistry 2011(ICVC-2011), Kalpakkam, India, Oct. 2011, e-mail:prabs@igcar.gov.in
2. 14th ISMAS Symposium cum Workshop on Mass Spectrometry Munnar, Kerala, Nov. 7-11, 2011, <http://www.ismas.org>
3. International Symposium on Chemistry and Complexity IACS, Kolkata, Dec. 6-8, 2011, e-mail:chemistry@iacs.res.in
4. ISEAC-WS-2011, International Symposium cum Workshop on Electrochemistry. Goa, India, Dec. 7-10, 2011, <http://www.iseac.org>
5. 56th DAE Solid State Physics Symposium (DAE - SSPS 2011) Kattankulathur, Tamilnadu, Dec. 19-23, 2011, e-mail:mukhop@barc.gov.in

Some of the International Conferences being organised in the year 2011-2012 are:

1. 2011 International Conference on Solid State Devices and Materials (SSDM2011) Nagoya, Japan, Sept. 28-30, 2011, e-mail:ssdm_secretariat@intergroup.co.jp
2. 7th International Symposium on Novel Materials and their Synthesis. Shanghai, China, Oct. 11-14, 2011, e-mail:nms@fudan.edu.cn
3. The 12th Pacific Polymer Conference (PPC12) Jeju Island, Seoul, Korea, Nov. 13-17, 2011, e-mail:info@ppc12.org,
4. 4th International Symposium on Structure-Property Relationships in Solid State Materials June 24-29, 2012, Bordeaux, France, e-mail:contact@spssm4.com
4. 15th International Congress on Catalysis Munich, Germany, July 1-6, 2012, e-mail:tagungen@dechema.de
5. ICACCE 2012 : International Conference on Applied Chemistry and Chemical Engineering Amsterdam, Netherlands, July 25-27, 2012. <http://www.waset.org>.
6. 4th EuCheMS Chemistry Congress Praha, Czech Republic, Aug. 26-30 2012, e-mail:info@euchems-prague 2012.
7. ISCRE 22, International Symposium on Chemical Reaction and Engineering Maastricht, Netherlands, Sept. 2-5, 2012, e-mail:info@iscre22.com,

Achievements, Honours and Awards received by the SMC members

Name of the member & affiliation	Name of the award/honour	Conferred by
Dr. M. K. Chattopadhyay <i>RRCAT, Indore</i>	Scientific & Technical Excellence Award	Department of Atomic Energy
Mrs. Sunaina Devi <i>University of Allahabad</i>	Prof. G. Gopala Rao Centenary Young Scientist Award	Annual Convention of Chemists
Dr. Dimple P Dutta <i>BARC, Mumbai</i>	Member, National Academy of Sciences, India	National Academy of Sciences, India
Neha Gupta <i>University of Allahabad</i>	Prof. G. Gopal Rao Centenary Young Scientist Award	Annual Convention of Chemists
Neha Gupta <i>University of Allahabad</i>	Prof. A.K. De memorial Award	Annual Convention of Chemists
Dr. Tanmay Kumar Ghorai <i>West Bengal State University</i>	BOYSCAST Fellowship	Department of Science & Technology
Dr. Vinita Grover Gupta <i>BARC, Mumbai</i>	Young Scientist Award	Indian Society for Chemists and Biologists
Atul Kumar Kushwaha <i>University of Allahabad</i>	Dr. U. V. Rao Memorial Award	Annual Convention of Chemists
Dr. G. P. Kothiyal <i>BARC, Mumbai</i>	INS Science Communication Award	Indian Nuclear Society
Dr. Raman Kumar Mishra <i>BARC, Mumbai</i>	IANCAS Prof. H.J. Arnikar Best Thesis Award - 2011	Indian Association of Nuclear Chemists and Allied Scientists
Dr. T. Mukherjee <i>BARC, Mumbai</i>	Lifetime Achievement Award	Free Radical Society of India
Prof. Anjali M. Rahatgaonkar <i>Institute of Science, Nagpur</i>	Nominated as National Representative for India to the IUPAC Division VII Committee. Division VII Committee.	International Union of Pure and Applied Chemistry (IUPAC)
Dr. Mainak Roy <i>BARC, Mumbai</i>	Young Associate of Maharashtra Academy of Sciences	Maharashtra Academy of Sciences
Prof. Nandlal Singh <i>The M.S. University of Baroda</i>	Fellow- Gujarat Academy of Sciences	Gujarat Academy of Sciences
Dr. V. Sudarsan <i>BARC, Mumbai</i>	Young Achiever Award for the Year 2010	DAE Solid State Physics symposium 2010 (DAE-SSPS 2010)
Dr. A. K. Tyagi <i>BARC, Mumbai</i>	Fellow, Royal Society of Chemistry (FRSC)	Royal Society of Chemistry, UK
Prof. Sandeep Varma <i>IIT, Kanpur</i>	Shanti Swarup Bhatnagar Prize in Chemical Sciences	CSIR, New Delhi
Prof. Sandeep Varma <i>IIT, Kanpur</i>	Fellow, Indian Academy of Sciences	Indian Academy of Sciences, Bangalore
Dr. P. R. Vasudeva Rao <i>IGCAR, Kalpakkam</i>	MRSI-ICSC Superconductivity and Materials Science Senior Award	Materials Research Society of India
Dr. P. R. Vasudeva Rao IGCAR, <i>Kalpakkam</i>	CRSI Silver Medal	Chemical Research Society of India

Printed by:

Ebenezer Printing House

Unit No. 5 & 11, 2nd Floor, Hind Service Industries

Veer Savarkar Marg, Shivaji Park Sea-Face, Dadar (W), Mumbai - 400 028

Tel.: 2446 2632 / 2446 3872 Tel Fax: 2444 9765 Email : eph@vsnl.com / outworkeph@gmail.com

In this issue

Feature articles

- | | | |
|---|--|----|
| 1 | Chemistry and applications of nanomaterials
<i>A.K. Tyagi</i> | 1 |
| 2 | Evaporation induced self assembly of nanoparticles by spray drying
<i>D. Sen, J. Bahadur, S. Mazumder, J.S. Melo and S.F. D' Souza</i> | 12 |
| 3 | Light absorption and emission in gold nanoplates assembled in small groups via poly(vinylidene fluoride) molecules
<i>B. Susrutha, A.D. Phule and S. Ram</i> | 22 |
| 4 | Preparation and characterization of Collagen-based Liposome Nanoparticles composite matrix
<i>Krishnamoorthy Ganesan, Praveen Kumar Sehgal, Asit Baran Mandal and Sadulla Sayeed</i> | 29 |
| 5 | Application of nanophosphors in solid state white light generation
<i>Dimple P. Dutta</i> | 34 |
| 6 | Photocatalytic Properties of mixed oxides of BaCrO ₄ and TiO ₂
<i>Tanmay K. Ghorai, Chirantan Roy Chaudhyry, Suman Biswas, Mukut Chakraborty, Ranjan Das, Jhimli Sengupta</i> | 40 |
| | News and Forthcoming Events | 48 |
| | Honours and Awards | 49 |

Society for Materials Chemistry

C/o. Chemistry Division Bhabha Atomic Research Centre, Trombay, Mumbai, 400 085 (India)

E-mail: socmatchem@gmail.com,

Tel: +91-22-25592001